# Fibre Placement Architectures for Improved Damage Tolerance

# Fibre Placement Architectures for Improved Damage Tolerance

Proefschrift

ter verkrijging van de graad van doctor
aan de Technische Universiteit Delft,
op gezag van de Rector Magnificus prof. ir. K. C. A. M. Luyben,
voorzitter van het College voor Promoties,
in het openbaar te verdedigen op dinsdag 10 december 2013 om 15:00 uur

door

Martin Herman NAGELSMIT

vliegtuigbouwkundig ingenieur
geboren te Leiderdorp.

Dit proefschrift is goedgekeurd door de promotor:

prof. dr. Z. Gürdal

Copromotor: dr. C. Kassapoglou

Samenstelling promotiecommissie:

| | |
|---|---|
| Rector Magnificus, | voorzitter |
| prof. dr. Z. Gürdal, | Technische Universiteit Delft, promotor |
| dr. C. Kassapoglou, | Technische Universiteit Delft, copromotor |
| prof. dr. ir. R. Benedictus | Technische Universiteit Delft |
| dr. L. Lessard | McGill University, Canada |
| prof. dr. C. Soutis | University of Manchester, UK |
| prof. dr. ir. R. Akkerman | Universiteit Twente |
| ir. H.G.S.J. Thuis | Nationaal Lucht- en Ruimtevaartlaboratorium |
| prof. dr. A. Rothwell, | Technische Universiteit Delft, reservelid |


This research was funded by the National Aerospace Laboratory NLR

*Keywords:* Composites, damage tolerance, fibre placement

*Printed by:* Sieca Repro, Delft



ISBN 978-94-6186-243-3

An electronic version of this dissertation is available at
`http://repository.tudelft.nl/`.

# Preface

The research described in this thesis originated from a true believe that we should never be satisfied with the solutions and techniques available. Originating from an improvement in the manufacturing process by developing the fibre placement machine, people started to realise that this same manufacturing process could also increase the design space of composite materials. Some of those people happened to be working at TUDelft and NLR, and combined the powers of excellent design tools with outstanding manufacturing knowledge and industry experience. First with the amazing variable stiffness laminates with curved fibre paths, improving amongst others the buckling load of composite laminates. Next, the impact damage issue in composites was taken on with dispersed laminates and this research. A strong combination of theoretical design tools and experimental work, together with vision and a bit of fantasy is a prerequisite for the generation, validation and acceptation of new ideas. Just like in composites, the result of cooperation is always more than the sum of its constituents. With the solutions and ideas from this research I hope to inspire people for future steps and contribute humbly to safer and more sustainable aviation. We must always improve!

Martin

Rotterdam, 18 November 2013

# Summary

For obvious reasons, composites have been used in aerospace structures for years, but only recently on a very large scale. One of the downsides of composites is the poor impact behaviour. After having suffered a foreign object impact, their residual strength is decreased considerably while not showing clear signs of damage. This combination of residual strength and detectability determines the damage tolerance of a structure, and is notoriously poor in composites as compared to metals. Most current methods to improve the damage tolerance of composite laminates use reinforcements in the thickness direction to prevent delaminations.

The weight saving achieved by composites is not sufficient anymore; the manufacturing costs have to be decreased significantly as well. This has led to the introduction of fibre placement technology and this automated manufacturing technology also makes new structural concepts possible. Laminates do not only have to be made of straight fibres in the 0°, 90° and 45° directions, but they can have any orientation and do not have to be straight anymore. Significant improvements in for instance the buckling load can be achieved with this increase in design freedom, by applying the variable stiffness principle. An increased damage tolerance can be achieved by optimising the adjacent fibre angles to decrease the delamination tendency, while maintaining the in-plane stiffness. Promising test results are achieved by these so-called dispersed laminates.

In this thesis, a new fibre placement architecture is proposed that combines an automated production process with through-the-thickness reinforcements. Normally in fibre placement fibre tows are placed adjacent to each other, creating laminates with unidirectional layers and relatively poor damage tolerance. In the AP-PLY fibre architecture, room is left in between adjacent fibre tows. In a second passing of the machine head, the same series of tows is placed in a second direction. For the third and fourth time, the machine fills up the gaps left open in the first and second passing of the machine head. Continuing like this, a laminate can be created with a uniform thickness that has fibres running across the resin interface between adjacent layers. A virtually endless amount of patterns can be thought of when varying the bandwidth, orientation angle, number of tows to skip and amount of interwoven layers. In a second approach, a package of two interwoven layers is interwoven with the package above and the package below, creating a laminate without open resin interfaces.

In a 'design of experiments' approach the influence of each abovementioned parameters is investigated to determine the best performing AP-PLY pattern. In compression after impact tests at a series of energy levels the indentation depth, projected delamination size and resid-

ual compressive strength are compared. Overall, an increase in residual strength after impact is achieved between 5 and 10%. A smaller bandwidth gives a higher residual strength, and skipping more than one bandwidth does not yield a sufficient increase in residual strength to justify the increase in fabrication time. Interweaving more plies increases the residual strength, but also increases the amount of undulations possibly reducing in-plane strength and stiffness. The best performing pattern has a bandwidth of 1/4 inch, 45° between adjacent plies, skips only one bandwidth and interweaves each package of two interwoven layers with the package above and below. In section cuts, it was observed that although delaminations are smaller with AP-PLY, more fibre breakage and matrix cracks are present. A redistribution amongst damage mechanisms dissipates a similar amount of energy in both types of laminates. Due to this notion, it is expected that even better damage tolerance can be achieved by interweaving a limited number of layers in a laminate.

Also mechanical properties other than the compression after impact strength have been investigated. Virgin compression after impact specimens have been used to test the stiffness, and no differences between baseline laminates with unidirectional layers and laminates with the AP-PLY configurations have been measured. In open hole compression, bolt bearing and pin bearing the average test results did not show a clear difference between AP-PLY and unidirectional laminates, but the scatter was considerably lower in AP-PLY, which could result in higher A- and B-basis allowables. Also in a sandwich configuration, the specimens with interwoven facesheets show an increase in after impact residual compressive strength of 10%.

One of the mechanisms in AP-PLY increasing the damage tolerance is thought to be an increased fracture toughness. To measure these values, specimens are designed with an AP-PLY unit cell and tested in Mode I and Mode II for fracture toughness. In Mode I an 89% increase in fracture toughness was measured and in Mode II 20%.

In an attempt to predict the tendency of composite laminates to delaminate, a new analytical model is proposed that can calculate the deflection of composite plates with asymmetric and unbalanced stacking sequences under an out-of-plane load. Using Legendre polynomials instead of Fourier sine and cosine series, results were achieved that matched values from literature and a simple linear finite element model. From this model, the stresses and strains in each layer interface can be calculated, and together with a failure criterion the layers that fail under impact induced bending can be calculated. In a parallel fracture mechanics approach, a model from literature was adapted and used to determine the delamination size under an out-of-plane load. These two methods were combined to get a delamination profile for the lower half of a composite laminate. First, using fracture mechanics, the largest delamination is determined. Next, the laminate is split up at that delamination location reducing the stiffness. This reduced stiffness is used in the bending failure model using the Tsai-Hill failure criterion. The results are supported by the C-scans from the impacts, where the largest delaminations are located near the bottom side of the laminate.

Using the observation of the redistribution of energy dissipation, two new AP-PLY configurations are proposed that do not interweave all layers in the laminate. In a first configuration, only the outside +/-45° layers of a quasi-isotropic laminate are interwoven, interweaving 4 out

of 24 layers. After impact residual strength is increased by 10% as compared to its unidirectional counterpart, yielding a similar increase as laminates with all layers interwoven with only a 17% increase in manufacturing time. In a second configuration, the layer interfaces at the outside which are prone to fail under bending and do not contribute much to the stiffness are sacrificed to dissipate energy. Two packages of 5 layers are interwoven, resulting in 10 out of 24 interwoven layers. Test results show a 15% increase in compressive residual strength after impact with a 42% increase in manufacturing time. This supports the hypothesis that strengthening all layer interfaces does not result in the highest damage tolerance, because the impact energy has to be dissipated by damage creation.

# Samenvatting

Composiet materialen worden al jaren om evidente redenen gebruikt in de lucht- en ruimtevaart, maar pas recent op zeer grote schaal. Eén van de nadelen van composieten is de slechte bestendigheid tegen inslag. Nadat het composiet een inslag te verduren heeft gekregen is de sterkte onder druk sterk verminderd zonder zichtbare tekenen van schade. Deze combinatie van reststerkte en detecteerbaarheid bepaalt de 'damage tolerance', oftewel schadetolerantie, van een constructie. Bij composieten is deze schadetolerantie berucht slecht vergeleken met metalen. De meeste huidige methodes om de schadetolerantie van composieten te verbeteren gebruiken versterkingen in de dikterichting om delaminaties te voorkomen.

Alleen de gewichtswinst die te behalen is bij het toepassen van composieten is niet meer interessant genoeg; ook de productiekosten moeten drastisch worden verminderd. Dit heeft geleid tot de uitvinding van 'fibre placement'; het machinaal plaatsen van de vezels op een mal. Deze automatische productietechnologie maakt ook nieuwe structurele concepten mogelijk. Laminaten hoeven niet meer alleen uit rechte vezels in de 0°, 90° en 45° richting te bestaan, maar ze kunnen in elke richting gelegd worden en hoeven zelfs niet meer recht te zijn. Significante verbeteringen in bijvoorbeeld de kniklast kunnen bereikt worden met deze nieuwe ontwerpvrijheid door het toepassen van het variabele stijfheids principe. Een verbetering van de schadetolerantie kan bereikt worden door het optimaliseren van de vezelrichtingen van naastgelegen lagen, terwijl de in-het-vlak stijfheid gelijk blijft. Met deze zogenaamde 'dispersed' of verspreide laminaten zijn bemoedigende testresultaten behaald.

In dit proefschrift wordt een nieuwe vezelplaatsing architectuur voorgesteld die een geautomatiseerd productieproces combineert met versterkingen in de dikterichting van het laminaat. Normaal gesproken worden bij 'fibre placement' de vezelbundels direct naast elkaar geplaatst waardoor laminaten worden verkregen met unidirectionele lagen en relatief slechte schadetolerantie. Bij de AP-PLY vezel architectuur wordt ruimte gelaten tussen naastgelegen vezelbundels. Tijdens een tweede gang van de machinekop wordt een vergelijkbare serie vezelbundels in een tweede richting geplaatst. In de derde en vierde gang van de machinekop worden de opengebleven stukken opgevuld met vezelbundels. Als op deze manier wordt doorgegaan kan een laminaat met een uniforme dikte verkregen worden waarin vezels de volledige harslagen overbruggen. Een schier oneindige hoeveelheid variaties kunnen bedacht worden als de bundelbreedte, vezelrichtingen, aantallen vezelbundels die worden overgeslagen en verweven lagen worden gevariëerd. In een tweede methode wordt elk pakket met twee verweven lagen verbonden met het pakket eronder en het pakket erboven waardoor een laminaat ontstaat zonder volledig uit hars bestaande lagen.

Door gebruik te maken van 'design of experiments' kan de invloed van elke hierboven beschreven parameter onderzocht worden om het best presterende AP-PLY patroon te vinden. Door 'compression after impact', oftewel 'druk na inslag', testen uit te voeren op verschillende energieniveaus van de inslag kunnen de putdiepte, geprojecteerde delaminatiegrootte en reststerkte worden vergeleken. Over de hele breedte wordt een verbetering in de reststerkte na inslag gemeten tussen de 5 en 10%. Een smallere bundelbreedte geeft een hogere reststerkte, en meer dan één bundel overslaan geeft niet een dusdanige verbetering dat het de langere fabricagetijd rechtvaardigt. Meerdere lagen met elkaar verweven verhoogt weliswaar de reststerkte, maar vergroot ook de golvingen van de vezelbundels wat de in-het-vlak stijfheid en sterkte nadelig zou kunnen beïnvloeden. Het best presterende patroon heeft een bundelbreedte van 1/4 inch, 45° tussen naastgelegen lagen, slaat één bundel over en verweeft elk pakketje van twee vervlochten lagen met het pakketje erboven en het pakketje eronder. In doorsnedes werd ontdekt dat delaminaties weliswaar kleiner zijn als AP-PLY wordt toegepast, maar dat deze laminaten meer vezelbreuk en harsscheurtjes vertonen. Een herverdeling onder de schademechanismes vindt plaats om dezelfde energie te kunnen dissiperen in beide laminaattypes. Door dit inzicht is de verwachting dat een grotere verbetering van de schadetolerantie bereikt kan worden door niet alle lagen in een laminaat te verweven.

Naast de druksterkte na inslag zijn ook andere mechanische eigenschappen van AP-PLY laminaten onderzocht. Onaangetaste proefstukken zijn gebruikt om de stijfheid te testen, en deze vertoonden in geen geval een verschil tussen laminaten met unidirectionele lagen en laminaten met een AP-PLY patroon. Geen significante verschillen in de gemiddelde waardes tussen AP-PLY en unidirectionele laminaten zijn gemeten voor open gat druk, pin lagering en bout lagering, maar de spreiding was significant kleiner voor AP-PLY, hetgeen zou kunnen duiden op hogere toegestane ontwerpwaardes. Ook in een sandwichconstructie laten proefstukken met AP-PLY dekplaten een verbetering van de druksterkte na inslag zien van 10%.

Het vermoeden bestaat dat breuktaaiheid één van de mechanismes is die de schadetolerantie van AP-PLY laminaten verbetert. Om deze waardes te meten zijn speciale proefstukken ontworpen met een AP-PLY patroon en getest voor de breuktaaiheid in Mode I en Mode II. In Mode I is de breuktaaiheid verbeterd met 89% en in Mode II met 20%.

In een poging om de delaminatieneiging van composiet laminaten te voorspellen is een nieuw analytisch model ontwikkeld dat de doorbuiging van een composieten plaat met een onsymmetrische en ongebalanceerde stapeling onder een uit-het-vlak belasting kan berekenen. Door Legendre polynomen te gebruiken in plaats van sinus en cosinus series werden resultaten behaald die overeen kwamen met resultaten uit de literatuur en een simpel eindige elementen model. Met dit model kunnen ook de rekken en spanningen in elke laagovergang berekend worden, en door het toepassen van een faalcriterium kunnen de laagovergangen die bezwijken onder door inslag veroorzaakte buiging worden bepaald. Parallel hieraan is een breukmechanica model uit de literatuur aangepast en gebruikt om de delaminatiegrootte veroorzaakt door een uit-het-vlak belasting te bepalen. Deze twee methodes werden gecombineerd om een delaminatieprofiel te verkrijgen voor de onderste helft van een composietlaminaat. Eerst werd door middel van breukmechanica bepaald waar de grootste delaminatie ontstaat. Vervolgens wordt

het laminaat opgesplitst op deze locatie waardoor de stijfheid afneemt. Deze gereduceerde stijfheid wordt gebruikt in het Legendre model in combinatie met het Tsai-Hill faalcriterium. De resultaten worden ondersteund door de C-scans na de inslagen, waar ook de grootste delaminaties zich bevinden aan de onderkant van het laminaat.

Door gebruik te maken van het inzicht van de herdistributie van de inslagenergie zijn twee nieuwe AP-PLY configuraties ontwikkeld die niet alle lagen in het laminaat verweven. In een eerste configuratie worden alleen de buitenste +/-45° lagen verweven, waardoor vier van de vierentwintig lagen zijn verweven. De reststerkte na inslag is verbeterd met 10% vergeleken met zijn unidirectionele versie, terwijl de fabricagetijd met slechts 17% is toegenomen. In een tweede configuratie worden de buitenste lagen, die weinig bijdragen aan de stijfheid en vroeg bezwijken onder buiging, opgeofferd om inslagenergie te dissiperen. Twee pakketjes van vijf lagen worden verweven, resulterend in tien uit vierentwintig verweven lagen. Testresultaten laten een verbetering zien in de reststerkte na inslag van 15% met een 42% toename in fabricagetijd. Dit ondersteunt de hypothese dat het versterken van álle laagovergangen niet resulteert in de hoogste schadetolerantie omdat de inslagenergie moet worden gedissipeerd door schadevorming.

# Contents

# List of Abbreviations

| | |
|---|---|
| AFP | Automated Fibre Placement |
| AITM | Airbus Industry Test Method |
| AP-PLY | Advanced Placed Ply |
| ASTM | American Society for the Testing of Materials |
| ATL | Automated Tape Layer |
| BVID | Barely Visible Impact Damage |
| CAI | Compression After Impact |
| CFRP | Carbon Fibre Reinforced Plastic |
| DCB | Double Cantilever Beam |
| DLL | Design Limit Load |
| DS | Delamination Size |
| DUL | Design Ultimate Load |
| ENF | End Notch Flexure |
| FHC | Filled Hole Compression |
| ID | Indentation Depth |
| LVDT | Linear Variable Differential Transformers |
| MDD | Maximum Design Damage |
| NCL | Non-Conventional Laminate |
| NLR | Nationaal Lucht- en Ruimtevaartlaboratorium |
| OHC | Open Hole Compression |
| RDD | Readily Detectable Damage |
| RS | Residual Strength |

| | |
|---|---|
| SBC | Short Block Compression |
| TP | Thermoplast |
| TS | Thermoset |
| TUDelft | Delft University of Technology |
| UD | Unidirectional |
| VSL | Variable Stiffness Laminate |

# Chapter 1

# Composites and Damage Tolerance

## 1.1 Introduction

Literally, composite means a material composed of several materials, and combinations of materials have long been used in construction. Very early versions of composites include wattle and daub for walls in early building and horn and wood Scythian bows with animal glue. Nowadays, plywood and reinforced concrete are used extensively in construction and the more sophisticated fibre and resin type in sports equipment such as tennis rackets and skis. In the field of engineering, composites are known as a material composed of fibres and a resin. Although fibres are unable to carry loads in compression and a resin by itself is very weak, particularly in tension, when combined they form a winning team.

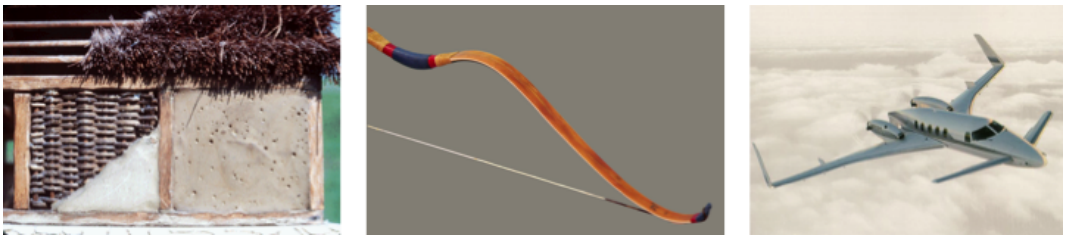

Figure 1.1: Wattle and daub for walls (loki.stockton.edu), a Scythian bow (www.grozerarchery.com) and a Beech Starship composite airplane (www.rps3.com)

Modern composites have been used in aircraft structures for over four decades. The aerospace specific advantages of composites are:

- Their high specific strength and stiffness
- The possibility to optimise strength and stiffness directionally due to their anisotropy
- The possibility to integrate parts and thus removing the need for expensive, in terms of cost and weight, joints
- Aerodynamically smoother shapes
- Their relative insensitivity to fatigue and environmental degradation as compared to metals

Due to the brittle nature and multiple failure mechanisms of composites, one of their main disadvantages compared to metals is how they behave under impact. This is one of the main topics of this thesis.

### 1.1.1 Structural Concepts

In aircraft, a stiffened thin-walled shell is the most commonly occuring structural design concept in metals and such shells are increasingly made of composite materials. Below, the two main ways to construct a stiff panel using composites are discussed. Both are being used in aerospace applications, and both have their specific advantages and disadvantages [Niu, 1992].

#### Sandwich

In the same way as an I-beam, the geometry of a composite can be used to increase its moment of inertia and thus its bending stiffness. A stiffer structure can be constructed for the same weight by placing two sheets of composite further apart using a low density core. Core materials can be for instance foam or metal or paper honeycomb. The disadvantages of this method for aerospace applications are moisture ingression, joining and facesheets vulnerable to impact and poor handling. The advantages are in the inherent thermal and acoustic insulating properties present when this type of composite is used for a fuselage, and its high buckling strength.

#### Monolithic Shells

Instead of using a different core material in the composite, a thicker shell structure can be stiffened by stringers, analogous to a metal stiffened skin design. Due to their lower density, composite skins will be thicker than comparable aluminium skins, while stringers can be bonded or co-cured, resulting in a lighter construction than a riveted joint.

### 1.1.2 Aerospace Applications

Innovation often comes from military applications, and this is no different for composites. In the 1970's, Chinook rotorblades were made from fibreglass composites which made maintenance and inspection less costly. For military applications, apart from the previously mentioned advantages, a composites stealth potential also plays an important role. First carbon composite applications in military aircraft include the AV8-B Harrier and B2 stealth bomber.

Composite use in civil aircraft began with fibreglass tertiary structures such as interiors, to secondary structures, such as flaps and ailerons, via vertical and horizontal stabilizers on the Boeing 737 in the 1980's and evolved to primary carbon fibre structures such as center wing boxes (Airbus A380), wings (Airbus A400M) and complete fuselages (Boeing 787). The first passenger airplane with more than 50% of its structural weight consisting of composites was the Boeing 787 'Dreamliner', see Figure 1.2 for a list of the different materials used in this aircraft.


Figure 1.2: Boeing 787 Dreamliner material profile [Roeseler, Sarh, and Kismarton, 2007]

In Boeing's 787 the material advantage of composites has resulted in a plane with 20% improved fuel efficiency due to the lower weight, higher cabin pressure and larger windows due to the higher fatigue strength and higher cabin humidity and lower maintenance costs due to the relative insensitivity to environmental degradation.

The challenge for future aeronautic structures as foreseen by EADS, one of the leading aerospace vehicle manufacturers, is depicted in Figure 1.3. Where current composite structures are lighter but more expensive, future composite structures have to be both lighter and cheaper. This important notion will be addressed later in this chapter when different manufacturing technologies are discussed.

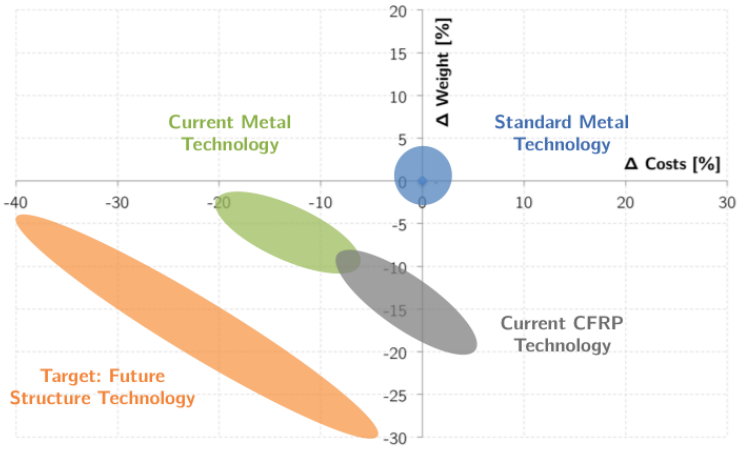


Figure 1.3: The future of aerospace structures according to EADS (EASN Workshop 2007)

## 1.2 Damage Tolerance

As a design philosophy, damage tolerance has been around since the 1970's. In contrast to preceding design philosophies such as fail-safe and safe-life, damage tolerance uses knowledge about the presence of flaws and predictions of their growth. Fail-safe design implies redundancy: when a part fails, it should not be catastrophic to the functioning of the structure. This redundancy some times implies an over-engineered, hence too heavy, design. The safe-life approach is nowadays only used for structures where inspections are not feasible, such as for helicopter blades. Knowledge of presence of flaws in a component and their growth implies detection and previously unavailable analysis techniques. No single definition of damage tolerance exists [Sierakowski and Newaz, 1995], but related to composite laminates and the topic of this thesis, the following definition of damage tolerance will be used:

*The ability of a structure to sustain its design loads despite being damaged*

In many cases, especially for aluminium structures, aircraft design is limited by fatigue requirements. With the introduction of composite materials, which show flatter fatigue curves, other types of damage have become dominant in the design process. Together with the poor detectability of impact damage in composite laminates, which is further explained in the next section, this has given rise to a new approach to damage tolerance in composites. In this new approach, the detectability of impact damage, rather than (fatigue) cracks, is related

to the strength of the structure. As graphically depicted in Figure 1.4, when no damage is

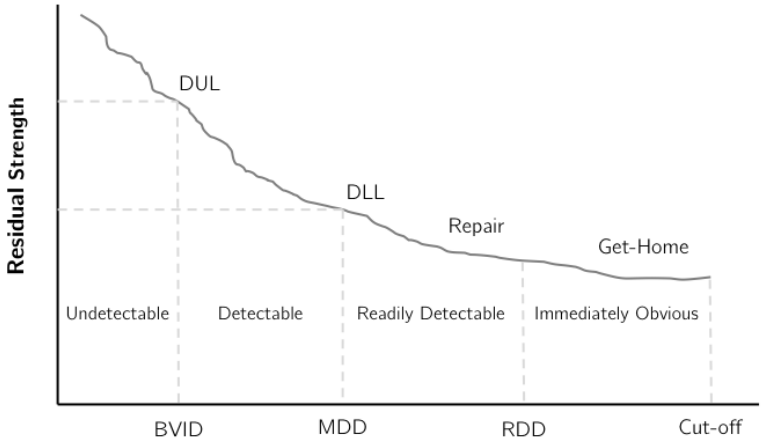


Figure 1.4: Requirements for damage size and residual strength

visible below the barely visbile impact damage (BVID) level, the structure should still be able to withstand its design ultimate load (DUL). With clearly visible damage, the maximum design damage (MDD), the structure should still be able to carry its design limit load (DLL) and the damage should be repaired during planned maintenance. Readily detectable damage (RDD) calls for immediate repair, and after an in-flight event the residual strength should be sufficient to 'get-home'.

As impact damage in composites is hard to detect from the outside, but detrimental internally, this poses a great challenge to designers using composites.

The damage tolerance of a structure can be regarded and evaluated at different levels. A building block approach is prescribed in MIL-HDBK-17-3F (2002), where most tests are performed on simple coupon specimens, and the more complex the part and the test, the fewer tests are performed. This concept is based on an increasing understanding of the behaviour of the composite material used, where analysis plays an important role and is depicted in Figure 1.5. After each step in the pyramid, the test results are fed into a model which is then verified and updated. This loop is performed after every step. Ideally, on the top of the pyramid only the airworthiness of the structure in question has to be demonstrated without any unpleasant surprises.

A structure can be damage tolerant when a single crack, or other type of damage, is arrested by a structural element such as a stringer or a joint. Further down in the pyramid, a composite laminate can be damage tolerant when it can still carry the design loads whilst containing damage caused by, for instance, an impact. This research focuses on the laminate level, hence damage tolerance will also be evaluated at this level.

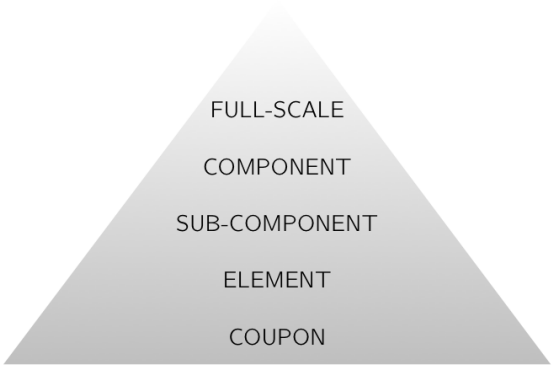


Figure 1.5: Building block approach

## 1.3 Composites

When designing with composites, there is a strong correlation between design, manufacturing and the materials used: the composite material is 'made' at the same time the product is made, and the way the product is made influences the mechanical properties of the material, in turn influencing the design. This is a slight adaptation of the trinity essence for lightweight design as explained elegantly by Beukers and Van Hinte (2005), and graphically depicted in Figure 1.6.

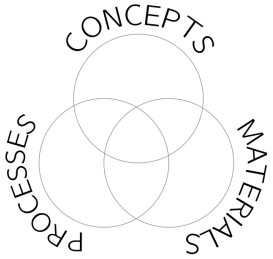


Figure 1.6: Trinity essence [Beukers and Van Hinte, 2005]

In this thesis, these three aspects of composite design are looked at from the *damage tolerance* point of view at the *laminate* level.

In aerospace applications, the most widely used composite is made of carbon fibres and polymer resin and is often erroneously referred to as carbonfibre, while carbon fibre reinforced plastic (CFRP) would be more accurate. As depicted in Figure 1.7, fibres and resin are combined in layers, and these layers can be stacked on top of each other to construct a laminate with the needed stiffness properties, and composite parts are constructed from these laminates.

Material is a confusing word to describe a composite, so the two main ingredients of composites used in aerospace applications are discussed below.

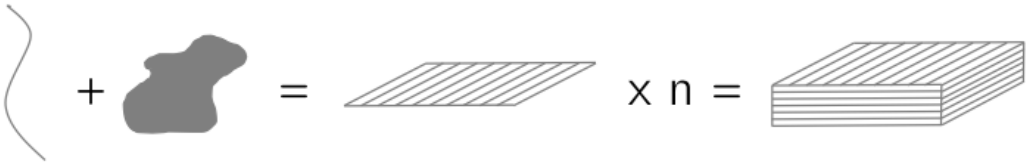

Figure 1.7: Fibres and resin are combined into layers, and a multiple of layers forms a laminate

### 1.3.1 Fibres

In a composite material, as used in aerospace engineering, the fibres are the main load carrying constituent. Their important characteristics are a high degree of anisotropy and poor compressive stiffness. Due to these characteristics their orientation, stacking and interweave determine the performance characteristics of the final material. Many types of fibres exist with a wide variety of stiffness and strength characteristics, however the three most widely used families of fibres in engineering are carbon, glass and aramid.

Some typical values for the three main fibre families are given in Table 1.1. In aerospace applications mainly carbon fibres are used because of their superior stiffness and strength properties. Glass fibres are mainly used in structures where costs are more important than weight such as in smaller wind turbines and construction. High strain-to-failure fibres like Aramid are a suitable choice for areas where protection is required as in armoured vehicles, bullet-proof vests and helmets.

Table 1.1: A comparison of typical values for carbon, glass and aramid fibres (www.carbon-fibre.com)

| | Tensile Strength [GPa] | Tensile Modulus [GPa] | Density [g/ccm] | Specific Strength [GPa] | Specific Modulus [GPa] |
|---|---|---|---|---|---|
| Carbon | 5.5 | 294 | 1.81 | 3.03 | 162 |
| Glass | 3.4 | 22 | 2.60 | 1.31 | 8 |
| Aramid | 3.6 | 60 | 1.44 | 2.50 | 42 |

### 1.3.2 Reinforcement Types

How the fibres are located in a matrix and how they interact plays an important role in the damage tolerance characteristics of a composite [Bibo and Hogg, 1996]. As out-of-plane loading and resulting delaminations are the most important source of failure, reinforcement in the thickness direction of the laminate is needed. An overview of current fibre architectures providing through-the-thickness reinforcement is given below. In general, improvements in out-of-plane properties come at the cost of a reduction in the in-plane properties of a composite.

#### Weaving

From the start, woven fabrics have been used in composite materials. Analogous to the textile industry, several weave styles exist with specific properties such as plain, satin and twill weaves.

Woven fabrics are convenient to handle in a manual production process but an important downside of weaving is that the fibre yarns undulate, which is also called crimp. Tighter weaves, such as the plain weave, have a high degree of weaving and are thus hard to drape around a mould and have relatively poor in-plane properties. A satin weave will have fewer undulations yielding better in-plane properties and drapeability, but it will be less damage tolerant.

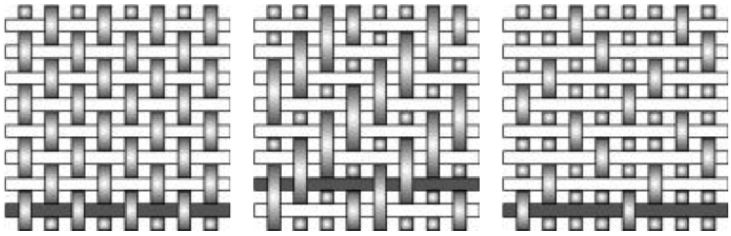

Figure 1.8: Plain, twill and satin weave from left to right (www.netcomposites.com)

### Multi-dimensional Fabrics

Three dimensional or 2.5D fabrics boast reinforcement yarns in the thickness direction [Khokar, 1996], as multiple warp yarns are used to create the three-dimensional structure. Its amount of interwoven layers, and thus thickness, can be varied depending on the application. This technology appears to be suited mainly for flat or simply shaped preforms with an orthogonal architecture [Tong, Mouritz, and Bannister, 2002]. Three dimensional fibre architectures possess higher residual strength after damage compared to their two-dimensional counterparts, despite having a lower undamaged compressive strength [Bibo and Hogg, 1996].

### Braids

In braids, two or three fibre directions can be interwoven, also in the thickness direction. Reinforcement characteristics, and thus mechanical properties, are very similar to weaving, with the main difference in the production process which will be discussed in the next section.

### Z-Pinning

Apart from stitching, small pins, made of carbon, titanium or steel, can be introduced into the composite preform [Mouritz, 2007]. Being discontinuous, they provide less reinforcement than stitching but are less invasive leading to less of a reduction of the in-plane mechanical properties of the composite. A z-pin content by volume of 2-4% will yield an improvement of impact damage resistance of 50% with a loss of in-plane modulus and strength of 5-10%. In compression after impact, z-pinning can reduce the damage size by 19-64% and the residual strength increase can be as high as 45% [Zhang, Hounslow, and Grassi, 2006]. However, the procedure to Z-pin a preform is laborious, time consuming and expensive, which tends to limit its application.

### Stitching

Stitching fabric plies, either as preforms or prepregs, introduces a needle and a thread into the preform, yielding both advantages and disadvantages [Dransfield, Baillie, and Mai, 1994]. In some cases the improvement in compression after impact strength is 75-95%, depending, amongst other things, on stitch density, thread material and thread diameter [Thuis et al., 1998], however, stitching introduces resin pockets and fibre failures that have a detrimental effect on the in-plane properties of the composite, mainly in compression.

### Knitting

Knitting is a process that closely resembles stitching, but intermeshes previous made loops with new loops by using a needle (Figure 1.9). It produces preforms with a wide variety of sizes and shapes with highly curved fibres. These high curvatures, combined with damage induced in the knitting process, lead to very flexible preforms, but decrease the in-plane mechanical properties significantly [Leong et al., 2000].

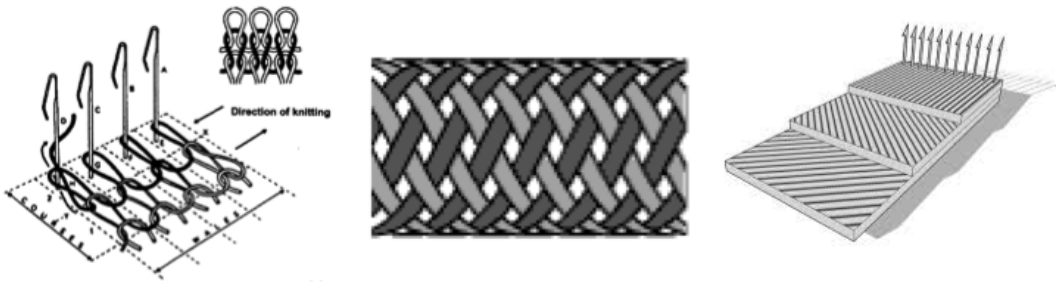


Figure 1.9: Knitting process (left, [Leong et al., 2000]), triaxial braid (middle, openprosthetics.org) and non-crimp fabric (right, www.noncrimpfabrics.com)

### Non-Crimp Fabrics

In non-crimp fabrics, to improve the in-plane properties of fabric, straight unidirectional fibres are stitched or knitted looseley together, generally in two directions, to create a fabric without undulations. High layup rates can be achieved and applications of this type of composite can be found in the fields of wind energy and automotive engineering. A disadvantage of this method is that the needles tend to damage the fibres and introduce resin pockets, which seriously reduces the fatigue life of structures produced this way.

## 1.3.3 Resins

In general, composite resin systems are divided into thermoset and thermoplastic resins. Where thermoset resins still have to perform a chemical reaction during cure, thermoplastic resins only have to be molten and cooled down. This difference on the molecular level plays an important role in the manufacturing process, as it determines amongst other things the temperature and length of the curing or consolidation cycle. Another difference is the generally higher toughness

of thermoplastic resin systems when compared to thermoset resin systems. When designing composite laminates for damage tolerance, it is mainly this toughness of a composite that is of interest.

### Thermoset Resin Systems

Thermosetting polymers, in aerospace application often epoxies, form crosslinked chemical bonds creating a stiff and strong three-dimensional molecular structure. However once cured, they cannot be melted back to the liquid form making them hard to recycle, and because of the chemical reaction taking place, thermoset resins have, once mixed, a limited processing window and shelf life. Their low viscosity makes them more suitable for resin infusion and low temperature processing. The strong bonds imply a more brittle behaviour when cured. This brittle behaviour also implies less favourable damage tolerance characteristics.

### Thermoplastic Resin Systems

Instead of chemical bonds, the molecules of thermoplastics form chains through intermolecular forces, meaning they can be remolded after heating. Because of their weaker bonds, thermoplastics are in general tougher than thermosetting polymers. Tougher resins are capable of absorbing more energy, resulting in higher compression after impact strengths [Cantwell and Morton, 1991].

Thermoplastics are, due to their reversible chemical reaction, very suitable to multi-step forming processes like press-forming, and they also have a virtually unlimited shelf life and do not need a time and energy consuming autoclave process.

### Resin Additives

Several techniques are developed to increase the Mode I and Mode II fracture toughness of composite laminates by adding materials to the resin. Nanotubes added to the resin can increase the CAI strength with about 12-15% [Kostopoulos et al., 2010] and (thermoplastic) interleaves and veils [Kim, 1998] can increase the CAI strength with about 50%, but will also decrease the in-plane properties. Disadvantages of these methods are the high costs and increases in manufacturing time.

### Overview

An attempt is made to show the trade-off between in-plane stiffness and out-of-plane, compression after impact, properties of the several discussed fibre reinforcement types and resins in a qualitative way in Figure 1.10. All reinforcement architectures are compared to woven fabric thermoset composite laminates, whose properties are taken as zero. The empty upper right quadrant is where the very difficult combination of excellent in-plane and out-of-plane properties has to be found.

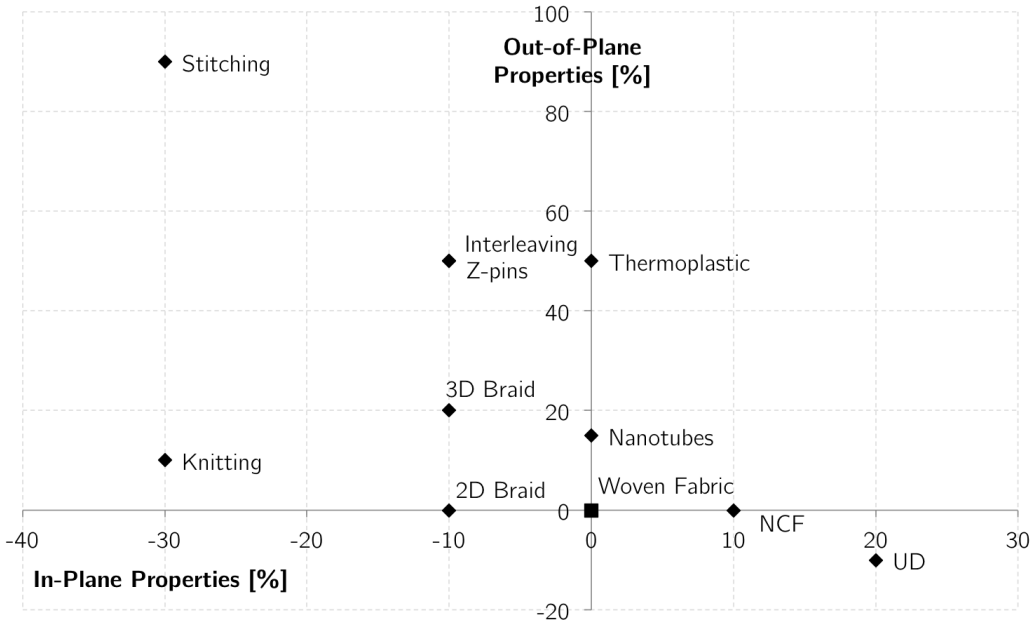


Figure 1.10: Qualitative comparison between in-plane (stiffness) and out-of-plane (CAI) mechanical properties of fibre reinforcement architectures

## 1.4 Manufacturing

Production techniques for composite structures differ mainly in the order the constituents are combined, in their forming process and how the products are cured, and often have a substantial influence on the damage tolerance behaviour. As automated processes are necessary for the cost-efficient production of composite structures, a short description of automated processes used to lay down fibres is given below, with the emphasis on automated fibre placement.

Figure 1.11: Automated production techniques from left to right: braiding (bfcarter.co.uk), filament winding (us.industrysourcing.com) and pick and place (Airborne Technology Centre)

### 1.4.1 Automated Fibre Layup Techniques

Here only braiding, filament winding and pick-and-place will be discussed as these are the main techniques used to automatically lay down fibres.

#### Braiding

Braiding is a very fast production process with high interlocking of the fibre yarns for products with closed, convex cross-sections and high length to width ratios, such as stringers or landing gears [Bannister, 2001]. Braiding angles can vary from 10°-85°, with the possibility of adding 0° yarns or manually adding other plies or patches of, for instance, woven fabrics. Part geometry has to be small in diameter, with preferably a fairly straight longest dimension. As the ratio between the diameter of the braiding machine and the diameter of the part can be as high as 50:1, the cross-sectional size of the braided part is very limited.

Three dimensional braiding techniques are under development, but commercial applications are still limited due to the high complexity of this technique, the costs of the machines and the small part diameters (<100mm) [Mouritz et al., 1999].

#### Filament Winding

One of the oldest automated production techniques, filament winding, has been used since the 1960's. Fibre yarns are literally wound around a mould, which has to be convex and closed. The placing of the yarns is based on friction resulting from applied tension to the filament being wound, so no 0° yarns are possible unless a secondary process is used to add these fibre tows. To make a completely filled layer, the geometry of the mould and the width of the yarn determine the winding angle. In terms of material, the winding can either be 'dry' or 'wet'. In wet winding, the yarns first go through a resin bath before continuing onto the mould. In filament winding, it is difficult if not impossible to cover the poles of the product, as this is where it is connected to the machine. Different winding patterns are depicted in Figure 1.12, where polar, helical and hoop winding is illustrated. These patterns can be varied and combined depending on the part geometry, application and material used [Rousseau, Perreux, and Verdière, 1999]. Disadvantages of this technology are that they have high void contents, they are restricted to surfaces of revolution and their resin content is difficult to control [Niu, 1992].

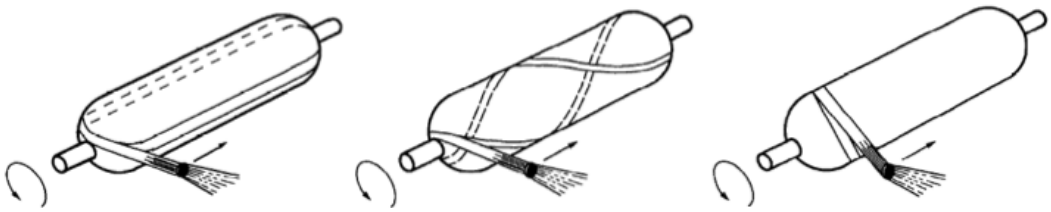

Figure 1.12: Winding Patterns from left to right: polar, helical and hoop winding [Shen, 1995]

**Pick-and-Place**

A recent advance in composite manufacturing automation is picking and placing preforms and/or plies using an industrial robot. Plies are cut from fabrics or prepregs on a cutting machine, and placed on a mould using a robot with a specific tool capable of handling the composite plies [Reinhart, Glück, and Ehinger, 2012]. Complex shapes are not possible, and vacuum bagging or resin infusion always has to be done manually. This is a fast and cheap way to automate the production process for fairly small and simple preforms.

### 1.4.2 Automated Tape and Fibre Placement

As the composites manufacturing process is laborious and time consuming, automation is key for large scale implementation. Large scale in terms of output, but also in the sheer size of the products produced. Large structures such as wings and fuselages need 'infinite' raw material dimensions, which cannot be provided by woven fabrics. Braiding machines would get too large and complex and thus cost inefficient, and filament winding cannot handle the complex shapes, particularly doubly curved concave parts, and variety of ply orientations needed. Automated tape laying machines and later the slightly more complex but more flexible fibre placement machines were developed to overcome these problems. Some of the current aircraft structures made using fibre placement are Boeing 787 fuselage barrels and Airbus A350 doors. Aircraft wings are, due to their 'flatter' shape, more suited for tape laying, for example the Airbus A400M and A350 wings are made in this way.

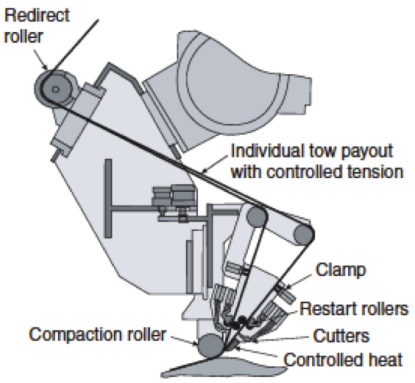


Figure 1.13: Schematic tape/fibre placement head IJsselmuiden (2011)

In fibre placement, the composite material is laid down on a tool by a robot or gantry fitted with a complex fibre placement head. Tows are fed from a storage that is either placed on the head or in a separate module of the fibre placement machine, depending on the machine manufacturer. The larger the head the more the flexibility and reach of the machine will be decreased. An overview of the Coriolis fibre placement facility at NLR is given in Figure 1.14, where there is a robot on a rails and the material is stored in the creel at the base of the robot.

Automated tape layers (ATL) place tapes of typically 30 cm wide, while fibre placement machines use a multiple of much smaller tows with a typical width of 6.35 mm (1/4 inch). This

makes more complex shapes possible and reduces material waste.

The fibre tapes placed with the fibre placement machine tend to buckle and wrinkle when placing paths with an in-plane curvature, negatively influencing the laminate quality and mechanical properties. When the mould has a concave curvature in the out-of-plane direction, the size and shape of the head of the machine could decrease the reach of the fibre placement machine.

Figure 1.14: Coriolis fibre placement facility at NLR

### Fibre placement specific material

Woven fabrics are mainly used in manual production processes, which in most cases also have to be impregnated with resin in a second step. Originally in fibre placement, thermoset prepregs were used, however with the advance in machine technology and materials nowadays thermoset prepregs, thermoplastic tape and dry fibre materials can be used.

### Thermoset Fibre Reinforced Tape

In fibre placement, the most widely used material is thermoset prepreg tape. One of its main advantages in the fibre placement process is that it sticks to most mould materials. The disadvantages that thermoset prepreg tape has are limited shelf life and a tackiness that causes contamination of the complex components of the fibre placement machine which results in downtime. The creel, tubes and head have to be cooled to prevent the material from getting stuck and because of the tackiness, both sides of the tape have to be covered in plastic backing tape to prevent the material from getting stuck to itself. This backing tape then has to be removed during the fibre placement process, meaning a complex fibre placement machine and an expensive production process for the tape.

### Thermoplastic Fibre Reinforced Tape

Thermoplastics are more challenging materials to handle during fibre placement than thermosets, as they have to be heated above their melting points to attach them to the previous layers in the structure and the mould. The main heating systems used are gas torches (ADC) and laser (Coriolis), but ultrasonic techniques are also used (Fokker) to melt (parts of) the fibre bands. Another practical issue that has to be solved is attachment of the tapes to the mould; after placing, the material cools down to its consolidated state where it is no longer tacky. Another issue with this in-between consolidation is that the layers of the composite become so well connected that they form asymmetric and unbalanced laminates during production, resulting in large warping deformations. One of the possible advantages of using thermoplastics is in-situ consolidation, meaning that the material is in its consolidated state directly after placing it on the mould, which means that an extra consolidation cycle is not needed [Naumann et al., 2012].

### Dry Fibre Tape

Dry fibre material for fibre placement is never really dry, as it would disintegrate when moving through the machine. Often, a binder material is added to the yarn (Toho Tenax) or a veil of a different material is added (Cytec) to prevent the yarn from disintegrating and to make a coherent preform. The resin is added in a subsequent infusion step. One of the main advantages of using dry fibre is the low cost of the material [Naumann et al., 2012].

### Process Parameters

During fibre placement, the following process parameters influence the smoothness of the process and the quality of the product:

- Compaction force
- Placement speed
- Heating of the tape

A specific set of parameters has to be determined for each material. Heating and compaction force influence the width of the placed tapes in the sense that higher values result in a wider tape width. Too low values for these parameters result in poor compaction and reduced preform stability. Excess heating can damage the material. Tapes placed too fast, especially during starting and stopping, can result in bad tack or inaccurate placement. When steering fibres, this is even more important. With thermoplastics, the placement speed can also determine the degree of curing, as the heating of the tape is a function of the energy put in and the amount of time the tape is exposed to that energy. When in-situ consolidation of the composite is desired, the placement speed of the machine has to be kept low.

## 1.5 Design

In laminate design one can alter the orientation and sequence of the plies used. A prerequisite for design is analysis of the mechanical properties and the producibility of the part. Until

recently, composite parts were mainly produced using hand lay-up which limits accuracy and repeatability. With advances in computing power it has become possible to do more detailed structural analyses at lower costs, with the result that more advanced optimisations are possible. Hence, there is no longer any excuse not to produce composite layups that deviate from the conventional fibre orientations of 0°, 45° and 90°.

### 1.5.1 Conventional Laminates

Looking at current laminate design practice, the damage tolerance considerations at the laminate level are [MIL-HDBK-17-3F, 2002]:

- ±45° layers on the outside; more flexible laminates can absorb more energy with less damage
- minimize orientation difference between adjacent plies; the mismatch in Poisson's ratio and bending stiffness increases interlaminar stresses
- woven fabrics as outer plies; woven fabrics have higher damage resistance
- load carrying plies on the inside of the stacking sequence; they are shielded by less important plies
- at least 10% of every ply orientation should be present in the laminate to provide enough strength in every direction [Hart-Smith, 1993]

As the first and the second considerations for a damage tolerant laminate are contradictory what is often seen in industry is that the +45° and -45° plies are separated by a 90° or a 0° ply.

All these considerations are currently taken into account in composite laminate design, together with improvements in the materials used to form the composite. Improvements are however approaching a limit, and revolutionary new ideas are needed to get a step-change improvement in damage tolerance characteristics of composite laminates.

### 1.5.2 Non-Conventional Laminates

New possibilities for design have arisen with the introduction of automated fibre placement machines. The new class of laminates that are made possible by fibre placement can be divided in two categories:

- Variable stiffness laminates (VSL), [Gürdal and Olmedo, 1993]
- Dispersed laminates, [Lopes et al., 2009]

#### Variable Stifness Laminates

In these laminates variable stiffness is achieved by steering fibres in-plane. Other possibilities to vary the stiffness include changing the thickness, stacking sequence or materials used in the laminate. When optimising the stiffness at every location, the critical buckling load can be increased [Setoodeh et al., 2009] or the vibration response of a laminate can be improved [Abdalla, Setoodeh, and Gürdal, 2007], [Akhavan and Ribeiro, 2011]. An elegant method for

optimising the stiffness of variable stiffness composite laminates by the use of lamination parameters is presented by Setoodeh, Abdalla, and Gürdal (2006). After this stiffness optimisation, the next step is to convert the optimised lamination parameters to actual fibre angles [Campen, Kassapoglou, and Gürdal, 2012]. Not only flat plates, but also cylinders subjected to a bending load [Blom, Stickler, and Gürdal, 2010] and the natural frequency of conical shells [Blom et al., 2008] could be improved by using variable stiffness. Apart from a high buckling load and natural frequency, improving the strength of a laminate can also be an objective of variable stiffness design [Khani et al., 2011]. An overview of the multi-step optimisation approach for variable stiffness laminates can be seen in Figure 1.15. No damage tolerance considerations in designing variable stiffness laminates have been found so far.

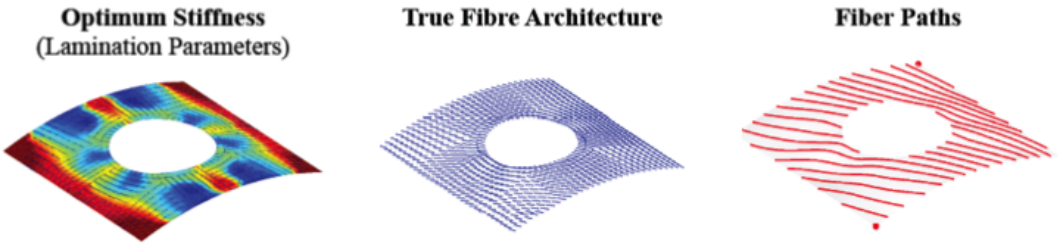


Figure 1.15: Multi-step optimisation approach for variable stiffness laminates [IJsselmuiden, 2011]

### Dispersed Laminates

A laminate with similar if not identical stiffness properties but different stacking sequences can be found with a similar optimization procedure as in variable stiffness laminates, bound by considerations such as a maximum difference in ply orientation between plies. For instance, the conventional stacking sequence:

Baseline : $[\pm 45/90/0/45/0_4/\text{-}45/0_2]_S$

has at least the following two alternatives with similar in-plane and out-of-plane stiffnesses [Lopes et al., 2009]:

Alternative 1 : $[\pm 45/0/70/\text{-}70/0/15/10/\text{-}10/\text{-}15/15/\text{-}15]_S$
Alternative 2 : $[\pm 45/80/5/20/\text{-}20/10/\text{-}80/\text{-}10/\text{-}5/15/\text{-}15]_S$

Although experimental results of compression after impact tests do not show a clear improvement in residual strength yet, there are indications that the strategy might work if constraints on the fibre angle difference between neighbouring plies and on the through-the-thickness location of delaminations are imposed.

In subsequent work [Sebaey, 2012], an ant colony optimisation algorithm was used to optimize a baseline stacking sequence $[45/0/\text{-}45/90]_{3S}$ for damage tolerance, using analytical formulations for the prediction of damage area and the delamination threshold load. Two alternative stacking sequences with similar in-plane and out-of-plane stiffnesses were tested, with

a maximum mismatch angle between 10° and 30°:

$[10/35/65/85/65/35/5/-25/-35/-45/-55/-80]_S$

And with a maximum mismatch angle between 5° and 80°:

$[-65/15/90/30/-45/30/-25/55/-10/70/-10/-80]_S$

It was found that dispersed laminates with a maximum mismatch angle of 10° showed smaller permanent indentation, less damage absorbed by a smaller number of delaminations and a higher residual compressive strength. The reason given for the improvement in residual compressive strength was the formation of thicker sublaminates with a higher buckling load.

## 1.6 Damage Tolerance Issues in Composites

Due to their brittle nature, composites exhibit different challenges when dealing with damage than the inherently tougher metals like aluminium do. When damage in a composite starts growing, it tends to grow rapidly, making it more challenging to apply the damage tolerance philosophy to composites.

To illustrate, the difference in stress and strain levels in the most critical failure modes [Campbell, 2010] for both a representative aluminium (Al7075-T6) and a quasi-isotropic CFRP (Hexply AS4/8552) are shown in Figure 1.16. In aluminium, the most critical failure mode is considered to be the fatigue limit with a stress intensity factor of 3 at one million cycles, which is taken from MIL-HDBK-5J (2003). For composites the compression after impact strength at barely visible impact damage is taken as the most critical failure load, and compared to the pristine compressive strength from test results generated in this research.

Immediately clear is that on the one hand the advantage of composites is lost when damage without fatigue considerations is included in the comparison, which is a prerequisite in aircraft design. On the other hand, more room for improvement is at disposal of the designer to approach the pristine strength more closely, and together with the relatively flat S-N curves of composites they can contribute to even more efficient aircraft structures. But, to make use of the full potential of composites, the damaged strength has to be improved.

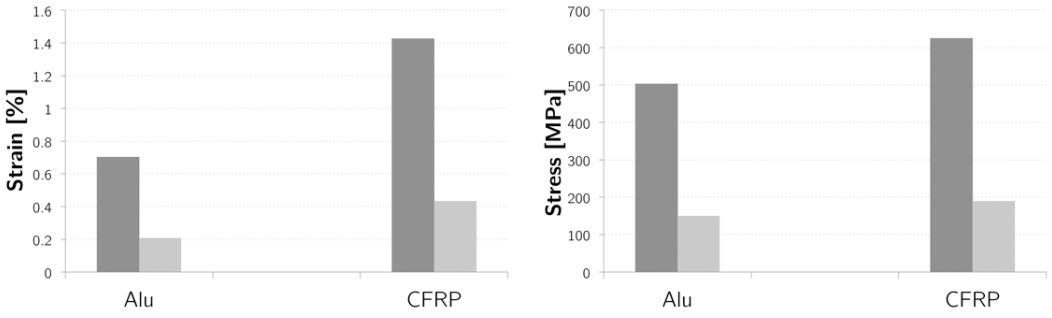


Figure 1.16: Comparison of pristine (dark grey) and damaged (light grey) properties. Critical failure mode taken for aluminium is fatigue and for CFRP compression after impact.

Next to the structural strength behaviour, also the detectability of damage plays an important role when attempting to design more damage tolerant structures, and it is this combination of strength and detectability that determines the damage tolerance of a structure. The next sections discuss the causes for the poor damage behaviour and the implications on detectability.

### Damage

Damage in composites can result from manufacturing defects, environmental effects such as moisture and radiation, or from mechanical damage during operation [Baker, Jones, and Callinan, 1985]. Both the fibres and the matrix of a composite can fail, as can the interface between them, making it very hard to predict damage initiation and propagation in composites. Assuming no manufacturing defects, and that environmental effects are a different field of study, the focus of the research discussed here was on mechanical damage during operation. In practice, this type of mechanical damage has a number of causes, most of which are due to foreign object impact, for example tooldrop, runway debris, hail, birdstrike and baggage lorries.

### Impact in composites

The most critical form of damage in composites is a low-velocity foreign object impact. In contrast to metals, in composites this type of damage is hard to detect *and* it causes a significant reduction in the strength of a composite: a dangerous combination from the damage tolerance point of view. To illustrate this, the front and backside of an impacted composite laminate and an ultrasonic C-scan of the internal damage is shown in Figure 1.17.

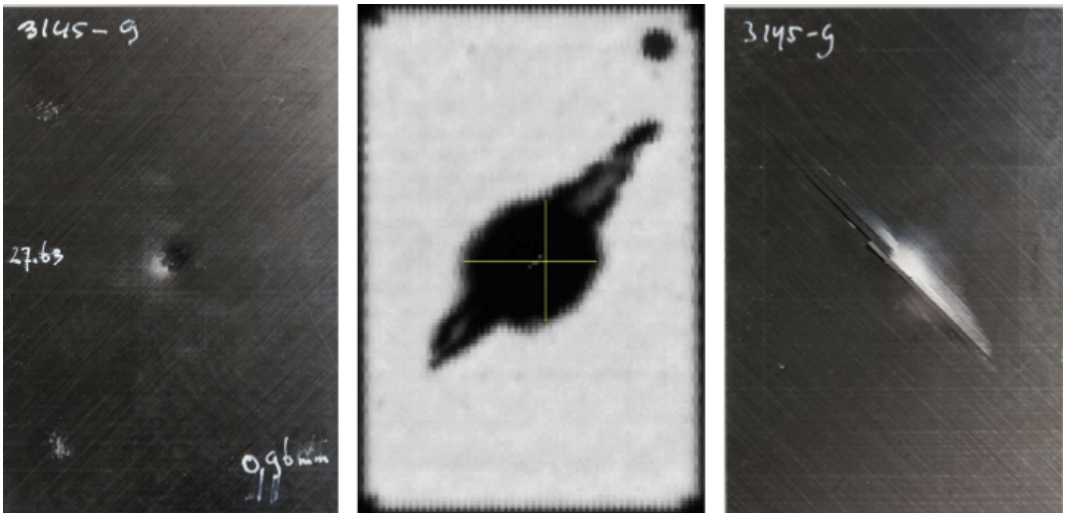


Figure 1.17: Frontside, C-scan and backside of a specimen impacted at BVID energy level

Upon impact, as depicted in Figure 1.18, fibre breakage (C), matrix cracks (A) and delaminations (B) are present and will interact. Delaminations can start from matrix cracks or can result from high interlaminar shear stresses, both are a result of bending deformations which are highest in the bottom half of the laminate. At the point of impact, the high contact stresses will crush fibres and create matrix cracks [Abrate, 1991].


Figure 1.18: Section cut of an impacted specimen

### Loading after impact

Depending on the loading, different damage forms will be the most critical at the damage site. In tension, fibre breakage will be more critical as fibres are the main load carrying constituent. In compression, the sublaminates formed by the delaminations will become unstable and start to buckle, growing the damage, which can also be the case in shear loading. The relative difference between virgin and damaged strength of the laminate is greatest for compression, making delaminations after impact loaded in compression the most critical failure mode in a composite and the main indicator for damage tolerance of a composite laminate.

### Composite Characteristics Influencing Damage Tolerance

When seeking to improve damage tolerance in composites at the laminate level, the following characteristics of a composite laminate influence its ability to tolerate damage:

- Laminate thickness
- Ply thickness
- Stacking sequence (subsequent ply angles)
- Fibre architecture
- Matrix toughness

Thickness and stacking sequence influence the out-of-plane stiffness (primarily bending) of a laminate. In stiffer laminates, damage may be confined to the contact area, where delaminations also start from lower level damage such as matrix cracks[Abrate, 1991]. Flexible laminates tend to bend more, resulting in tensile stresses in the lower side of the laminate cracking the matrix and shearing the interface between plies, which also results in delaminations. This difference between rigid and flexible targets is shown in Figure 1.19.

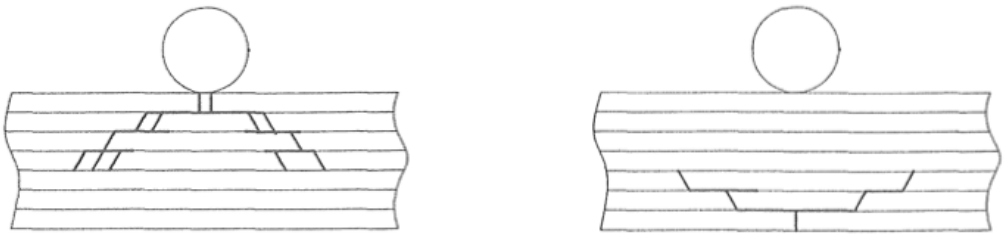

Figure 1.19: Difference in impact damage creation between rigid (left) and flexible (right) targets [Abrate, 1991]

Another aspect in the stacking sequence of a composite laminate is the orientation of directly adjacent plies. Large differences in ply orientation cause high interlaminar stresses, promoting delaminations [Sebaey et al., 2013]. A thicker ply, or several plies with the same orientation stacked, will not delaminate but matrix cracks will propagate more easily. Due to energy redistribution, the delaminations that are formed will be larger in size. Thinner plies will form more unstable sublaminates [Dost et al., 1991]. The fibre reinforcement architecture will influence the damage tolerance behaviour in the way described previously in this chapter; the more reinforcement in the thickness direction, the higher the damage tolerance of the composite laminate. This higher damage tolerance comes at the cost of lower in-plane properties, which is a trade-off for the designer to make. As all these characteristics can be varied by the designer, the implication is that the damage behaviour of a composite laminate can be tuned to the needs of the application.

## 1.7 Conclusion

In conclusion to this review of composites and damage tolerance, a few important observations, assumptions and decisions for the continuation of this thesis are made below:

- Compression after impact is the most critical damage state and loading for composite damage tolerance, and will be only considered in this research
- Improvements in CAI behaviour will be sought in laminate stacking sequence optimisation, made possible by fibre placement
- In compression, delamination is the most critical failure mode for structural integrity and damage tolerance
- In the typical impact damage sensitive laminates, the main delamination driver is bending of the laminate during impact
- Fewer, thick sublaminates formed by delaminations increase the residual compressive strength of impacted composite laminates
- Through-the-thickness reinforcements can significantly increase the ability of a composite laminate to withstand delaminations resulting from impact
- Only damage initiation during impact is considered; it is assumed that when less damage is present, also less damage will propagate

**Research Question**

Currently fibre placement is one of the most efficient manufacturing methods for large composite structures. An often mentioned drawback is the perceived limitation of unidirectional layers. Through-the-thickness reinforcements are one of the best options to increase the damage tolerance of composite structures, as is demonstrated by for instance braids and fabrics. Their drawback however is the limitation in size and the inefficient manufacturing process.

The research question was formulated as follows:

*Is it possible to improve the damage tolerance of composite laminates using the flexibility*

*fibre placement technology provides in terms of laminate design?*

In this thesis a new fibre placement architecture called AP-PLY will be presented that combines the manufacturing advantages of fibre placement with the favourable damage tolerance characteristics of laminates with through-the-thickness reinforcements.

Instead of placing fibre bands directly adjacent to each other, room is left in between for exactly one or a multiple of tows. In a second direction, the exact same pattern is laid down with the gaps between the fibre tows. After this step the gaps in the first direction are filled up by shifting the pattern sideways. When this is also done in the second direction a two-directional interwoven laminate with constant thickness is achieved. As this configuration has fibres crossing the resin layer in the thickness direction, it is believed to have improved damage tolerance characteristics.

In chapter 2 the AP-PLY pattern is explained in more detail and in chapter 3 the behaviour under impact will be investigated experimentally. Chapter 4 discusses tests performed to understand the behaviour of AP-PLY laminates better and its influence on other mechanical properties. As various variations on the AP-PLY pattern are possible, the influence of the several parameters defining the pattern will be investigated in chapter 5. In chapter 6 an attempt is made to predict the delamination behaviour of composite laminates with the intention to find the best through-the-thickness distribution of the AP-PLY pattern, which is tested in chapter 7.

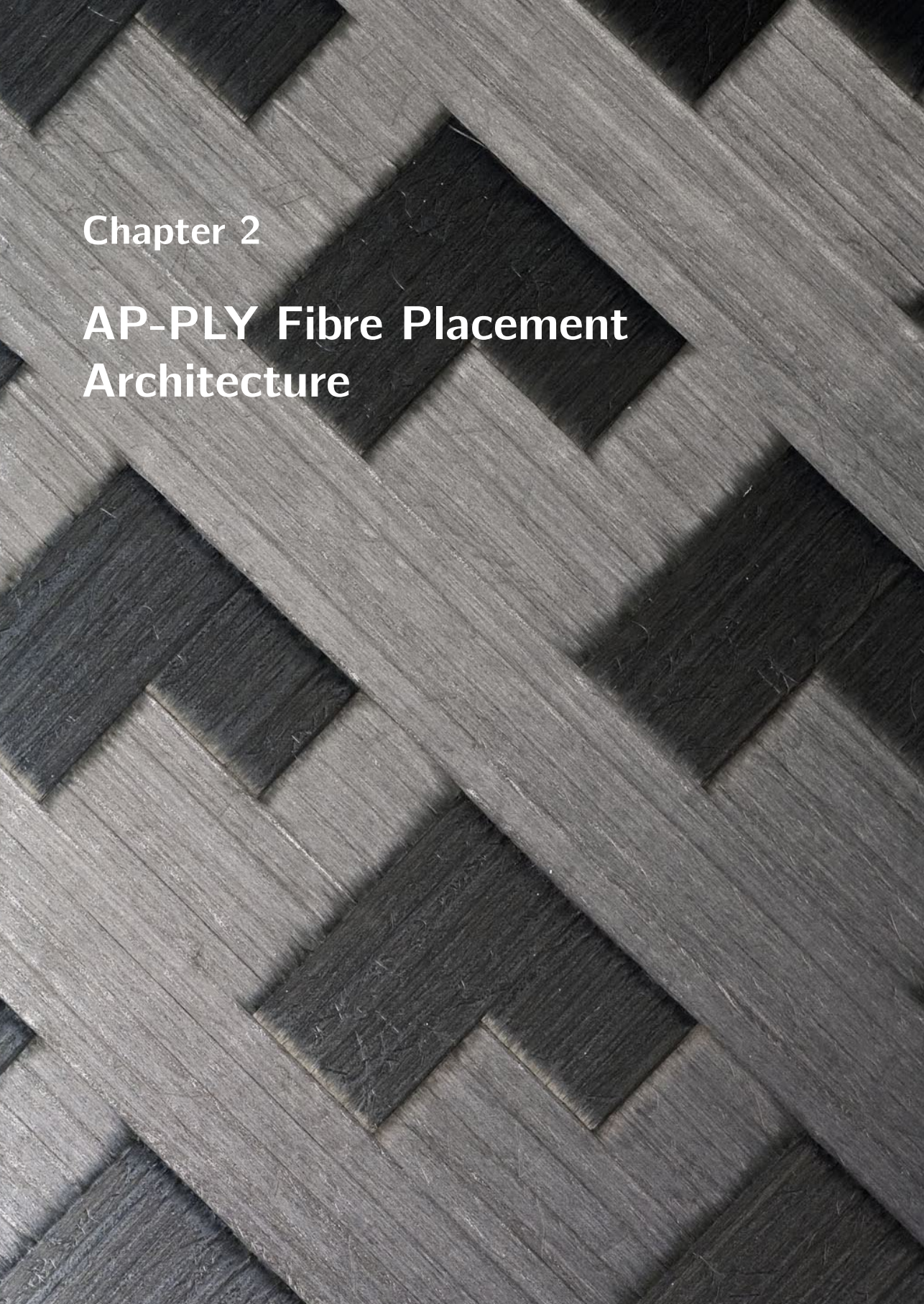

# Chapter 2

# AP-PLY Fibre Placement Architecture

## 2.1 Introduction

From the first chapter, it can be concluded that an automated production process and 3D fibre reinforcements are important characteristics for a composite, but fairly difficult to combine in a cost effective manner. Automated production processes are needed for cost-efficient manufacturing of large structures and 3D fibre reinforcements improve the damage tolerance characteristics. This damage tolerance, the combination of residual strength after damage and detectability, is one of the main limiting factors in the large scale use of composite materials in the aerospace industry.

Fibre placement is identified as one of the most promising automated manufacturing methods, but currently in fibre placement only laminates with unidirectional layers are used. This chapter presents a fibre architecture called AP-PLY (Advanced Placed Ply) that combines through-the-thickness reinforcements with an automated fibre placement process.

## 2.2 Concept

Traditionally, fibre placed laminates consist of unidirectional layers, each constructed by aligning all the passes of the machine head to be parallel to one another, and ensuring that each pass is adjacent to the previous pass without leaving any gap between them. The laminates constructed this way will have perfect coverage of continuous fibres over the part surface, but they will be susceptible for the delamination failures that would result from impact damages due to weak bond between the successive layers. In this thesis a new concept of producing laminates using automated fibre placement is introduced to improve the through-the-thickness strength of a laminate by introducing some level of connectivity between the successive layers of a laminate. The concept is somewhat similar to "weaving" of the successive passes of a fibre placement machine head pass, even though true weaving is not possible. In this new concept, instead of placing multiple fibre bands directly next to each other, bands are placed in two directions leaving space in between adjacent bands. These spaces are filled up with alternating bands in both directions, such that on every location two bands are positioned on top of each other. Basically two plies are interwoven, where the number of bands to skip and the angle between them can be infinitely varied, resulting in an endless number of possible patterns. The resulting configurations are referred to as advanved placed ply, or "AP-PLY" configurations. These AP-PLY fiber architectures very much resemble a filament winding pattern, but have never been used in fibre placement to the authors knowledge. Differences with respect to filament winding are in addition to the higher laminate quality and thus mechanical performance and more flexibility in geometry, the fact that also the fibre angles are not limited and, independent of geometry, any pattern can be created. In a sense, these are also variable stiffness laminates; the stacking sequence changes locally resulting in a slightly different bending stiffness in a repetitive pattern.

#### Series Pattern

For example, the pattern in Figure 2.1 is created by placing a group of fibre bands in one direction, leaving a gap of exactly one bandwidth in between. A second group of fibre bands is placed in a second direction, creating the pattern shown in the second picture of Figure 2.1.

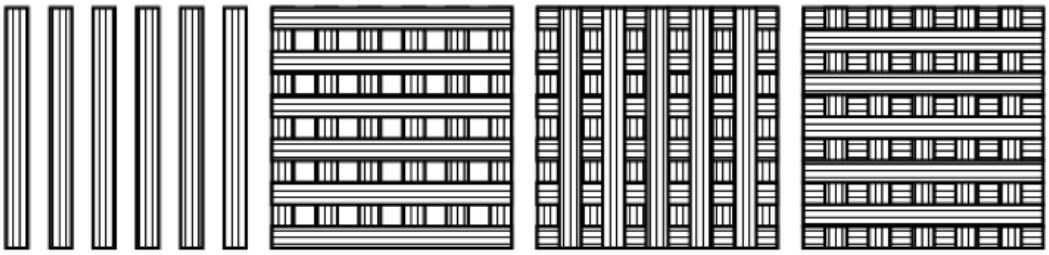

Figure 2.1: Buildup of the most straightforward AP-PLY Pattern

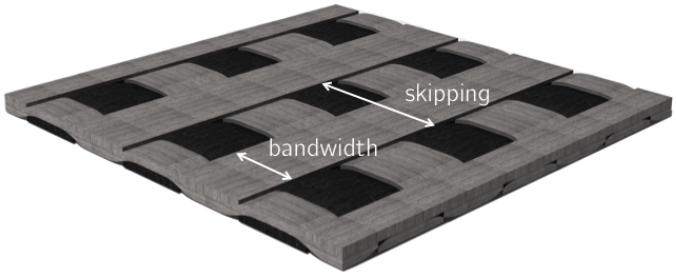


Figure 2.2: 3D CAD drawing of the most straightforward AP-PLY Pattern

Next the empty spaces shown in the first picture are filled up by a second group of fibre bands in the first direction shifted over one bandwidth. Finally in the last passing of the machine head the second direction is filled up creating a two-ply laminate with a uniform thickness.

### Alternating Pattern

Instead of placing a series of fibre bands in one direction first, the orientation of the courses can be changed every fibre band, which is similar to the helical filament winding pattern. However, this will result in more 'airtime' of the fibre placement machine, reducing its efficiency. Tests will have to be performed to judge whether this can be compensated by better mechanical performance of the laminate.

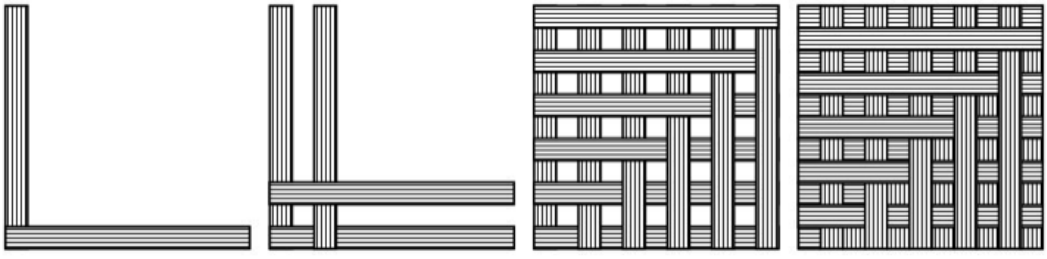

Figure 2.3: Buildup of the alternating AP-PLY Pattern

### Multiple Directions

In previous examples, only tow fibre orientations were interwoven. After the second step in the series pattern, a third, fourth and even more directions can be added before the first passings are filled up. This will result in a higher degree of interweaving, but will also increase the undulations and overall irregularities in the laminate.

### Totally Interwoven

In all previous patterns, between the two or more interwoven layers, still straight resin interfaces exist without fibres in the thickness direction that may thus easily delaminate. After some experimentation, a pattern was found that would interweave the last layer of that previously mentioned package of interwoven layers with the first layer of a next package of interwoven layers. A patent was filed for this configuration [Nagelsmit et al., 2010]. As can be seen in Figure 2.4, after step 3 of the original series pattern, a third orientation is added. After this first series of fibre bands in the third orientation, the last series of the first package is placed. From this point on, the second two orientations will be continued like the original pattern, creating a laminate with four orientations, where two packages of two orientations are interwoven. This pattern can be repeated indefinitely, until an entire laminate is created without open resin interfaces between layers. At the symmetry plane however, a problem arises as in a laminate with an even number of layers two layers with the same orientation are adjacent to eachother and cannot be interwoven. A solution for this could be to slightly rotate these layers both in a different direction, for instance +5° and -5°, creating a slight deviation from the intended fibre angle but still a completely interwoven laminate.

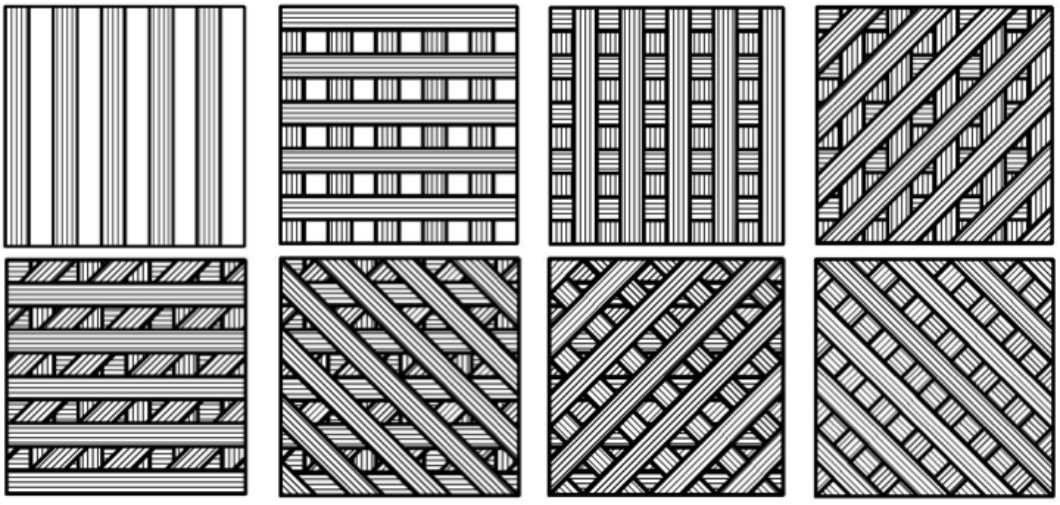

Figure 2.4: Buildup of the fully interwoven AP-PLY Pattern

Also instead of the above shown 90° angle between the two plies, any angle is possible. Depending on the application and preferred layup, the angle can be varied. Any layup can be created with this approach, and the location of the interwoven layers can be chosen at will, even combining unidirectional plies and AP-plies. Finally the width of the bands used determines the

resolution of the pattern, which influences the homogeneity of the laminate, performance and production time. As this fibre architecture does not involve curved fibre paths it does not have to deal with the gap and overlap issues often encountered in new fibre placement concepts with steered fibers.

## 2.3 Pattern Details

In constructing AP-PLY patterns, the following parameters determine the degree of interweaving and thus mechanical performance, but also manufacturability:

- Bandwidth ($w$)
- 'Skip Factor' ($n$)
- Angle ($\theta$)
- Number of layers to interweave
- Complete interweave

In Chapter 4 a design of experiments test campaign is carried out to determine the individual influence of each parameter on the damage tolerance performance of the laminate. The AP-PLY pattern parameters are graphically depicted in Table 2.1

### 2.3.1 Notation

Throughout this thesis, the following notation will be used for the AP-PLY configurations with the series patterns which are most used:

$[(\theta_1/\theta_2)_{n\times w}/(\theta_3/\theta_4)_{n\times w}]_{3S}$

Where the round brackets denote the layers that are interwoven, $n$ denotes the amount of fiber bands that are skipped and $w$ is the bandwidth. In the previous case, the $\theta_1$ and $\theta_2$ layers are interwoven.

The totally interwoven pattern will be denoted by:

$[(\theta_1/\theta_2/\theta_3/\theta_4)^{total}_{n\times w}]_{3S}$

The alternating pattern will be denoted as:

$[(\theta_1/\theta_2)^{alt}_{n\times w}/(\theta_3/\theta_4)^{alt}_{n\times w}]_{3S}$

#### Naming Convention

For a clearer understanding in writing, in Table 2.2 the naming convention used in this thesis is explained for reference purposes.

Table 2.1: Pattern Parameters

| | | | | |
|---|---|---|---|---|
| Skipping | 1 | 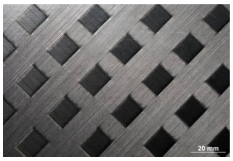 | 2 |  |
| Layup Angle | 45° |  | 90° | 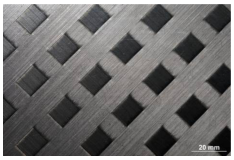 |
| Pattern | Alternating | 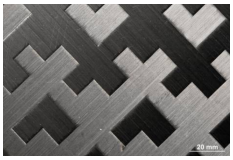 | Series |  |
| Bandwidth | 1/2" |  | 1/4" | 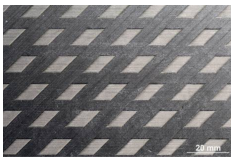 |
| Interwoven Layers | 2 |  | 4 | 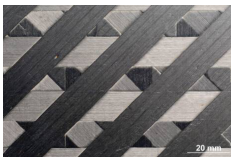 |
| Completely Interwoven | Yes | 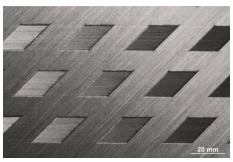 | No | 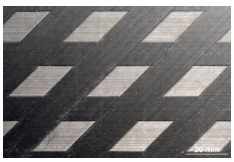 |

### 2.3.2 Degree of Interweave

To be able to compare the different patterns in their through-the-thickness reinforcement characteristics, the degree of interweaving, as described by [Rousseau, Perreux, and Verdière, 1999] is used:

$$D_W = \frac{\text{Undulating Area}}{\text{Unit Cell Area}} \tag{2.1}$$

For calculating this factor and to compare different patterns, the area of one undulation, the repetitive unit cell and the amount of undulations, meaning the crossings of fibers between layers, in that unit cell need to be determined.

Table 2.2: AP-PLY Naming Convention

| | |
|---|---|
| **Thermoset (TS)** | |
| $[45/\text{-}45/90/0]_{3S}$, Baseline | TS UD 90° |
| $[45/90/\text{-}45/0]_{3S}$, Baseline | TS UD 45° |
| $[(45/\text{-}45)_{2\times1/2}/(90/0)_{2\times1/2}]_{3S}$ | TS AP-PLY 2 90° 1/2 |
| $[(45/90)_{2\times1/2}/(\text{-}45/0)_{2\times1/2}]_{3S}$ | TS AP-PLY 2 45° 1/2 |
| $[(45/\text{-}45)_{1\times1/2}/(90/0)_{1\times1/2}]_{3S}$ | TS AP-PLY 1 90° 1/2 |
| $[(45/90)_{1\times1/2}/(\text{-}45/0)_{1\times1/2}]_{3S}$ | TS AP-PLY 1 45° 1/2 |
| $[(45/\text{-}45)^{alt}_{2\times1/2}/(90/0)^{alt}_{2\times1/2}]_{3S}$ | Alternating TS AP-PLY 2 90° 1/2 |
| $[(45/90/\text{-}45/0)_{1\times1/2}]_{3S}$ | TS AP-PLY 1 45° 1/2 Four |
| $[(45/90)_{1\times1/4}/(\text{-}45/0)_{1\times1/4}]_{3S}$ | TS AP-PLY 1 45° 1/4 |
| $[(45/90)^{total}_{1\times1/2}/(\text{-}45/0)^{total}_{1\times1/2}]_{3S}$ | Total TS AP-PLY 1 45° 1/2 |
| **Thermoplastic (TP)** | |
| $[45/90/\text{-}45/0]_{3S}$, Baseline | TP UD 45° |
| $[(45/90)_{1\times1/2}/(\text{-}45/0)_{1\times1/2}]_{4S}$ | TP AP-PLY 1 45° 1/2 |

### Undulations

A close-up of a single undulation in a manufactured AP-PLY laminate is shown in Figure 2.5. The geometry of a single 0°/90° undulation is derived by measuring the dimensions in the micrograph. In this case, the thermoset prepreg AS4/8552 is used, of which mainly the ply thickness of 0.18 mm and the tape width of 6.35 mm is of interest for the undulation.

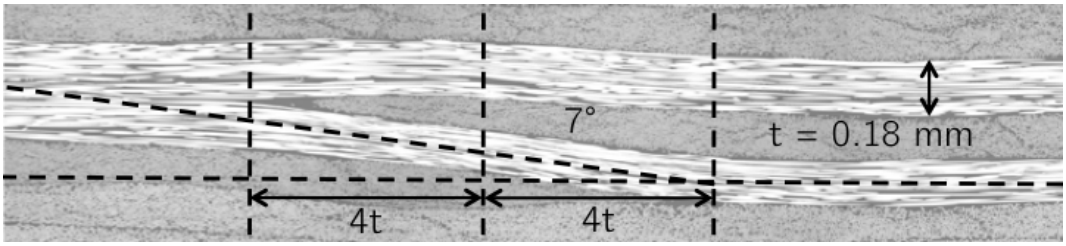


Figure 2.5: Close-up of a single undulation in AS4/8552 0/90 AP-PLY

Interesting to see is that the edge of the tape is smeared out by the undulation, smoothening the angle of the undulating tow. As these tows are slit from a wider sheet of UD material, their edges are originally straight. The middle dashed red line shows the edge where the edges of the two tows should be located. The undulating area is calculated by assuming that the undulating fibre tows are going straight up in the thickness direction, making the undulating area of one tow $bandwidth \times thickness$. Based on this approach, a larger ply thickness will thus result in a higher degree of interweave.

### Unit Cell

From every pattern, a repetitive and representative unit cell can be extracted which repeats itself and can be used in calculations. For the two distinct patterns interweaving two plies, these unit cells can be found in Figure 2.6 where the undulating tow edges are represented by a thicker line. The angle between the interwoven plies does not change this unit cell significantly except for the visual appearance.

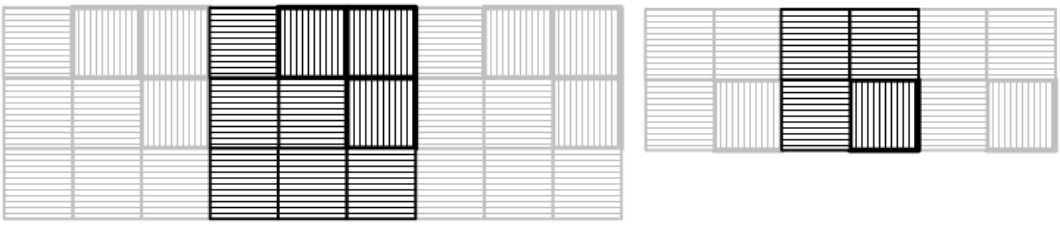

Figure 2.6: Unit Cell for Skip 2 (left) and Skip 1 (right)

### Pattern Comparison

Based on the degree of interweave of 2 plies, the different AP-PLY patterns are compared in Table 2.3. From Table 2.3 it is immediately clear that skipping more than one fibre band

Table 2.3: Degree of Interweave Comparison

| Pattern | DoW [%] |
|---|---|
| UD | 0 |
| $(0/90)_{1\times1/4}$ | 2.83 |
| $(0/90)_{2\times1/4}$ | 2.52 |
| $(0/45)_{1\times1/4}$ | 2.83 |
| $(0/45)_{2\times1/4}$ | 2.52 |
| $(0/90)_{1\times1/2}$ | 1.42 |
| $(0/90)_{2\times1/2}$ | 1.26 |

does not result in a significantly higher degree of interweave. Also, the angle between the interwoven plies does not influence the percentage of fibres in the thickness direction. What does increase the degree of interweave is the bandwidth of the tows used; the 'resolution' of the pattern. A smaller bandwidth and thus a higher resolution of the pattern should result in better out-of-plane properties.

## 2.4 Mechanical Properties

For this thesis, the main area of interest is the damage tolerance, and thus impact behaviour of AP-PLY laminates. As was seen in Chapter 1 however, the in-plane behaviour usually suffers from an improvement in out-of-plane behaviour. For this reason, the in-plane mechanical behaviour of AP-PLY laminates was looked at comprehensively.

### 2.4.1 Laminate Quality

In Figure 2.7 three different cross-sections of comparable composite laminates with different fibre architectures are shown and the difference between laminates with unidirectional layers, 5 harness satin woven fabric layers and AP-PLY can be appreciated. A clear conclusion could be that woven fabric laminates have large and more numerous undulations and resin rich areas. The compaction force of the fibre placement machine is largely responsible for the improvement in quality of the undulations in AP-PLY, together with the more stable fibre architecture created with the prepreg tows. Figures 2.8 and 2.9 zoom in on the difference in cross-section of the

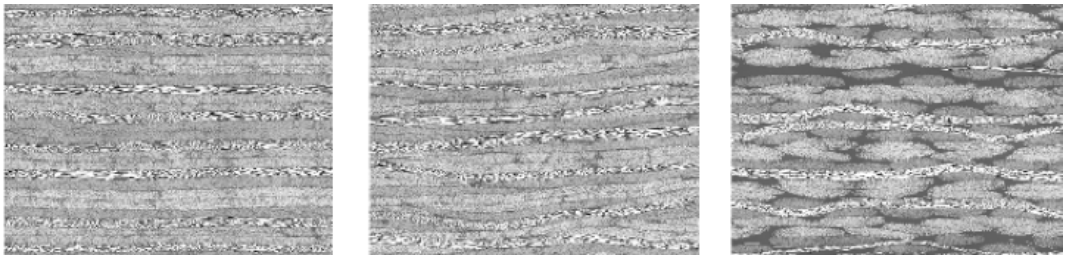

Figure 2.7: Unidirectional, AP-PLY and woven fabric laminate cross-section from the same AS4/PEEK material

baseline and AP-PLY laminates. The thermoplastic tape is thinner than the thermoset prepreg tape; 0.125 mm cured ply thickness for the thermoplastic versus 0.18 mm for the thermoset. To meet the test standard thickness of 4 mm, for the thermoplastic specimens 32 plies were used whereas the thermoset specimens only needed 24 plies. The consequence of this thickness difference is that the undulations in the thermoplastic AP-PLY laminate are even smaller than the thermoset, namely 5° versus 7°. In theory, this should result in a higher in-plane stiffness for the thermoplastic AP-PLY laminates.

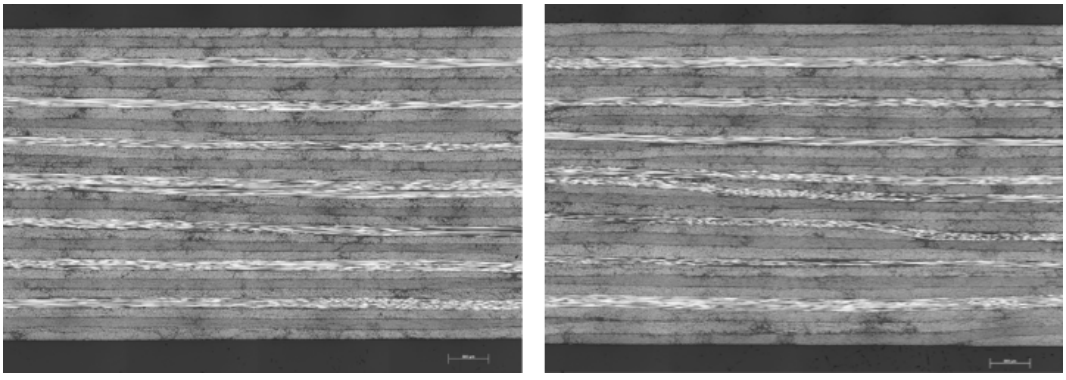

Figure 2.8: Microscopical image of a unidirectional (left) and AP-PLY (right) laminate cross-section from thermoplastic AS4/PEEK

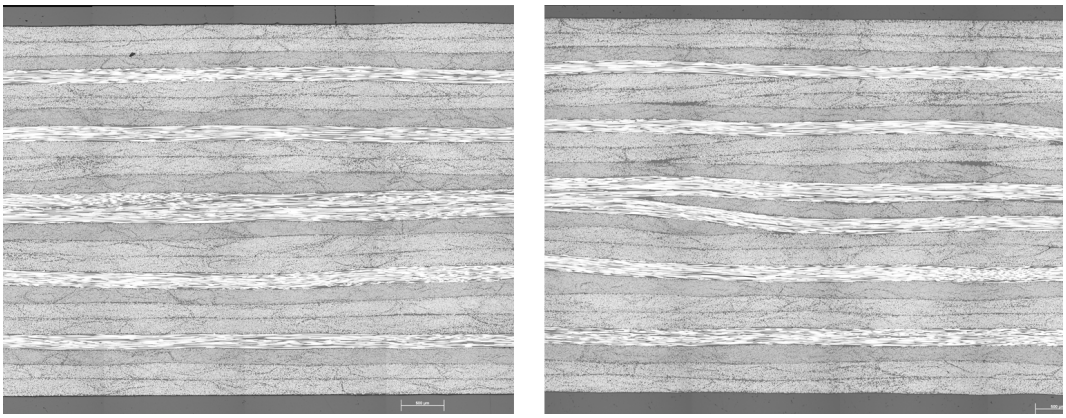

Figure 2.9: Microscopical image of a unidirectional (left) and AP-PLY (right) laminate cross-section from thermoset AS4/8552

### 2.4.2 Thickness

As the AP-PLY architecture introduces undulations, it is expected that the thickness will be influenced. Also in unidirectional layers the tows will always have small gaps and overlaps between them because of variations in the tow width, which can only be cut by the manufacturer to a certain tolerance. In general, gaps are considered favourable over overlaps, as overlaps will build up when subsequent layers are placed on top of them. Before testing, the thickness of every specimen is measured on four locations and the average is taken. For these series of 12 specimens, the mean thicknesses and the standard deviations are shown in Table 2.4. For thermoset, only negligible deviations from the thickness of the baseline are measured, with all values for AP-PLY smaller than the baseline unidirectional laminate. An explanation for the smaller thickness could be that the effective compaction pressure is higher because in AP-PLY the fibre placement machine uses 4 tows instead of 8. For the thermoplastic specimens only one AP-PLY configuration was tested, which was slightly thicker than the baseline. This could have to do with the fact that the thermoplastic tape width is changing with heating and compaction force, which are hard to control, especially between the first ply on the mould and subsequent plies that are placed on the material itself.

### 2.4.3 Stiffness

By adding undulations, it is expected that the in-plane stiffness of AP-PLY laminates will be different from laminates with unidirectional layers. To measure this property, before impact one virgin CAI specimen is tested in compression in the elastic regime, to avoid the creation of damage. As these specimens are not designed for undamaged compression testing, the absolute values are less illustrative than the relative comparison. Table 2.4 shows that in all thermoset cases the AP-PLY laminates are actually slightly stiffer. Only one thermoset baseline laminate was tested, meaning that the baseline could also be on the lower side of the scatter region, explaining the perceived higher stiffness of AP-PLY laminates. In the thermoplastic material the AP-PLY specimen was slightly less stiff, but in this case only one pattern was tested. The overall conclusion is that from the current tests AP-PLY does not show a stiffness difference

Table 2.4: Thickness and stiffness measurements of AP-PLY laminates

| | **Mean Thickness** [$mm$] | **St. Dev.** [%] | **Normalised Stiffness** |
|---|---|---|---|
| **TS** | | | |
| $[45/\text{-}45/90/0]_{3S}$, Baseline | 4.46 | 0.70 | 100.0 |
| $[(45/\text{-}45)_{2\times1/2}/(90/0)_{2\times1/2}]_{3S}$ | 4.35 | 0.84 | 101.0 |
| $[(45/\text{-}45)_{1\times1/2}/(90/0)_{1\times1/2}]_{3S}$ | 4.45 | 0.73 | 100.5 |
| $[(45/\text{-}45)^{alt}_{2\times1/2}/(90/0)^{alt}_{2\times1/2}]_{3S}$ | 4.29 | 0.59 | 101.7 |
| $[45/90/\text{-}45/0]_{3S}$, Baseline | 4.38 | 0.43 | 100.2 |
| $[(45/90)_{2\times1/2}/(\text{-}45/0)_{2\times1/2}]_{3S}$ | 4.32 | 0.85 | 100.7 |
| $[(45/90)_{1\times1/2}/(\text{-}45/0)_{1\times1/2}]_{3S}$ | 4.39 | 0.50 | 101.7 |
| | | | |
| Standard Deviation [%] | 1.44 | | 0.68 |
| **TP** | | | |
| $[45/90/\text{-}45/0]_{4S}$, Baseline | 3.96 | 0.43 | 100.0 |
| $[(45/90)_{1\times1/2}/(\text{-}45/0)_{1\times1/2}]_{4S}$ | 4.10 | 0.42 | 98.1 |
| | | | |
| Standard Deviation [%] | 2.46 | | 1.39 |

from composite laminates with unidirectional layers.
In a later phase, also Short Block Compression (SBC) specimens were produced and tested as described in Chapter 5. Being smaller, they are more suited for compression stiffness and strength measurements. The results of these tests support the previous findings.

## 2.5 Manufacturing

Manufacturing laminates with AP-PLY patterns poses some challenges that will be addressed in this section. In general, any fibre placement process can be adapted fairly easily to AP-PLY, but making it efficient requires some extra adaptations.

### 2.5.1 Manufacturing Time

Because of the open spaces in the courses needed for AP-PLY patterns, manufacturing them with current fibre placement machines will always take longer than a laminate with unidirectional layers. The AP-PLY laminates manufactured for this research were fibre placed with a machine having 8 tows directly adjacent to each other. In order to fibre place the AP-PLY patterns, only 4 of the 8 tows were used to achieve the gaps between the tows. Obviously this resulted in a doubling of the fibre placement time. A slight adaptation to the machine head, as shown in Figure 2.10, where a same amount of tows are separated instead of directly adjacent to eachother, could yield the same manufacturing times. As the compaction roller and the machine head would get wider, this could be a problem for highly curved or small parts. In the proposed configuration, for $N$ tows, an extra width of $(N-1) \times tow_{width}$ would be added to the width of the original compaction roller.

Figure 2.10: Current compaction roller with 8 tows (left) and possible adaptation for AP-PLY (right)

### 2.5.2 Practical Manufacturing Issues

When manufacturing AP-PLY laminates, some practical issues will arise during production that are not a problem with unidirectional layers [Nagelsmit, Kassapoglou, and Gürdal, 2011a]. First of all, depending on the pattern, the programming of the fibre placement machine is different. Depending on the machine and its software, this can be challenging or rather straightforward. On the Coriolis machine at NLR, tows can be turned on and off by the operator. To fibre place an AP-PLY pattern, unidirectional plies are programmed and during the placement process these are placed with specific tows turned on and off. This involves a lot of hand labour of the operator, which is not efficient in an actual production process.

As thermoplastic material will not 'stick' to the mould, the first courses will not have an inherent sideways stability which is provided in unidirectional layers by the adjacent fibre bands. In placing the second passing, also the fibre bands below will be heated and will move over the mould. To prevent this unwanted behaviour, fibre bands in the second passing are placed in a different order to secure the lower bands in their position first, as can be seen in Figure 2.11.

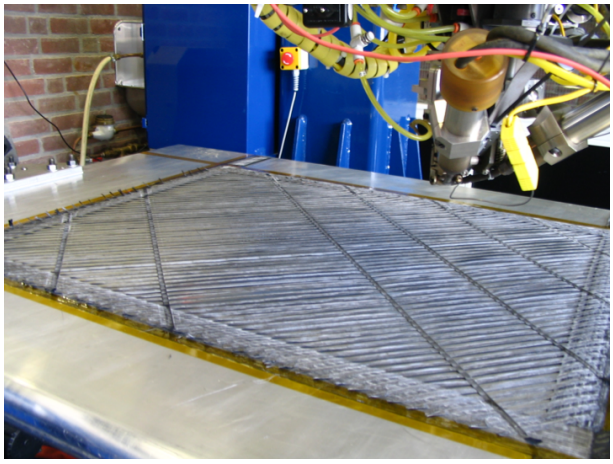

Figure 2.11: Placing the second layer in a thermoplastic AP-PLY Laminate

Chapter 3

# Impact Behaviour of AP-PLY Laminates

## 3.1 Introduction

Now that the background of composites and damage tolerance and the AP-PLY fibre placement architecture have been discussed, the performance of the AP-PLY laminates has to be investigated. Compression after impact (CAI) is the most representative test method to determine the damage tolerance of composite laminates. This chapter describes in a general fashion the difference in impact behaviour between composite laminates with the AP-PLY fibre placement architecture and composite laminates with unidirectional plies. The difference between different AP-PLY configurations will be discussed in detail in the next chapter.

## 3.2 Compression After Impact

In CAI tests, specimens are impacted first and then tested for compression strength. All tests are performed according to a combination of ASTM standard D7136 and AITM 1.0010 for impact and ASTM D7137 and AITM 1.0010 for residual compressive strength [ASTM, 2009b; ASTM, 2009c; AITM, 2009]. Where the ASTM standard does not prescribe the impact energy levels, the AITM standard proposes an approach for a series of 12 specimens to first find the barely visible impact damage (BVID) level from the impact energy level versus indentation relation. In the compressive residual strength part of the procedure, the two methods differ in the prescribed residual strength compression test velocity; where ASTM prescribes 0.5 $mm/min$, AITM prescribes 1.25 $mm/min$. Both velocities are well within the range which avoids strain rate effects, so the higher velocity was chosen to increase the efficiency of the test program.

### 3.2.1 Test Details

According to the standards, test specimens are 100 $\times$ 150 $mm$ with a quasi-isotropic stacking sequence and a thickness as close to 4 $mm$ as possible. Impactor tup diameter is 16 $mm$ and the weight of the impactor is 2.3 $kg$. Before impact testing, the width and length of the specimens are measured at two locations and the thickness at four locations.

### 3.2.2 Impact and Indentation Depth

In the impact tests, the release height of the impactor can be adjusted to achieve the desired impact energy. Specimens are simply supported, and held in place by the clamps shown in Figure 3.1. First, the Barely Visible Impact Damage (BVID) level has to be determined. This level is prescribed as a 0.3 $mm$ dent depth after 2 weeks relaxation, meaning a 1 $mm$ dent depth directly after impact [MIL-HDBK-17-3F, 2002]. To determine this value, a small series of tests are performed first below, on and above the predicted value to generate an impact energy - indentation depth curve. From this curve, the BVID level is determined. Preferably three tests are performed at every energy level, as scatter is high in these dynamic tests.

Directly after impact, the indentation depth is measured using a micrometer. This indentation can be seen as a first measure of the damage resistance and the detectability of an impact event. A typical impact energy - indentation depth curve can be seen in Figure 3.2.

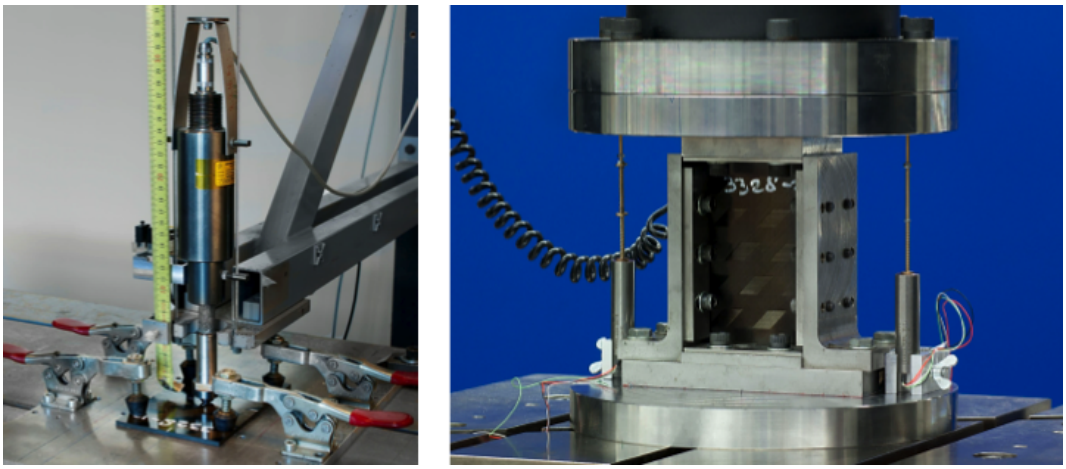

Figure 3.1: Test set up of impact (left) and compressive residual strength (right)

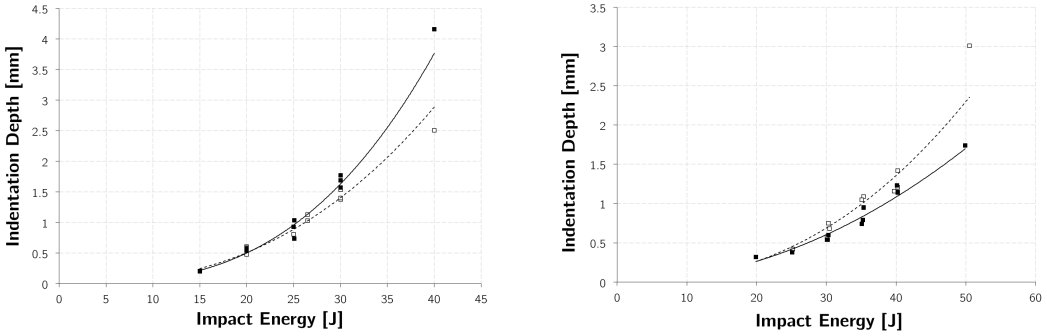


Figure 3.2: Indentation versus Impact Energy TS AP-PLY 1 90° 1/2 (black) and TS UD 90° (white) in the left picture and TP AP-PLY 1 45deg 1/2 (black) and TP UD 45° (white) in the right picture

Every thermoset AP-PLY configuration and layup behaves as the example in the left part of Figure 3.2; at higher impact energy levels the AP-PLY laminates have deeper indentations and the larger the energy level the larger the difference between AP-PLY and laminates with unidirectional layers. For the thermoplastic material system, the AP-PLY specimens have smaller indentation than their unidirectional counterparts as shown in the right part of Figure 3.2. This clear difference in indentation behaviour suggests that the impact energy is dissipated differently in AP-PLY compared to composites with unidirectional layers, and also a difference in AP-PLY behaviour between thermoset and thermoplastic resin systems. In Chapter 4 the impact behaviour will be studied more closely with section cuts of impacted specimens.

Every AP-PLY and unidirectional configuration tested has a different impact energy at which the indentation depth is 1 *mm*. Table 3.1 shows the difference in BVID energy level for every AP-PLY and unidirectional configuration tested.

Table 3.1: BVID energy levels corresponding to 1 *mm* indentation depth

| | **BVID energy level** [*J*] |
|---|---|
| **Thermoset** | |
| TS UD 90° | 26.5 |
| TS AP-PLY 1 90° 1/2 | 25.1 |
| TS AP-PLY 2 90° 1/2 | 25.9 |
| Alternating TS AP-PLY 2 90° 1/2 | 26.1 |
| TS AP-PLY 1 45° 1/4 | 28.8 |
| TS UD 45° | 27.6 |
| TS AP-PLY 1 45° 1/2 | 25.4 |
| TS AP-PLY 2 45° 1/2 | 26.3 |
| Symmetric TS AP-PLY 1 45° 1/2 | 26.0 |
| Total TS AP-PLY 1 45° 1/2 | 28.9 |
| Total TS AP-PLY 1 45° 1/4 | 27.2 |
| **Thermoplastic** | |
| TP UD 45° | 35.3 |
| TP AP-PLY 1 45° 1/2 | 38.5 |

### 3.2.3 Impact Location

When visually inspecting the impacted specimens, it was clear that different impact locations with respect to the AP-PLY pattern resulted in different damage behaviour, especially the fibre breakout on the backside of the specimens. In Figure 3.3 specimens are shown from the front- and backside and their c-scan images, with the same impact energy level (25 *J*) and different impact locations with respect to the pattern.

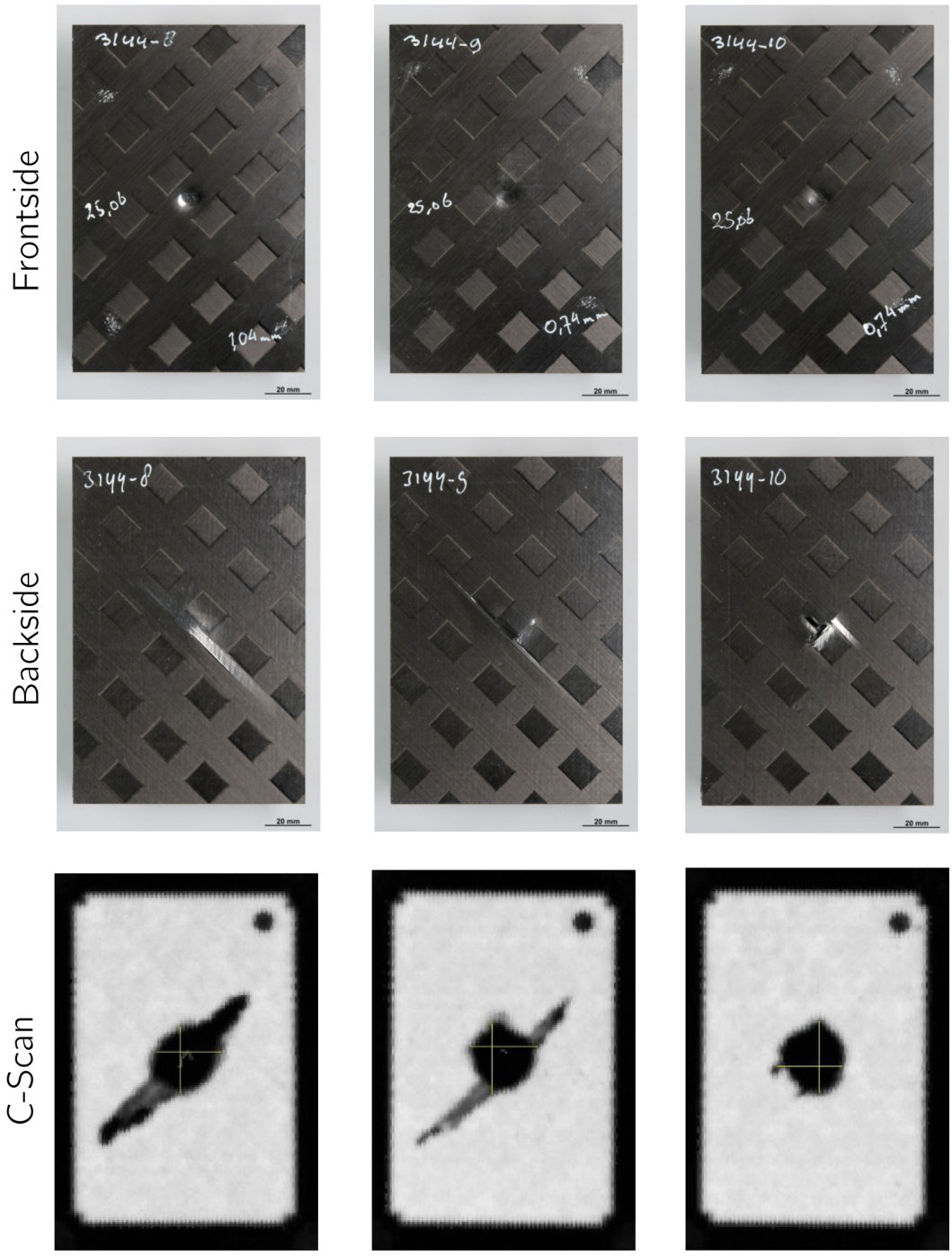


Figure 3.3: Influence of impact location on impact behaviour for three different impact locations shown in the top row from the front, the middle row from the back and C-scans of the internal damage are shown in the bottom row

Looking at the CAI test results (Appendix C) the indentation depth is similar for the middle and right specimen (0.74 $mm$), but considerably larger for the leftmost specimen (1.04 $mm$). On the backside, clear fibre breakout can be seen in the leftmost specimen, while the other two manage to contain the damage to a smaller region in the lower plies. Delamination sizes are similar when looking at the circular area of the delamination (808, 663, 680 $mm^2$), excluding the splitting of the lower ply. No information on the through-the-thickness location of the delaminations is known for these specimens. The most important feature, residual compressive strength after impact, is increasing from the left specimen (192 $MPa$), via the middle (209 $MPa$), to the right specimen (217 $MPa$).

Impact location does make a difference in AP-PLY laminates, but is uncontrollable in aircraft structures. A more homogeneous pattern with a higher 'resolution' and thus a smaler repetitive unit cell will most likely reduce the scatter and will thus be necessary to make full use of the benefits of AP-PLY.

### 3.2.4 Impact Force Measurements

During impact, a strain gauge attached to the impactor measured the force exerted by the impactor on the specimen. A high-frequency oscillation is present in the force-time curve, which is believed to be noise in the signal caused by the electronic equipment. The frequency of the oscillation is found to be 8.3 $kHz$ by using a fast Fourier transform (Figure 3.4), and it was equal for every layup, material and AP-PLY pattern. As this is a clear indication it is electronic noise, it was filtered out a-posteriori using a low-pass filter at 7.5 $kHz$. In Figure 3.5 the difference between the unfiltered and filtered curves can be appreciated.

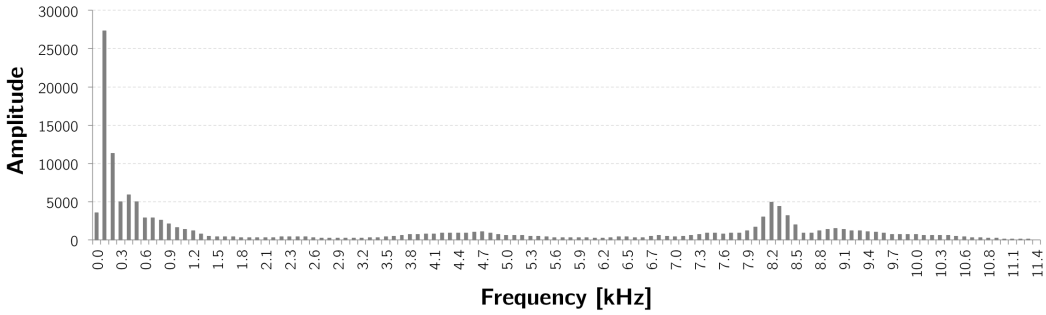


Figure 3.4: Fourier transform of the F-t signal

Force is a multiplication of mass and acceleration, implying that from the force data also the velocity and the displacement of the impactor can be derived. A simple integration procedure deriving Equations 3.2 and 3.3 from Equation 3.1 yields these results. Two examples of the calculated velocity and displacement curves are shown in Figure 3.6.

$$F = ma \tag{3.1}$$

$$v = \int \frac{F}{m}\,\mathrm{d}t \tag{3.2}$$

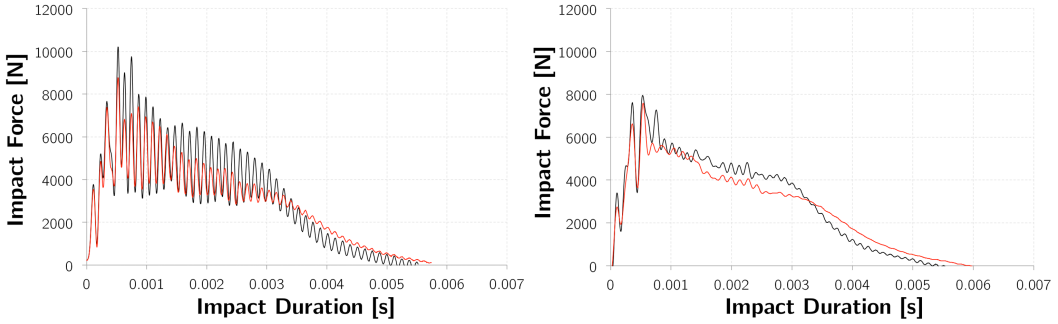


Figure 3.5: Raw (left) and filtered (right) force-time (F-t) curves for a UD 90° specimen (black) and AP-PLY 1 90° 1/2 (red) impacted at 40 *J*

$$s = \int v \, \mathrm{d}t \tag{3.3}$$

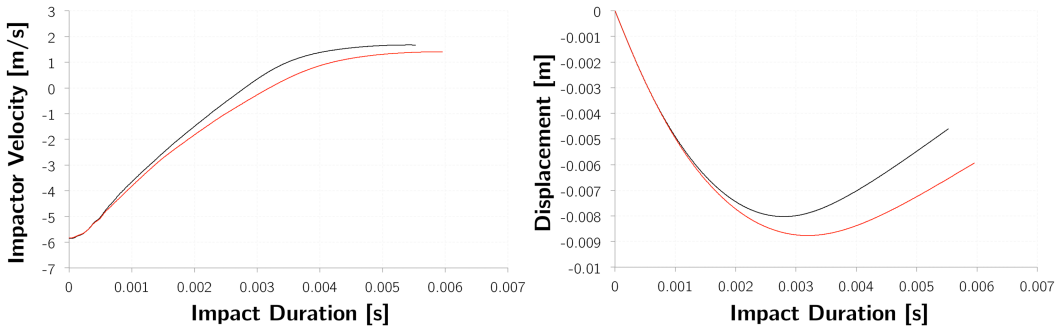


Figure 3.6: Calculated impactor velocity (left) and displacement (right) plots of a UD 90° specimen (black) and AP-PLY 1 90° 1/2 (red) impacted at 40 *J*

### Maximum Force

A purely elastic impact would show a sinusoidal shape of the F-t curve, while a discontinuity in the curve, as present in Figure 3.5 indicates plastic deformation and/or damage [Feraboli, 2006]. The area below the curve can be seen as the energy dissipated during impact. Velocity measurements of the impactor right before and right after impact can be used to check the validity of the force measurements when they are compared with the velocities calculated from the force measurements using Equation 3.2. Some measurement errors were found when comparing the measured and calculated values for the impactor velocity. In almost half the cases the measured velocity difference results in a higher rebound velocity than the impact velocity, which is physically impossible. Impact force measurements with this behaviour are ignored.

The AP-PLY configurations with half bandwidth and four interwoven layers have a 10% lower maximum force than their unidirectional counterpart (Table 3.2). The totally interwoven

pattern has a higher force again, which might indicate that not enough energy can be dissipated by damage creation.

### Impact Duration

The impact duration determines together with the impact force the dissipated energy during impact. A longer impact duration with a similar maximum force, will result in more deformation and/or damage. Except for two, all thermoset AP-PLY configurations have a longer impact duration than their unidirectional counterparts. In the thermoplastic material system, the one tested AP-PLY configuration has a shorter impact duration, which suggests that the AP-PLY laminate becomes less compliant during impact than the unidirectional baseline [Feraboli and Kedward, 2006]. This would indicate other damage mechanisms in thermoplastic AP-PLY laminates, discussed in more detail in the next chapter when section cuts of impacted specimens are analysed. More thermoplastic specimens should be tested to confirm this behaviour.

### Dissipated energy

The velocity of the impactor is measured right before and right after the impact using a light switch. Because there is a slight difference between the location of the light switch and the specimen, the impactor speed measurements are compensated. Although some of the dissipated energy values from the force measurements were unreliable, the same quantity can be calculated using the velocities right before and right after impact:

$$\Delta E = \tfrac{1}{2} m \left( v_1^2 - v_2^2 \right) \tag{3.4}$$

As average values of these impact parameters are not always representative of the behaviour on a large spectrum of impact energies, and because of the different impact energies between AP-PLY patterns caused by different BVID levels, plots are shown in Figure 3.7 of the dissipated energy versus the impact energy in the two tested material systems. An interesting observation is that the behaviour is linear for the impact energies tested, so the ratio between impact energy and dissipated energy is constant.

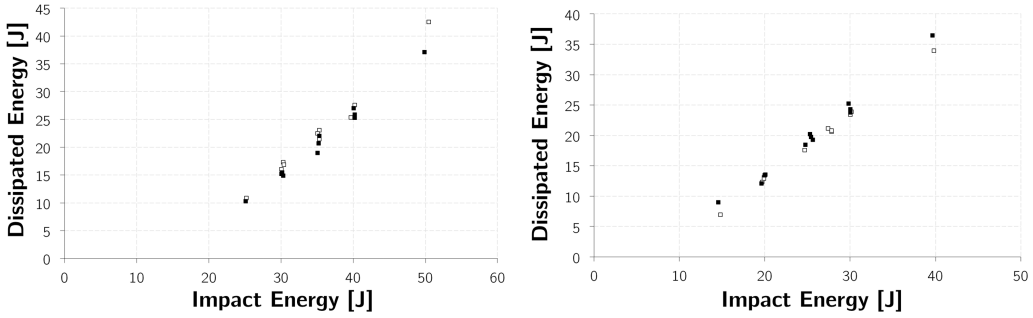


Figure 3.7: Dissipated Energy vs Impact Energy curves for thermoplastic (left) and thermoset (right) baseline (white) and AP-PLY (black) specimens

No clear difference is found between the dissipated energy during impact of different laminate configurations with the thermoset material system. Between the two series of specimens with the thermoplastic material system, a larger difference is seen. As only one thermoplastic AP-PLY configuration is tested, it is hard to draw a reliable conclusion.

#### Displacement

In the force-displacement curve, as depicted in Figure 3.8, clearly the hysteresis can be seen that results from non-elastic behaviour such as damage and the difference between AP-PLY and UD. As the values for impactor displacement are derived from the force, which is already discussed previously, these will not be treated separately.

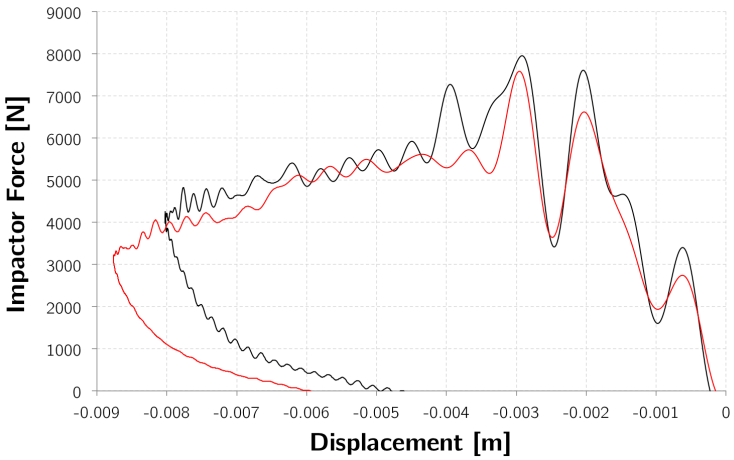


Figure 3.8: Force-displacement curve of UD 90° (black) and AP-PLY 1 90° 1/2 (red) impacted at 40 $J$

#### Overview of impact properties

Table 3.2 shows an overview of all the measured impact properties and maximum force calculated from the filtered force-time curve. The main conclusion is that no clear distinction can be found in the energy dissipated in AP-PLY laminates compared to their unidirectional baseline laminates, while maximum force and duration differ. This is an important realisation when continuing the analysis of AP-PLY impact behaviour.

### 3.2.5 Section Cuts

Of every AP-PLY configuration, a section cut is made of a specimen impacted at 25 $J$. First, the specimen is poured in resin, to prevent damage during cutting and sanding. Once cut adjacent to the middle of the impact location, the last bit is sanded off to have a perfectly smooth polished surface to view under the microscope. With the Zeiss Axioplan microscope a large amount of high definition images are captured which are combined in one single section cut image. One section cut is shown in Figure 3.9. In the next chapter, a closer look is taken at the difference found in section cuts between the several tested AP-PLY configurations.

Table 3.2: Impact Details for all tested laminate configurations (averages of three specimens impacted at 30 J)

| | **Dissipated Energy** $[J]$ | **Maximum Force** $[N]$ | **Duration** $[ms]$ |
|---|---|---|---|
| **Thermoset** | | | |
| TS UD 90 | 24.57 | 8230 | 4.20 |
| TS AP-PLY 1 90° 1/2 | 24.69 | 8176 | 4.39 |
| TS AP-PLY 2 90° 1/2 | 24.50 | 8472 | 4.34 |
| Alternating TS AP-PLY 2 90° 1/2 | 24.1 | - | 4.13 |
| TS UD 45° | 23.75 | - | 3.97 |
| TS AP-PLY 1 45° 1/2 | 24.47 | - | 4.46 |
| TS AP-PLY 2 45° 1/2 | 24.63 | - | 4.30 |
| Symmetric TS AP-PLY 1 45° 1/2 | 24.62 | 7664 | 4.52 |
| Total TS AP-PLY 1 45° 1/2 | 23.33 | 8210 | 3.90 |
| TS AP-PLY 1 45° 1/4 | 23.83 | 7436 | 4.28 |
| TS AP-PLY 1 45° 1/2 Four | 23.06 | 7353 | 4.12 |
| **Thermoplastic** | | | |
| TP UD 45° | 16.81 | - | 3.44 |
| TP AP-PLY 1 45° 1/2 | 14.95 | - | 3.29 |

In general, the AP-PLY laminates show more fibre failure and matrix cracks but fewer and smaller delaminations than their unidirectional counterparts. This suggests a possible mechanism for diverting energy from one type of failure mode to another. This, in turn can be used to improve compression after impact strength by using up impact energy in failure modes less critical for compression after impact. In subsequent chapters this is discussed in more detail.

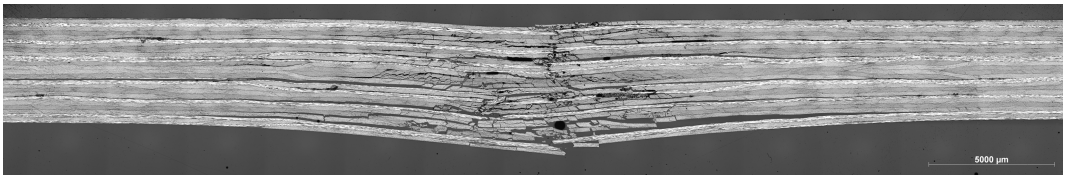


Figure 3.9: Section cut of an AP-PLY 1 45 1/2 specimen impacted at 25 J

### 3.2.6 C-Scan and Delamination Size

After impact, ultrasonic C-scan technology was used to determine the size and the extent of the delamination damage, by NLR's Ultrasonic Sciences C-scan system S 618/1. The specimens are fully immersed in water horizontally, which acts as a medium for the ultrasonic waves. Below the specimen a glass plate is positioned, which reflects the ultrasonic waves and they

are received back by the transducer. The threshold damping level for sizing the delamination damage was determined using a piece of cork attached to the specimen of which the size was known. The damping threshold was moved until the size of the ultrasonic image of the piece of cork matched its actual size. In practice, this was close to 8 $dB$. Time of flight data (B-scan) was recorded to determine the through-the-thickness location of the delaminations and the total projected delaminated area is determined. An example of these ultrasonic scans for UD and AP-PLY is shown in Figure 3.10, with the red circle being the piece of cork and the through-the-thickness time of flight images on top.

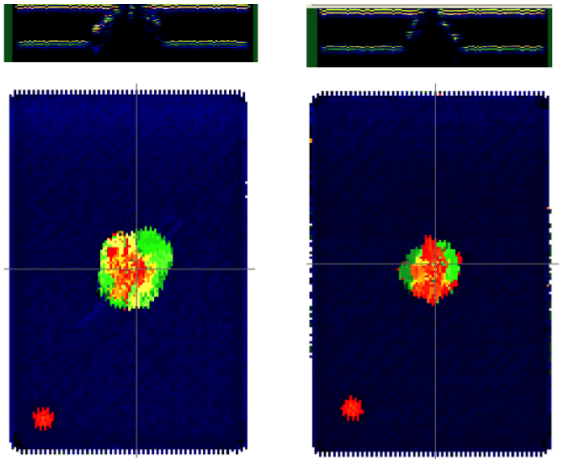

Figure 3.10: B-scans (top) and C-scans (bottom) of UD 90° (left) and AP-PLY 1 90° 1/2 (right) specimens impacted at 30 $J$

In a C-scan, only the projected delaminated area can be determined. It is more interesting however what the sizes of the individual delaminations are, and where they are located through the thickness. A slightly more detailed scan with this information is the B-scan shown in the top of Figure 3.10. It is clear from this picture that the delaminations in the AP-PLY specimen are smaller in size, through the entire thickness.

### Delamination Distribution

The section cuts confirmed the known behaviour that delaminations are largest in the direction of fibre orientation of the lower ply in the interface. No full distribution can be derived from the section cuts, as they were only made in one direction. In the B-scans, the top delaminations are blocking the lower ones, making it difficult to precisely determine the size and distribution of the delaminations. Therefore, in this research the total projected delamination area is taken as a measure for the size of the delaminations, with the previously mentioned reservation. The two curves in Figure 3.11 are representative of the difference in projected delamination area between AP-PLY laminates and laminates with unidirectional layers.

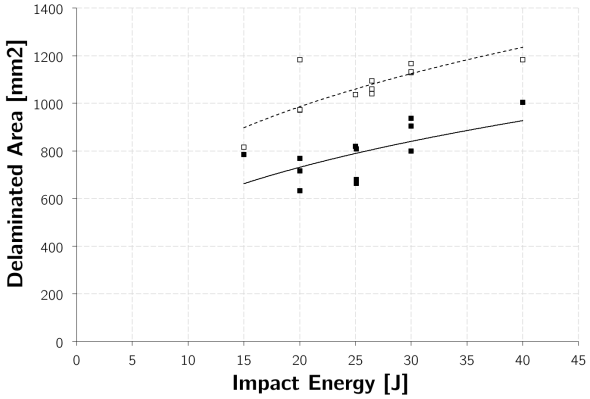


Figure 3.11: Projected delamination area versus impact energy for AP-PLY 1 90° 1/2 (black) and UD 90° (white)

### 3.2.7 Residual Compressive Strength

In an Instron 5882 static test machine using a standard CAI fixture (Figure 3.1), the residual compressive strength of the impacted specimens was determined and displacement and force were recorded. Two Linear Variable Differential Transformers (LVDT) were used to record the cross head displacement directly at the specimen.

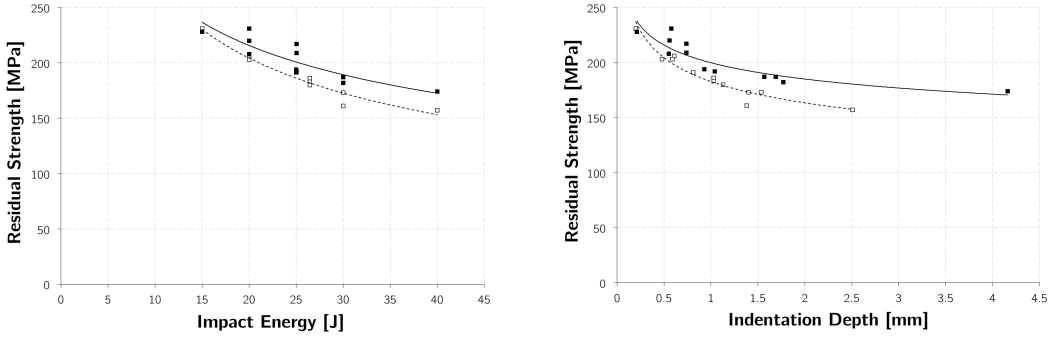


Figure 3.12: Residual strength versus impact energy (left) and versus indentation depth (right) for AP-PLY 1 90° 1/2 (black) and UD 90° (white)

Damage tolerance is determined by residual strength after impact and detectability of the damage. All test results in one series are plotted in Figure 3.12 to illustrate the trend and the associated scatter. In the right part of Figure 3.12 it can be seen that for the given, representative AP-PLY configuration, damage is easier to detect because the resulting indentation is greater, while the strength is higher. This is not the case however for all AP-PLY configurations. In the next chapter, the difference in residual strength for all AP-PLY configurations is treated in more detail.

# Chapter 4

# Design of Experiments

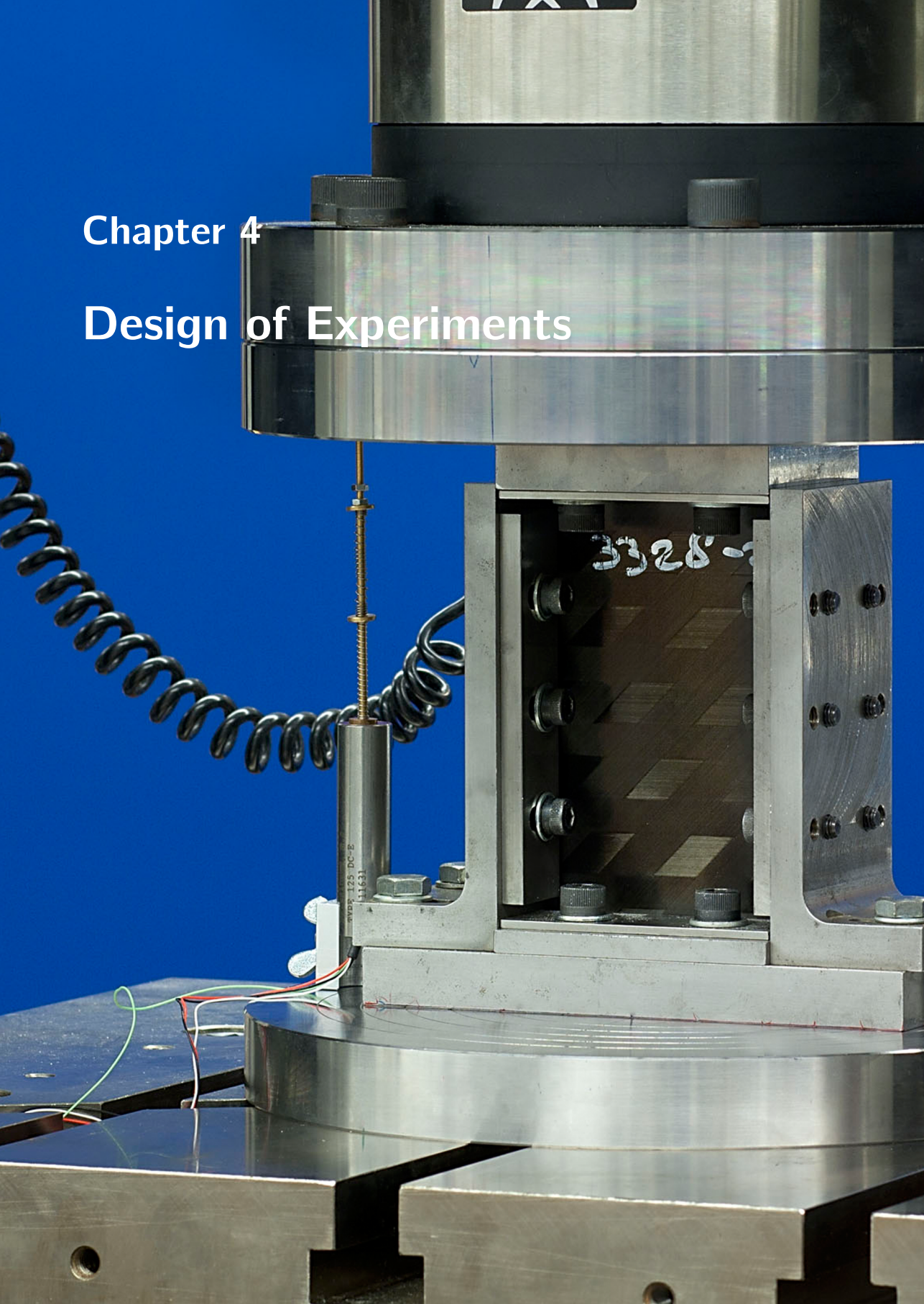

## 4.1 Introduction

In previous chapters the working principle of the AP-PLY pattern is proven to be effective in improving the damage tolerance of composite laminates, without compromising the other mechanical properties. This chapter is designed to show the relative influence of the six individual parameters of the AP-PLY patterns on the earlier defined result drivers from the CAI tests, using the factorial design of experiments approach first used by Fisher [Box, Hunter, and Hunter, 1978]. In such an approach, the influence of individual parameters can be deduced, also by changing more than one paramater at a time. Based on the results of this exercise, the best performing pattern can be chosen, where in this case an improved damage tolerance will be the ultimate goal.

## 4.2 Design

A complete overview of the tested laminate configurations with their result driver values can be found in Table 4.1, arranged in a factorial approach [Nagelsmit, Kassapoglou, and Gürdal, 2011b]. In the Pattern column, the *S* and *A* stand for series and alternating respectively. The *N* and *Y* in the Totally Interwoven column stand for "No" and "Yes". Impact energy levels were slightly different in every series because the BVID energy levels varied. For a fair comparison, average values were taken over the 3 impacts at 30 Joules that were performed in every series, except for the TS AP-PLY 2 45° 1/2 where a clear outlier blurred the results and only two values were used. 30 *J* energy levels were close to BVID for every series, except for the thermoplastic resin laminates, and thus deemed representative. When more than one configuration possess that certain parameter of the pattern that is investigated, their result driver values will be combined in an average. The tables in the next sections will show the relative difference of the combined values of one configuration compared to the other, which is described by "one" versus "the other".

For the complete picture, also graphs of all the test results of the indentation depth, delamination size and residual strength versus the impact energy are given for each parameter discussed. Relevant section cuts of specimens impacted at 25 *J* are shown for the pattern parameter discussed, as well as C-scans of the delaminations. If available, these C-scans include time-of-flight data on the through-the-thickness location of the delaminations.

## 4.3 Results

For every parameter that can be varied in the AP-PLY fibre architecture, the influence on the impact damage behaviour will be discussed in the following sections. Full test results can be found in C.

### 4.3.1 AP-PLY versus unidirectional

To determine the overall AP-PLY performance, 3 AP-PLY configurations will be compared to their unidirectional counterparts. Looking at the most important test results in Table 4.2 and Figure 4.1, it can be seen that for all configurations the residual strength of AP-PLY is higher than for unidirectional laminates, ranging from 5-10%.

Table 4.1: Design of experiments overview, with the average values at 30 $J$ impacts for the result drivers in the last three columns and Coefficient of Variation [%] in brackets

| | Skipping | Layup Angle | Pattern | Bandwidth | Interwoven Plies | Totally Interwoven | Residual Strength $[MPa]$ | Delamination Size $[mm^2]$ | Indentation Depth $[mm]$ |
|---|---|---|---|---|---|---|---|---|---|
| **Thermoset** | | | | | | | | | |
| TS UD 90° | - | 90° | - | - | - | - | 169 (4.1) | 1143 (1.8) | 1.44 (6.1) |
| TS UD 45° | - | 45° | - | - | - | - | 185 (1.9) | 1195 (6.6) | 1.28 (10.4) |
| TS AP 2 90° 1/2 | 2 | 90° | S | 1/2 | 2 | N | 180 (2.8) | 902 (10.5) | 1.64 (5.0) |
| TS AP 2 45° 1/2 | 2 | 45° | S | 1/2 | 2 | N | 193 (1.5) | 1197 (1.0) | 1.41 (15.6) |
| TS AP 1 90° 1/2 | 1 | 90° | S | 1/2 | 2 | N | 185 (1.6) | 880 (8.2) | 1.68 (6.0) |
| TS AP 1 45° 1/2 | 1 | 45° | S | 1/2 | 2 | N | 194 (1.9) | 1183 (8.6) | 1.52 (8.0) |
| Alt. TS AP 2 90° 1/2 | 2 | 90° | A | 1/2 | 2 | N | 185 (6.2) | 1158 (34.3) | 1.53 (12.9) |
| TS AP 1 45° 1/2 Four | 1 | 45° | S | 1/2 | 4 | N | 196 (3.1) | 1230 (15.3) | 1.22 (16.0) |
| TS AP 1 45° 1/4 | 1 | 45° | S | 1/4 | 2 | N | 203 (1.6) | 1079 (19.2) | 1.23 (3.3) |
| Total TS AP 1 45° 1/2 | 1 | 45° | S | 1/2 | - | Y | 199 (0.6) | 1033 (7.8) | 1.16 (12.9) |
| **Thermoplastic** | | | | | | | | | |
| TP UD 45° | - | 45° | - | - | - | - | 298 (6.4) | 648 (15.8) | 0.67 (13.6) |
| TP AP 1 45° 1/2 | 1 | 45° | S | 1/2 | 2 | N | 327 (5.8) | 554 (13.2) | 0.56 (6.2) |

In the 45° interface laminates the projected delamination size does not seem to be smaller for AP-PLY. The residual strength is however higher, implying that not only the size of the delaminations influences the residual strength, but also other factors such as the through-the-thickness distribution, which is supported by the section cuts in Figure 4.2. This could also be an indication that AP-PLY does not only play a role in damage initiation but also in damage propagation, which was already discussed in Chapter 5 on fracture toughness values of AP-PLY. Another question that can be raised is whether AP-PLY in a 90° configuration is more efficient than AP-PLY in a 45 ° configuration.

For the thermoplastic configurations the indentation behaviour is opposite; AP-PLY shows smaller indentations than the unidirectional laminate. An explanation for this could be the overall smaller amount of damage in the thermoplastic laminates with respect to the thermoset specimens, resulting in different damage mechanisms.

Going back to the thermoset specimens, on the C-scans in Figure 4.3, larger and more regularly shaped backside splits are visible for the UD specimens compared to the AP-PLY specimens in Figure 4.4, caused by the different impact location with respect to the pattern. The size of the delaminations is only taken for the circular part, as the backside splits are not considered to have a large negative influence on the residual compressive strength.

Table 4.2: AP-PLY versus UD

| | **45° ply interface, TS** | **90° ply interface, TS** | **45° ply interface, TP** |
|---|---|---|---|
| Indentation Depth | + 14.5% | + 15.2% | - 16.4% |
| Delaminated Area | - 0.4% | - 22.0% | - 14.5% |
| Residual Strength | + 4.6% | + 8.0% | + 9.9% |

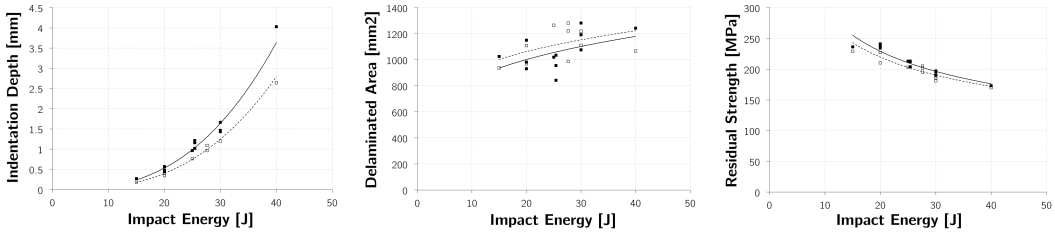


Figure 4.1: Comparison of TS AP-PLY 1 45° 1/2 (black) versus TS UD 45° (white)

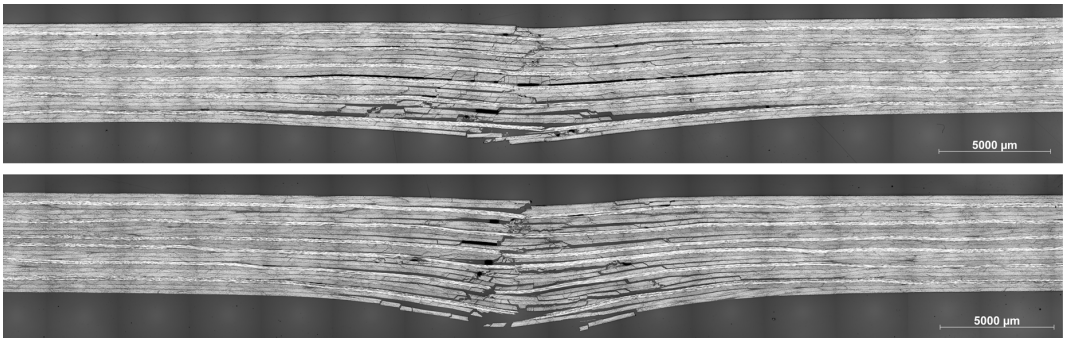


Figure 4.2: Section cuts of TS UD 90° (top) and TS AP-PLY 1 90° 1/2 (bottom) specimens impacted at 25 J

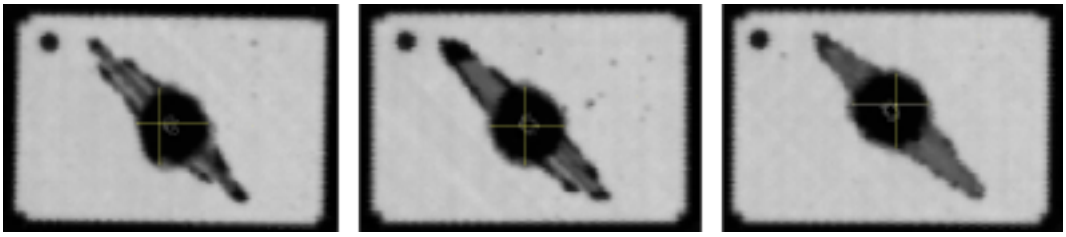

Figure 4.3: C-scans of three TS UD 90° specimens impacted at 30 J

### 4.3.2 Layup Interface Angle

An interesting phenomenon is the better performance in terms of residual strength of 45° interface laminates ($[45/90/\text{-}45/0]_{3S}$) as compared to the 90° interface laminates ($[45/\text{-}45/90/0]_{3S}$), both in UD and AP-PLY. As can be seen in Figure 4.5 the projected delamination size is significantly larger for the 45° interface, but the residual strength is higher. Apparently, not only

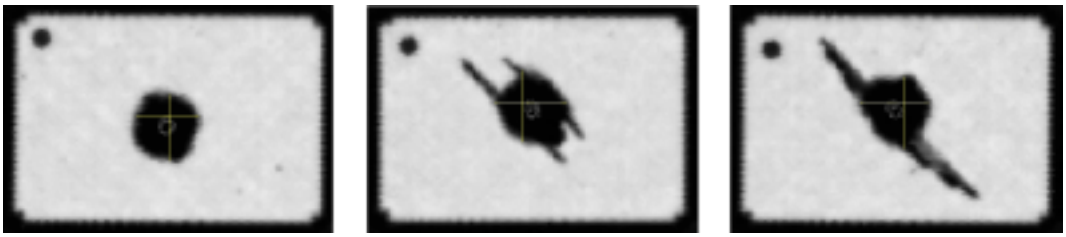

Figure 4.4: C-scans of three TS AP-PLY 1 90° 1/2 specimens impacted at 30 J

the size of the delaminations determines the residual strength, but also their locations. The in-plane stiffnesses of these two laminates are equal, which is confirmed by the stiffness measurements of the specimens presented in Table 2.4, but the out-of-plane stiffness $D_{11}$ is slightly higher for the 90° interface laminates. Due to this higher stiffness the bending deformation is smaller, resulting in lower interlaminar stresses due to bending than in the 45° interface laminates. Also in compression, the buckling load of the 90° interface laminate should be higher due to the higher out-of-plane stiffness. In Table 4.3, the averages of all three result drivers of *all* 45° interface laminates, so AP-PLY and UD, are compared to the averages of *all* 90° interface laminates, as well as the separate values for AP-PLY and UD. As these facts all point to a better behaviour of the 90° interface laminates, which is not supported by the experiments, this might indicate, together with the larger relative difference between AP-PLY and UD laminates, that the pattern behaves differently for different interface angles and that the ply interface angle has more influence on the damage behaviour than the stiffness of the entire laminate. In Figures 4.6 and 4.7 a cross-section and the C-scans of the specimens used for the comparison can be found, which will be compared to the other laminate configurations in the following sections.

Table 4.3: Influence of the layup angle (45° ply interface versus 90° ply interface) on the result drivers

| | **UD** | **AP-PLY** | **Average** |
|---|---|---|---|
| Indentation Depth | - 11.1% | - 11.4% | - 11.3% |
| Delamination Size | + 4.5% | + 33.6% | + 19.1% |
| Residual Strength | + 9.5% | + 6.0 | + 7.8% |

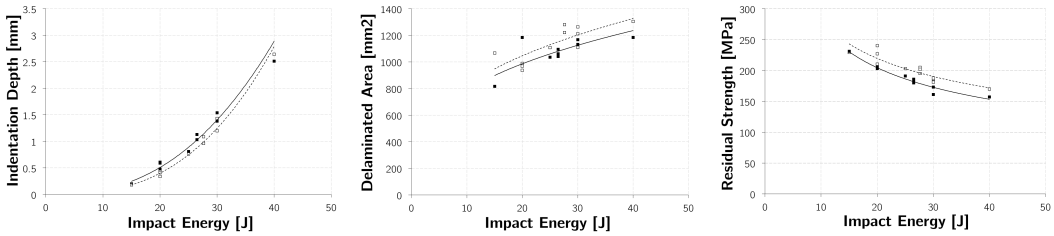


Figure 4.5: Comparison of TS UD 90° laminates (black) versus TS UD 45° laminates (white)

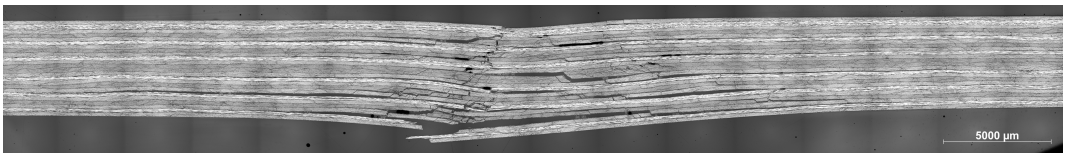


Figure 4.6: Section cut of a TS UD 45° specimen impacted at 25 J

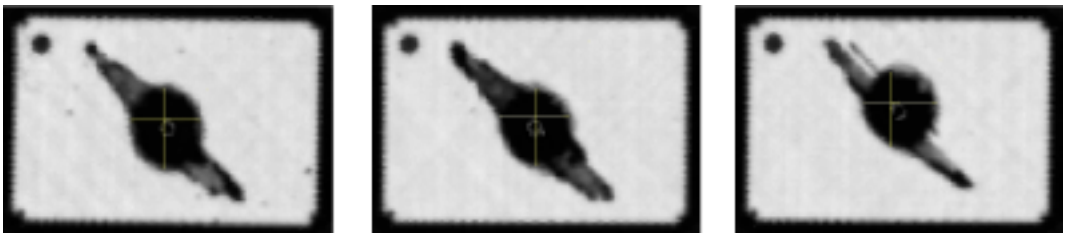

Figure 4.7: C-scans of three TS UD 45° specimens impacted at 30 J

### 4.3.3 Resin Systems

A first observation when looking at the results of laminates with different resin systems is the better performance in impact tests of laminates with a thermoplastic resin system compared to laminates with a thermoset resin system, for the same fibre and layup. BVID energy levels are significantly higher, projected delamination sizes are smaller and the residual strength is superior over thermoset laminates, as can be seen in Table 4.4 and Figure 4.8. The section cuts in Figure 4.9 show mainly delaminations, and significantly less fibre breakage or matrix cracks compared to laminates with a thermoset resin system as shown in Figure 4.6.

Table 4.4: Influence of the resin system on the result drivers, shown separately for AP-PLY and UD laminates

| | **TP AP-PLY versus TS AP-PLY** | **TP UD versus TS UD** |
|---|---|---|
| Indentation Depth | -60.5% | - 47.7% |
| Delamination Size | -62.6% | - 45.8% |
| Residual Strength | +68.7% | + 60.9% |

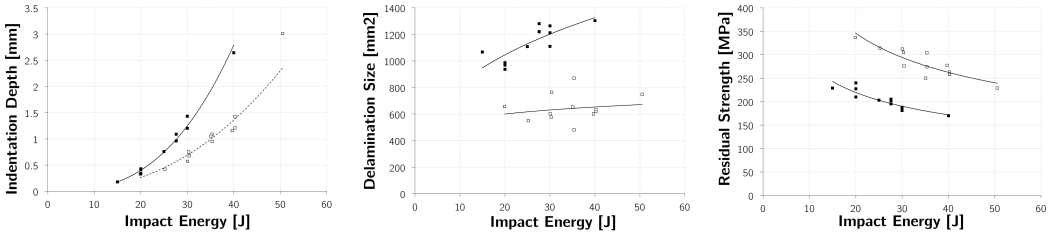


Figure 4.8: Comparison of TS (black) versus TP (white) for UD 45° interface laminates

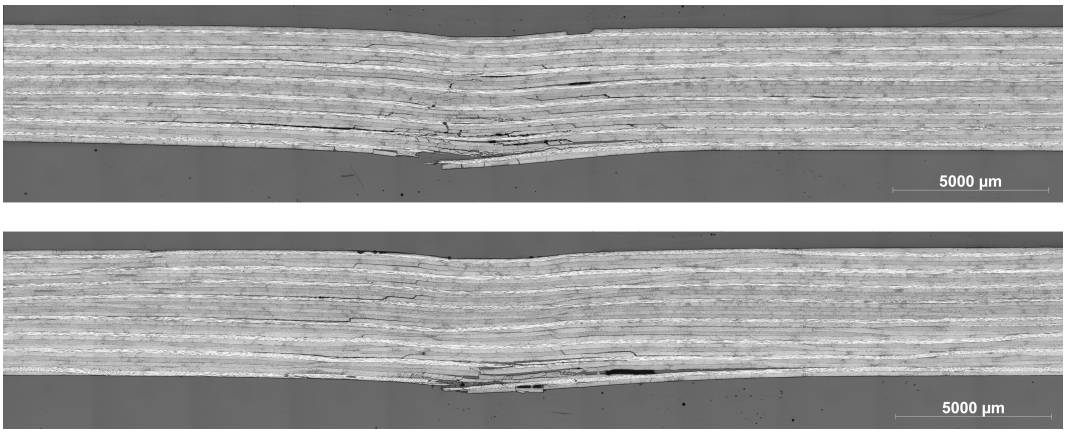


Figure 4.9: TP UD 45° (top) and TP AP-PLY 1 45° 1/2 (bottom)

### 4.3.4 Pattern

Two different AP-PLY patterns were tested: the series pattern places an entire group of fibre bands before changing to another direction, whereas the alternating pattern switches direction every fibre band, as explained in Section 2. This alternating pattern is more irregular and less homogeneous than the series pattern. As can be seen in Table 4.5 and Figure 4.10 the alternating pattern has a slightly higher residual strength, but the projected delamination size is higher. The irregular pattern can also be recognised in the section cuts in Figure 4.11, where the main difference is the larger backside split for the alternating pattern. On the C-scans shown in Figure 4.12 and 4.13 the specimens with the alternating pattern have more irregularly shaped delaminations, resulting from the more irregular pattern. In Figure 4.12 no backside splits are visible, which is a coincidence resulting from apparently favourable impact locations with respect to the pattern for these three specimens.

The more irregular and less predictive behaviour, together with the very limited improvement in residual strength and the longer and more difficult production process, renders the alternating pattern an undesirable option.

Table 4.5: Influence of the AP-PLY pattern on the result drivers

| | **Series versus Alternating** |
|---|---|
| Indentation Depth | + 7.2% |
| Delamination Size | - 22.1% |
| Residual Strength | - 2.8% |

### 4.3.5 Skipping

Results of the comparison between AP-PLY configurations with different bandwidths can be found in Table 4.6 and Figure 4.15. For all values except the indentation depth for 90° interface laminates, the influence of the amount of bandwidths that are skipped seems to be within

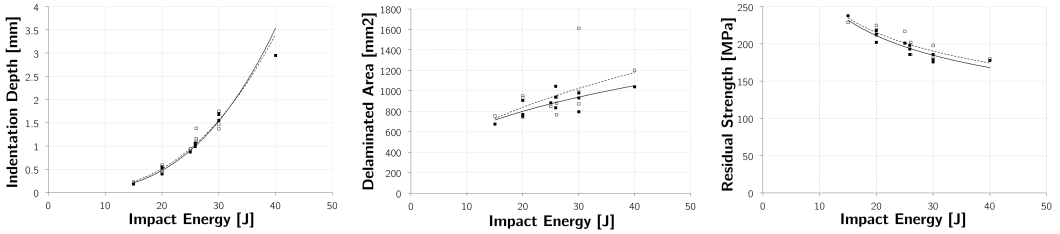


Figure 4.10: Comparison of TS AP-PLY 2 90° 1/2 laminates (black) versus Alternating TS AP-PLY 2 90° 1/2 laminates (white)

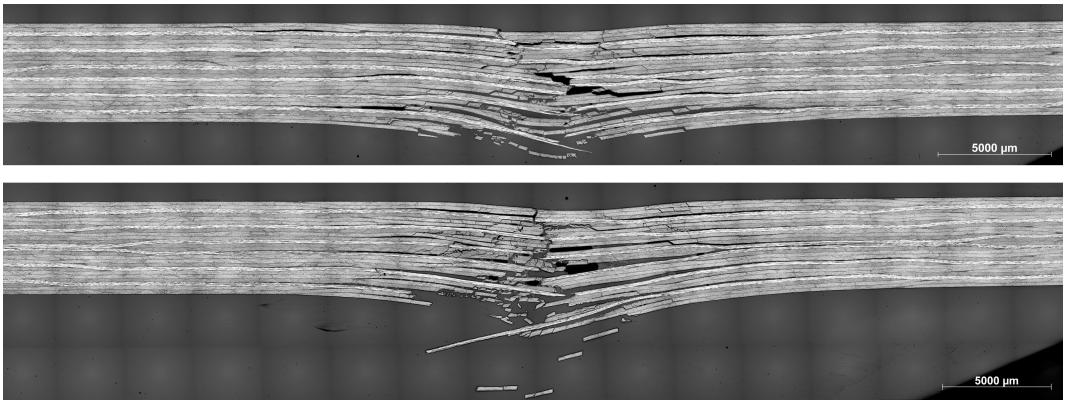


Figure 4.11: Section cuts of specimens with the regular TS AP-PLY 2 90° 1/2 (top) and the alternating AP-PLY 2 90° 1/2 (bottom)

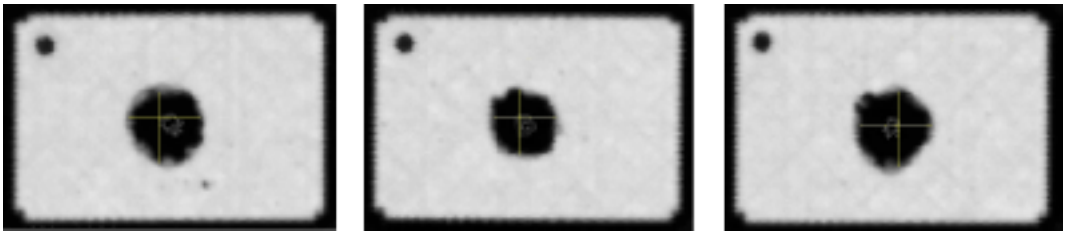

Figure 4.12: C-scans of three AP-PLY 2 90° 1/2 specimens impacted at 30 J

Figure 4.13: C-scans of three alternating AP-PLY 2 90° 1/2 specimens impacted at 30 J

experimental scatter. Also the C-scans in Figures 4.16 and 4.17 do not give clear indications of different behaviour. Skipping one is more advantageous and more efficient to manufacture than skipping two, so this choice will be made based on different criteria than the mechanical performance.

Table 4.6: Influence of number of bands that are skipped on the result drivers

| | **1 versus 2 (45°)** | **1 versus 2 (90°)** | **Average** |
|---|---|---|---|
| Indentation Depth | + 2.4% | + 7.8% | + 5.1% |
| Delamination Size | - 2.4% | - 1.2% | - 1.8% |
| Residual Strength | + 2.8% | + 0.5% | + 1.7% |

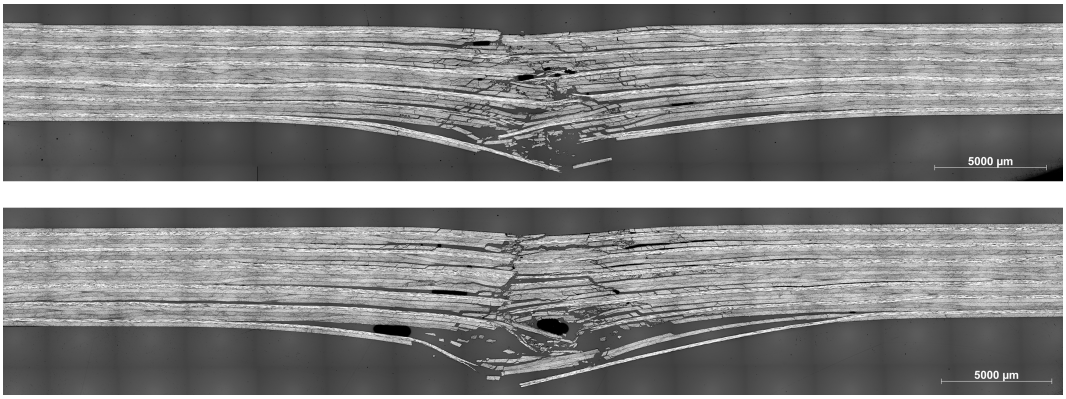


Figure 4.14: Section cuts of TS AP-PLY 1 45° 1/2 (top) and TS AP-PLY 2 45° 1/2 (bottom) impacted at 25 *J*

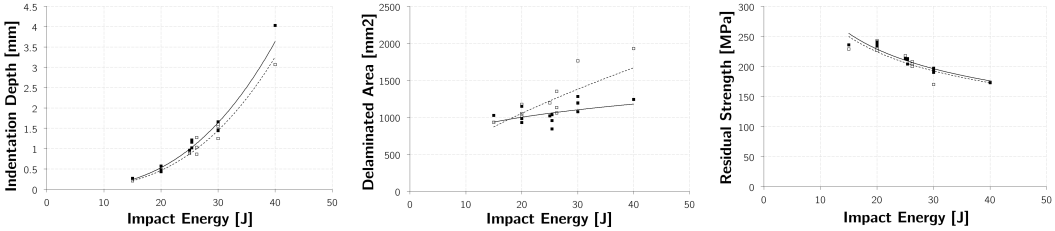


Figure 4.15: Comparison of TS AP-PLY 1 45° 1/2 (black) and TS AP-PLY 2 45° 1/2 (white)

### 4.3.6 Bandwidth

It is expected that reducing the bandwidth would positively influence the homogeneity of the laminates, thus reducing the impact location dependency and confining damage to a smaller region. As can be seen in Table 4.7 and Figure 4.18, the residual strength is increased significantly compared to the same AP-PLY configuration with twice the bandwidth. The projected delamination size is smaller, and the indentation depth is also lower. This means BVID is

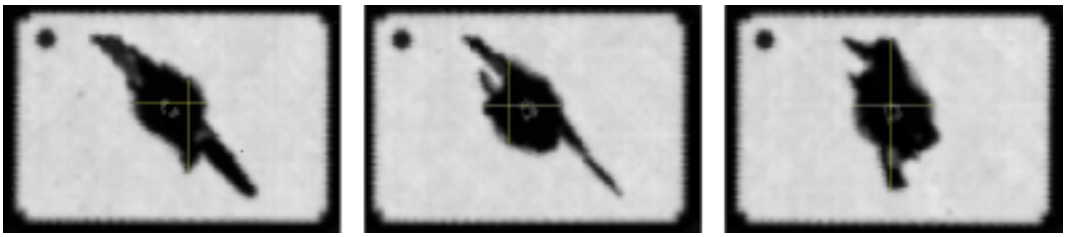

Figure 4.16: C-scans of three TS AP-PLY 1 45° 1/2 specimens impacted at 30 *J*

Figure 4.17: C-scans of three TS AP-PLY 2 45° 1/2 specimens impacted at 30 *J*

reached at a lower energy level, which could be considered a disadvantage because at this BVID energy level the residual strength is higher.

In the section cut in Figure 4.19 it can be seen that both delaminations and matrix cracks in the mid-plane are confined by AP-PLY undulations present. When comparing this cross-section with Figure 4.14 of the configuration with twice the bandwidth, the overall damaged area seems smaller for the smaller bandwidth.

The C-scans in Figure 4.20 show more regular behaviour when comparing them to the same AP-PLY configuration with twice the bandwidth in Figure 4.16. This observation supports the hypothesis that a smaller bandwidth will improve the homogeneity of the laminate.

Table 4.7: Influence of bandwidth

| | **1/4" versus 1/2"** |
|---|---|
| Indentation Depth | - 19.1% |
| Delamination Size | - 8.8% |
| Residual Strength | + 4.6% |

### 4.3.7 Interwoven Layers

The main difference between interweaving four and two layers is in the indentation depth as can be seen in Table 4.8. This trend is similar to the totally interwoven pattern, where also more plies are interwoven reducing the indentation depth. The projected delamination size involves a lot of scatter, and the residual strength shows practically the same curve for the four and two ply interwoven AP-PLY configurations (Figure 4.21). BVID is lower, but a lower indentation depth could also imply less fibre damage, which explains a slightly higher residual strength. The

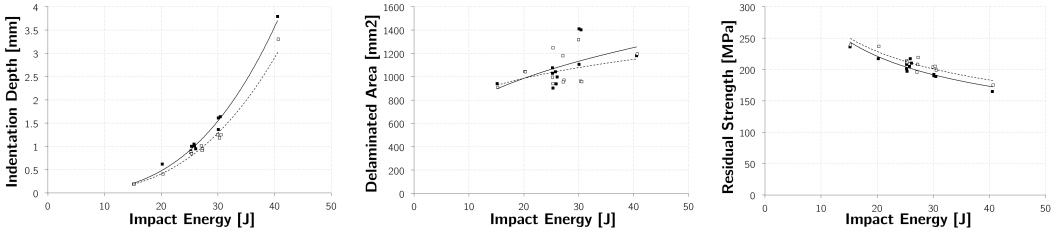


Figure 4.18: Comparison of AP-PLY 1 45° 1/2 (black) versus AP-PLY 1 45° 1/4 (white)

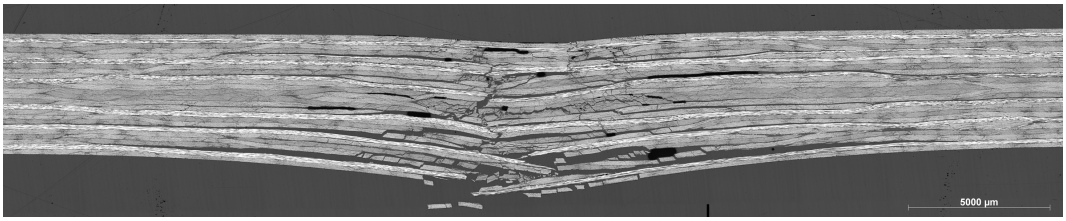


Figure 4.19: Section cut of a TS AP-PLY 1 45° 1/4 specimen impacted at 25 *J*

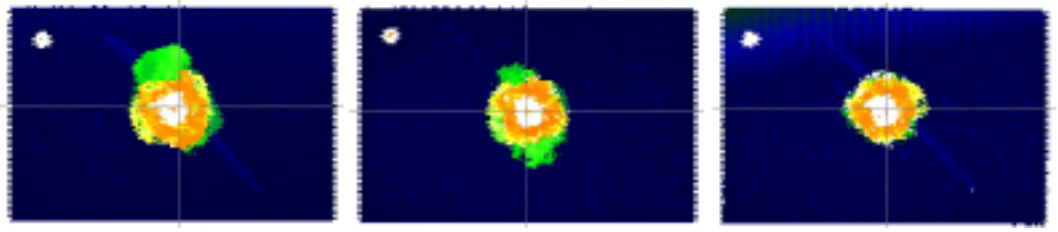

Figure 4.20: C-scans of three TS AP-PLY 1 45° 1/4 specimens impacted at 30 *J*

section cut in Figure 4.22 shows that the delaminations are still large and present, but larger sublaminates are still intact.

Further study should explain the influences of indentation depth and delamination size on residual strength.

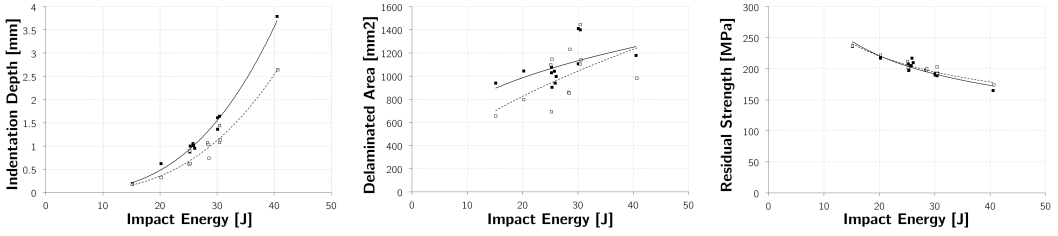


Figure 4.21: Comparison of TS AP-PLY 45° 1/2 interface laminates with 2 interwoven layers (black) versus TS AP-PLY 45° 1/2 interface laminates with 4 interwoven layers (white)

Table 4.8: Influence of interwoven layers

| | **4 layers interwoven versus 2 layers interwoven** |
|---|---|
| Indentation Depth | - 19.7% |
| Delamination Size | + 4.0% |
| Residual Strength | + 1.0% |

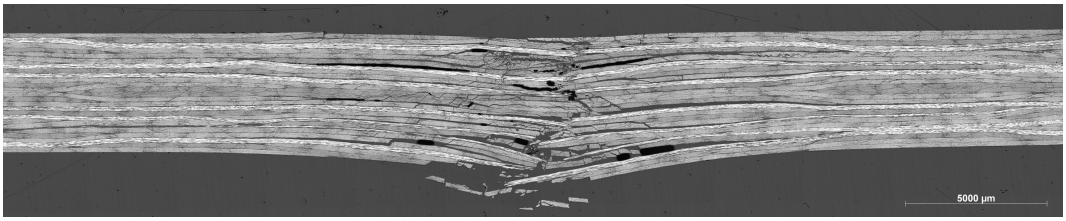


Figure 4.22: Section cut of a TS AP-PLY 1 45° 1/2 specimen with four interwoven layers impacted at 25 *J*

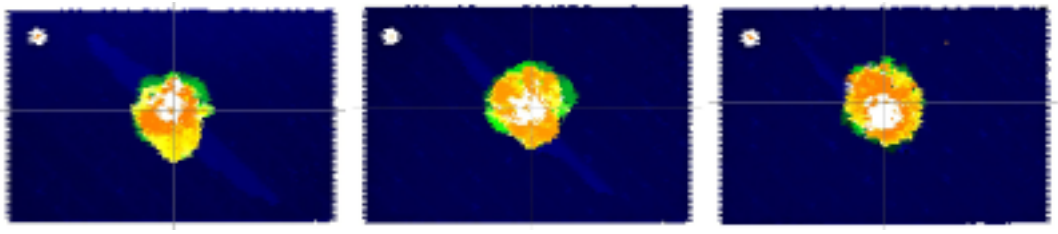

Figure 4.23: C-scans of three TS AP-PLY 1 45° 1/2 specimens with four interwoven layers impacted at 30 *J*

### 4.3.8 Totally Interwoven

In terms of residual strength the totally interwoven pattern shows a clear improvement over the two ply interwoven AP-PLY configurations. When looking at Figure 4.24, it can be seen that the indentation depth is much lower however, which could be a disadvantage. The delaminated area curve in the same Figure shows an interesting trend: it tends to stay constant with increasing impact energy, which is a clear hint where improvement can be found, namely in the higher impact energy levels.

In the section cuts in Figure 4.25 a very irregular damage pattern can be seen when comparing it to all the previous cross-sections where not all the layers were interwoven. Delaminations propagate differently in different directions, and more matrix cracks and fibre breakage is present in the lower half of the laminate than in the top half of the laminate. This implies that because of all the interwoven layers the energy tries to dissipate in different ways than delaminations. The mid-plane is however still non-interwoven, and indeed a large delamination can be seen here. Also in the C-scans in Figure 4.26 this large, green, delamination in the mid-plane is visible.

Table 4.9: Influence of complete interweaving

| | **Totally interwoven versus partly interwoven** |
|---|---|
| Indentation Depth | - 23.7% |
| Delamination Size | -12.7% |
| Residual Strength | + 2.6% |

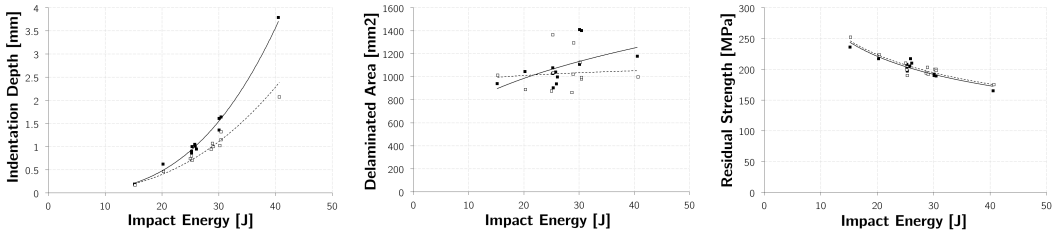


Figure 4.24: Comparison of TS AP-PLY 45° 1/2 interface laminates with 2 interwoven layers (black) versus TS AP-PLY 45° 1/2 interface laminates with totally interwoven layers (white)

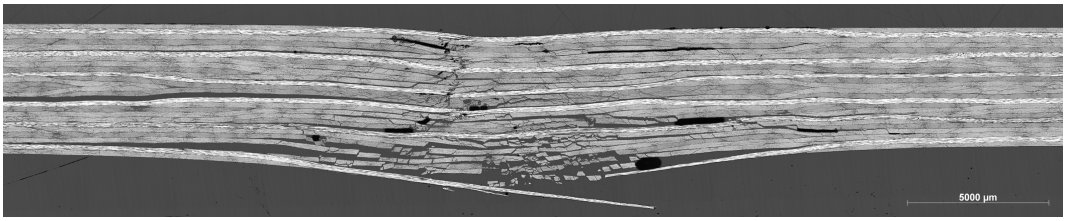


Figure 4.25: Section cut of a totally interwoven TS AP-PLY 1 45° 1/2 specimen impacted at 25 *J*

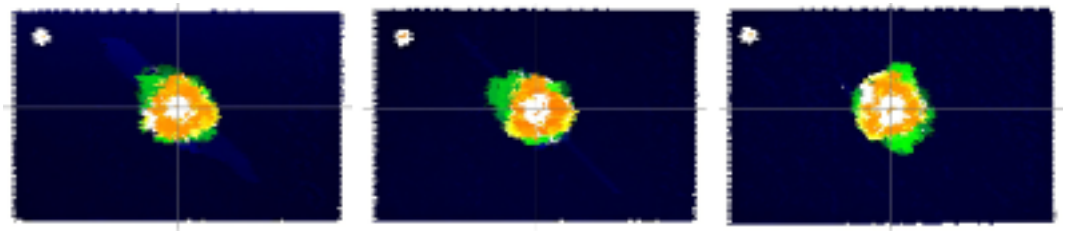

Figure 4.26: C-scans of three TS AP-PLY 1 45° 1/2 specimens with totally interwoven layers impacted at 30 *J*

## 4.4 Summary

An overview of all individual influences can be found in Table 4.10. The differences can mainly be found in the indentation depth and delamination size; improvements do not directly translate to a significantly higher residual strength in these tests with high scatter values. Especially for the amount of fibre bands to skip and the pattern, a conclusion will be drawn based on manufacturing considerations rather than an improvement in damage tolerance. At this moment, it can be concluded that the best AP-PLY configuration for compression after

impact performances has:

- a thermoplastic resin system
- a layup with 45° interface angles
- a series pattern that skips 1 fibre band
- a bandwidth of 1/4"
- a totally interwoven configuration

The AP-PLY configuration with the parameters described above will be used when investigating the influence of the AP-PLY pattern on other mechanical properties than the ones tested in compression after impact.

Table 4.10: Overview of influence of pattern parameters on result drivers

| | | **Indentation Depth [%]** | **Delamination Size [%]** | **Residual Strength [%]** |
|---|---|---|---|---|
| Layup Angle | 45 vs 90 | -11.3 | +19.1 | +7.8 |
| Resin System | TP vs TS | -60.5 | -62.6 | +68.7 |
| Pattern | S vs A | +7.2 | -22.1 | -2.8 |
| Skipping | 1 vs 2 | +5.1 | -1.8 | +1.7 |
| Bandwidth | 1/4 vs 1/2 | -19.1 | -8.8 | +4.6 |
| Interwoven Layers | 4 vs 2 | -19.7 | +4.0 | +1.0 |
| Totally Interwoven | C vs NC | -23.7 | -12.7 | +2.6 |

Chapter 5

# Mechanical Properties

## 5.1 Introduction

The majority of this thesis deals with the impact behaviour of composite laminates, with or without the AP-PLY fiber placement architecture. Other mechanical tests are also performed, to assess the influence of the new fiber architecture on non-impact related mechanical properties. Some of them will be used for modelling later in this thesis, such as the fracture toughness values, and some of them are for information, such as open hole and bearing tests, because it is important to verify that any improvements of AP-PLY in CAI performance do not come at the expense of any other properties.

## 5.2 Fracture Toughness

In damage creation and propagation, fracture toughness is an important measure. Fracture toughness is defined as the energy it takes to create a unit surface area of a crack, and is expressed in $J/m^2$. Three separate opening modes can be distinguished which are presented in Figure 5.1.

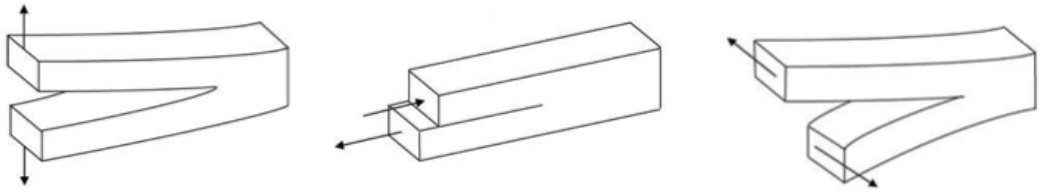

Figure 5.1: Crack Opening Modes I, II and III. (Source: Wyoming Test Fixtures Inc.)

To measure the fracture toughness, tests can be performed with specimens that already have a crack present in the form of a foil. From this initiation point, the cracks will grow through the actual material to be tested. Test standards [ASTM, 2007] and [ISO, 2002] require a fully unidirectional specimen with fibres in the length direction of the specimen, but this is impossible for AP-PLY due to the minimum of two fibre orientations involved. In order to capture the effect of the AP-PLY fibre architecture, specimens were designed such that one 'undulation' was present in the critical part of the specimen where the crack grows. In Figure 5.2 the undulation is shown that is included in the otherwise unidirectional specimen, and in Figure 5.3 the manufacturing of the specimens can be seen. The red delamination foil initiates the crack, and the fibre band on top of the foil is pulled upwards, which is counteracted by the bands running in the orthogonal direction. The green fibre band from Figure 5.2 is attached to the top half, above the delamination foil and thus pulled upwards in the Mode I test. Before and after this AP-PLY region all fibres are oriented in the lengthwise direction. Test details and AP-PLY behaviour are described in the following sections. Because these tests were performed in the scope of another research program, other material was used than in the CAI tests described before. As the AP-PLY effect is mainly geometrical, it is assumed that the relative difference in behaviour is independent of the material used and applicable to the material used in this program.

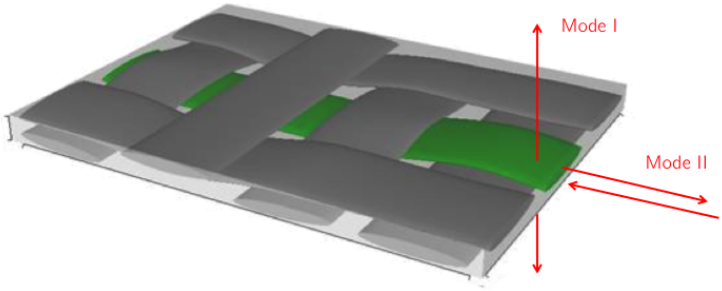


Figure 5.2: Mode I and II specimen, where the green fibre band is attached to the top half, above the delamination foil.

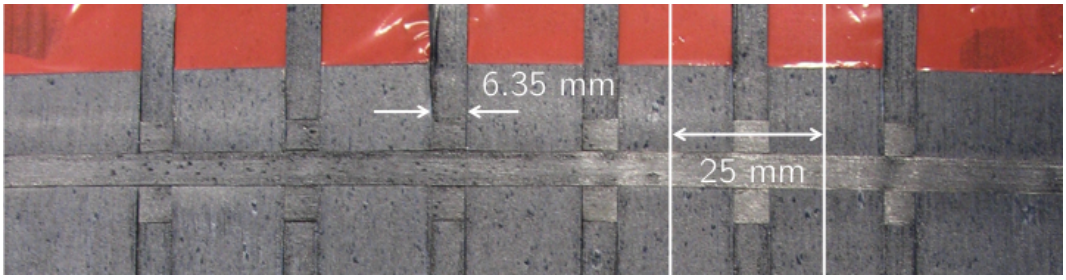


Figure 5.3: Manufacturing of the Mode I and II specimens.

### 5.2.1 Mode I

For mode I, the 'opening' mode, double cantilever beam (DCB) tests are used, according to standard ASTM D5528 ASTM (2007). Test specimens of 250 *mm* length, 25 *mm* width, 2 *mm* thickness and a foil insert of 45 *mm* are fitted with hinges to get pure tension forces that rotate with the bending of the specimen without creating moments. A schematic drawing of the test setup can be found in Figure 5.4, where the red line is the delamination foil, and the red arrows represent the pulling forces. The sides of the specimens are painted white, to be able to follow the crack tip with a digital camera taking pictures every second. After a first precrack loading to make sure the crack is propagated into the specimen, the test is started with a stroke rate of 1 $mm/min$. In Figure 5.5 a typical load-displacement curve of a Mode I test for a unidirectional specimen (black) and an AP-PLY specimen (red) are shown. The details of this figure are discussed in the next section.

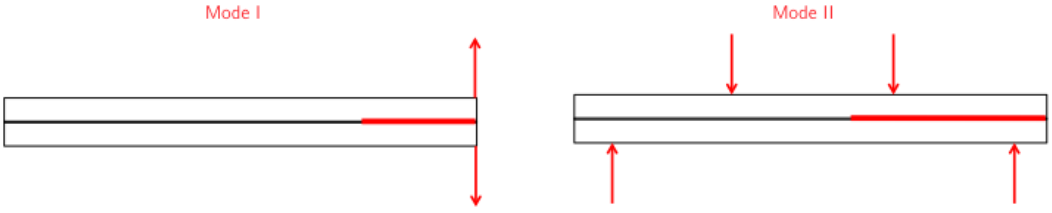


Figure 5.4: Mode I and Mode II test configurations

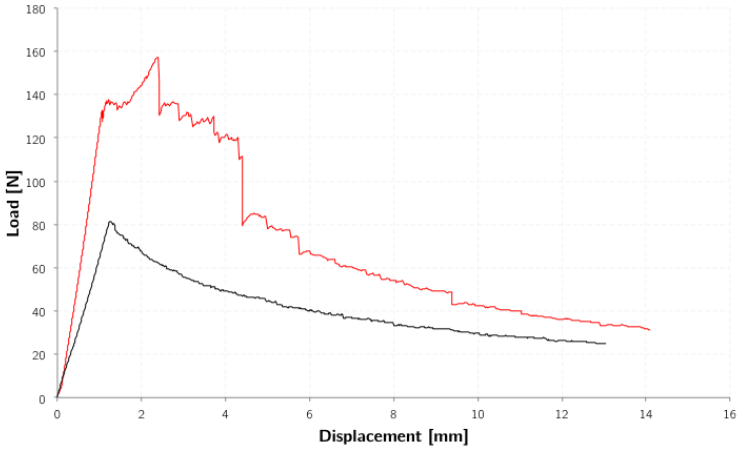


Figure 5.5: Mode I load-displacement curves for baseline (black) and AP-PLY (red)

### Mode I Results

The actual value for the Mode I fracture toughness is calculated by dividing the total energy put in the specimen by the crack area increment. The energy is taken from the area under the force-displacement curve, and the crack length is measured from the specimen:

$$G_{IC} = \frac{\int F d\delta}{aw} \tag{5.1}$$

Where $F$ is the force, $\delta$ is the displacement, $a$ is the crack length and $w$ is the width of the specimen. As can be seen in Figure 5.5 the AP-PLY curve is steeper, and the peak values before the crack starts growing are higher for AP-PLY, and after the peak the force displacement curves show a flatter behaviour. For all specimens, peaks after the initiation point are even higher than the initiation point itself, which is propably where the fibre band that is pulled up will encounter another undulation pulling it down. All these factors contribute to the higher energy needed for a crack to grow in AP-PLY in opening mode compared to a unidirectional composite laminate. Average calculated results for the fracture toughness of AP-PLY in Mode I compared to a reference [Garcia, Wardle, and Hart, 2008] can be found in Table 5.1, full results are included in Appendix E. In these tests, the AP-PLY configuration has an 89.2 % higher Mode I fracture toughness than a unidirectional specimen.

Table 5.1: Average Mode I results for Baseline and AP-PLY

| | **Mean [$J/m^2$]** | **St. Dev. [%]** | **Reference [$J/m^2$]** |
|---|---|---|---|
| Baseline | 204.6 | 6.83 | 210 |
| AP-PLY | 387.1 | 7.41 | - |

### 5.2.2 Mode II

A four-point bending end notch flexure test was used to determine the Mode II fracture toughness, as this is considered more accurate than three point bending due to the stable delamination growth [Martin and Davidson, 1999]. The test is conducted according to ISO Standard [ISO, 2002] with 6 specimens of 250 *mm* length, 15 *mm* width, 2 *mm* thickness and a foil insert of 65 *mm*.

#### Mode II Results

After performing a four-point bending fracture toughness test, the critical fracture toughness value can be calculated according to the previously mentioned standard:

$$G_{IIC} = \frac{9P_{cr}\delta_{cr}}{2W(9a + 5d - 4L)} \tag{5.2}$$

Where: $P_{cr}$ is the critical load, $\delta_{cr}$ is the corresponding critical machine head displacement, $W$ is the width of the specimen, $a$ is the initial crack length, $d$ is the distance between the two loading points and $L$ is the length between the supports. A typical plot of the force displacement curve of a Mode II test for a unidirectional specimen (black) and an AP-PLY specimen (red) can be found in Figure 5.6.

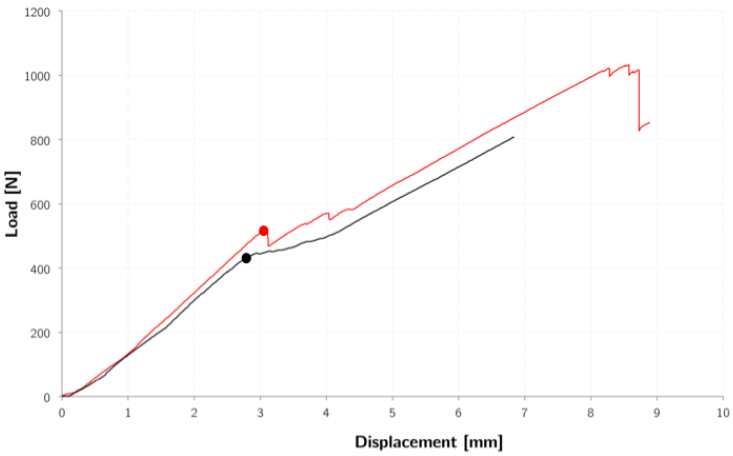


Figure 5.6: Mode II force-displacement curves for baseline (black) and AP-PLY (red)

In Mode II, AP-PLY does not seem to yield such a large improvement as in Mode I, but the behaviour is significantly different from the baseline. Instead of a gradual deviation from the linear line as in the baseline, AP-PLY specimens continue longer in a linear fashion and then show a sudden short drop, after which they continue again parallel to the baseline. The point where the load drops or deviates from the linear trend, shown with a colored dot in Figure 5.6, is taken as critical and used for the calculations. Average results from 6 specimens compared to a reference [Garcia, Wardle, and Hart, 2008] can be found in Table 5.2, full results are included in Appendix E. In these tests, the AP-PLY configuration has a 20.0 % higher Mode

II fracture toughness than a unidirectional specimen of the same material and with the same layup.

Table 5.2: Average Mode II results for Baseline and AP-PLY

| | **Mean [$J/m^2$]** | **St. Dev. [%]** | **Reference [$J/m^2$]** |
|---|---|---|---|
| Baseline | 366.9 | 5.16 | 350 |
| AP-PLY | 440.4 | 2.59 | - |

## 5.3 Short Block and Open Hole Compression Tests

In structures, often holes and connections are present, which in general weaken a structure. Greatly exaggerated, damage in a structure could be viewed as a hole, completely ignoring the material still present and thus even being conservative. It is expected that AP-PLY will show different behaviour in these elements with edge effects than in elements made from laminates with unidirectional layers.

### 5.3.1 Short Block Compression

Before testing the open hole specimens, the compression strength and stiffness of the pristine laminates are tested in short block compression (SBC). These small specimens are designed not to buckle but to fail under pure compression. The AITM 1-0008 standard is used with a slightly adapted specimen size of 32 x 50 *mm*. The standard prescribes a thickness of 3-5 *mm* and a quasi-isotropic layup, resulting for this material in a 24 layer laminate with a quasi-isotropic layup of 4.3 *mm* thickness. Specimens are fitted with strain gauges on the front and on the back side of the specimen, to be able to observe unwanted buckling behaviour. In Table 5.3 a summary of the results is shown for the baseline UD 45° and AP-PLY 1 45° 1/4 for 3 specimens each. Full results can be found in Appendix D.

As the results indicated a large difference in scatter between the baseline and AP-PLY specimens, estimates for the A and B basis allowables are also given in Table 5.3. These estimates are calculated using the procedure given in MIL-HDBK-17-3F (2002), and represent a knockdown of the average based on the standard deviation and the number of specimens tested.

The stiffness of the AP-PLY specimens for short block compression was higher than for the baseline, which was not expected due to the undulations present in AP-PLY. Because of the small number of specimens no reliable conclusion can be drawn, but the small or no influence on stiffness of AP-PLY was shown before in the compression tests of pristine CAI specimens. The considerably lower strength in compression was, to some extent, expected, as the undulations in AP-PLY act as crack initiators. Together with the higher scatter in AP-PLY, the calculated allowables are considerably lower than those for the baseline specimens with unidirectional plies.

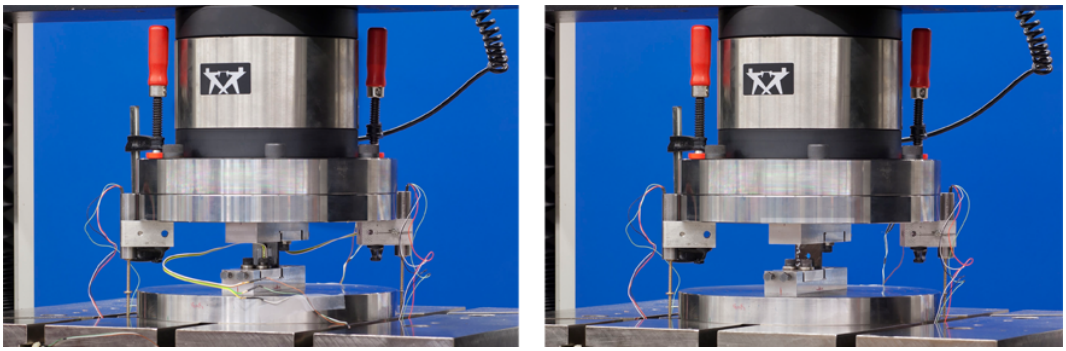

Figure 5.7: SBC (left) with strain gauge and OHC (right) test setups

Table 5.3: Short Block Compression results for Baseline TS UD 45° and TS AP-PLY 1 45° 1/4

| | AP-PLY | Baseline | Difference [%] |
|---|---|---|---|
| E-modulus (GPa) | 45.12 | 43.85 | + 2.9 |
| Mean maximum stress (MPa) | 599.0 | 625.0 | - 4.2 |
| Mean maximum strain ($\mu\epsilon$) | 13270 | 14250 | - 6.9 |
| B allowable stress (MPa) | 513.6 | 586.3 | - 12.4 |
| A allowable stress (MPa) | 452.6 | 558.7 | - 19.0 |

### 5.3.2 Open Hole Compression

Now that the pristine strength and stiffness under compression are known, the knock down for the presence of a hole can be determined. Specimens are exactly similar to SBC, with a hole of 6.35 *mm* right in the middle. No more room is left for strain gauges, but with the same LVDT's a reliable value for the stiffness can be computed. In Table 5.4 a summary is shown of the results for baseline TS UD 45° and TS AP-PLY 1 45° 1/4 with 6 specimens each. Full results can be found in Appendix D.

For open hole compression strength the maximum stress is higher for AP-PLY, meaning a positive influence on the compression strength in the presence of a hole. It is believed that the AP-PLY pattern slows down damage growth in the vicinity of the hole and is responsible for the moderate increases in strength observed here. On top of that, the scatter in the AP-PLY results is in this case considerably lower, leading to higher allowables. Although not a spectacular improvement, the results are promising for future work focussing on this aspect of the AP-PLY fibre placement architecture.

Table 5.4: Open Hole Compression results for Baseline TS UD 45° and TS AP-PLY 1 45° 1/4

| | AP-PLY | Baseline | Difference [%] |
|---|---|---|---|
| Mean maximum stress (MPa) | 329.3 | 327.2 | + 0.6 |
| B allowable stress (MPa) | 293.5 | 285.5 | + 2.8 |
| A allowable stress (MPa) | 262.9 | 251.3 | + 4.6 |
| Mean maximum strain ($\mu\epsilon$) | 6500 | 6530 | - 0.5 |

## 5.4 Bearing Tests

Bearing specimens should be designed such that they fail in the correct bearing failure mode, and not in shear-out or net-tension which is shown in Figure 5.8. Bearing tests are performed according to standard ASTM (2009a) with both a pretensioned bolt and a pin, resulting in a different behaviour. Specimens are 150 *mm* in length and 35 *mm* width, with the hole located 25 *mm* from edge in the middle of the specimen.

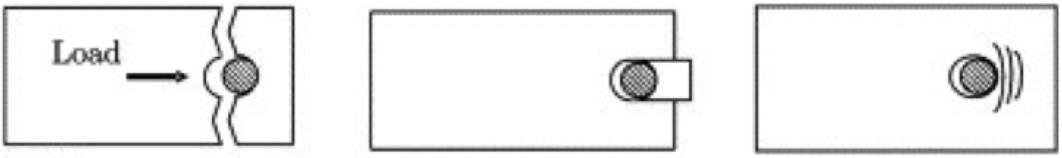


Figure 5.8: Net-tension, shear-out and bearing failure [Camanho and Lambert, 2006]

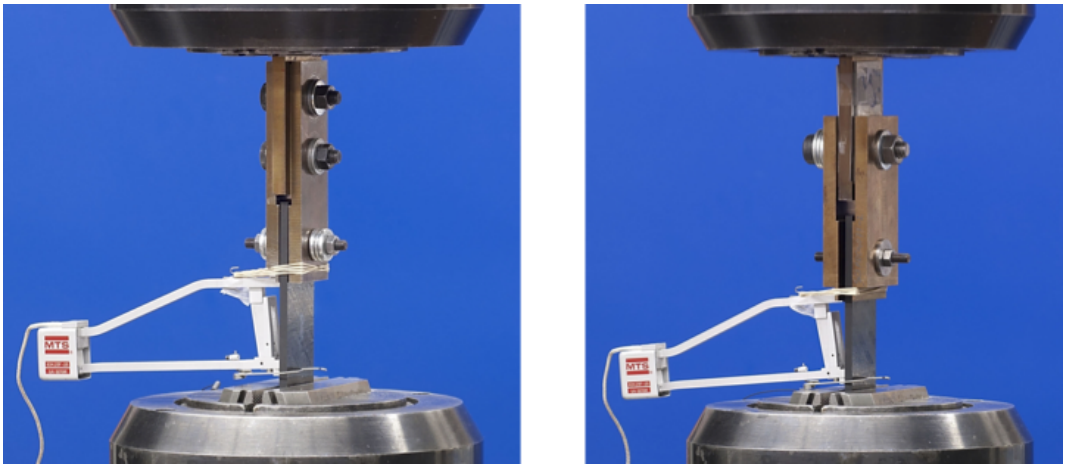

Figure 5.9: Bolt (left) and Pin (right) Bearing Test Set-Up

### 5.4.1 Pin Bearing

In pin bearing, the steel pin is not pretensioned but just kept in place by a nut and washer, with a spacing of 0.5 *mm* on both sides of the specimen. The right picture in Figure 5.9 shows the test set-up. Table 5.5 shows a summary of the results for baseline and AP-PLY, with 6 specimens each. Full results can be found in Appendix D.

### 5.4.2 Bolt Bearing

For bolt bearing, the pin is pretensioned with a torque of 1.3 Nm. All other specifications are the same as for pin bearing. The left picture in Figure 5.9 shows the test set-up. Table 5.6

Table 5.5: Pin Bearing results for Baseline TS UD 45° and TS AP-PLY 1 45° 1/4

| | AP-PLY | Baseline | Difference [%] |
|---|---|---|---|
| Mean maximum stress (MPa) | 685.0 | 676.7 | + 1.2 |
| B allowable (MPa) | 650.6 | 613.2 | + 6.1 |
| A allowable (MPa) | 622.4 | 561.2 | + 10.9 |

Table 5.6: Bolt Bearing results for Baseline TS UD 45° and TS AP-PLY 1 45° 1/4

| | AP-PLY | Baseline | Difference [%] |
|---|---|---|---|
| Mean maximum stress (MPa) | 1066.0 | 1076.0 | - 0.9 |
| B allowable (MPa) | 998.7 | 974.8 | + 2.5 |
| A allowable (MPa) | 943.6 | 891.8 | + 5.8 |

shows a summary of the results for baseline and AP-PLY, with 6 specimens each. Full results can be found in Appendix D.

A similar behaviour to the OHC tests is observed in the bearing tests; a similar average maximum stress, but due to a considerably lower scatter higher calculated allowable values. In these bearing tests, the material is pushed aside and thus out-of-plane by the pin. Fibres in the thickness direction present in the AP-PLY pattern act as (matrix) crack stoppers and delay or slow down delaminations, thereby increasing the bearing strength. This effect is larger in the pin bearing tests, possibly because in the bolt bearing specimens the laminate is obstructed in the thickness direction by the bolt pretension.

## 5.5 Discussion of AP-PLY performance

Even tough the un-notched strength of AP-PLY laminates is lower, notched and bearing strengths, which are the typical design conditions in an aerospace application, are higher. The ability of AP-PLY to slow down damage emanating from a stress riser such as a hole (open or bolted) offsets the negative effect the undulations have on un-notched strength.

## 5.6 Non-monolithic Configurations

Apart from non-impact related mechanical properties such as the above, also structural configurations other than monolithic flat panels were investigated during the research. Although less elaborated than the monolithic setup, two interesting configurations, namely a sandwich panel and a cylindrical structure, are presented below.

### 5.6.1 Sandwich

The thin facesheets that make a sandwich panel very efficient, are also its weakness. With a very limited amount of material a very high bending stiffness can be achieved. From a damage point of view however these thin facesheets are very easily penetrated by a foreign

object. Their high bending stiffness prevents damage due to in-plane stresses on the bottom facesheet, but the impact energy has to be dissipated. Once damaged, moisture builds up inside which increases the weight and negatively affects the mechanical behaviour. The vulnerability of the facesheets is one of the reasons why sandwich panels are not used more extensively in aerospace structures. To increase the damage tolerance of composite sandwich structures, AP-PLY was used to interweave the plies in the facesheet. CAI tests (Figure 5.10) were performed to assess the damage resistance and damage tolerance [Arzoni, Nagelsmit, and Van Langen, 2012]. The test set-up was taken similar to the monolithic CAI, with specimens of 100 x 150 *mm*. A representative configuration was chosen to have thermoset quasi-isotropic facesheets with four plies and a 0.5' honeycomb core, with the AP-PLY 1 45° 1/4 configuration.

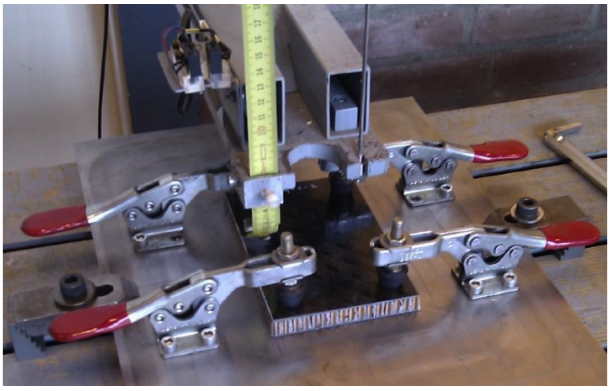

Figure 5.10: Sandwich impact test setup.

Compression after impact tests of which the results are shown in Table 5.7 indicate a comparable improvement for the AP-PLY configuration as in monolithic laminates. As the cross-section of the facesheets is difficult to measure, no stress levels but the loads at failure of the static test machine are compared.

Table 5.7: Sandwich CAI results, averages from 3 impacts at 2.5 J

| | **Indentation [mm]** | **Residual Strength [kN]** |
|---|---|---|
| Unidirectional | 0.90 | 26.5 |
| AP-PLY | 0.94 | 29.6 |

### 5.6.2 Cylindrical Tube

In a commercial R&D project at NLR, tubes with a diameter of 111 *mm* and a wall thickness of 1.1 *mm* were manufactured using fibre placement. Having only six plies, vulnerability was an issue combined with pressure carrying requirements. The design with unidirectional layers was adapted for AP-PLY by interweaving all six plies in the Skip 1 Total Half pattern. A large tube was cut into specimens of 50 *mm* length which were impact tested at different energy levels. A special fixture was manufactured out of wood, to support the cylindrical specimen during impact over its lower half and preventing sideways motion. A difference in manufacturing

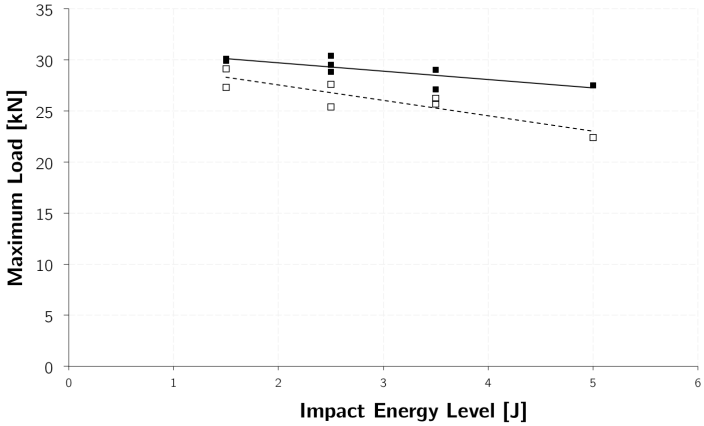


Figure 5.11: Sandwich CAI results for UD (white) and AP-PLY (black) facesheets

for the tubular structure compared to flat panels was that no cover plate was used during manufacturing, but a vacuum bag. In Figure 5.12 a cross-section of the laminate is shown. It is clear that the overlapping regions are less compacted and thickness differences arise. It will have to be investigated whether this also occurs in flat laminates without a cover plate, and whether this can be solved. After impact, the delamination sizes were measured using ultrasonic C-scan.

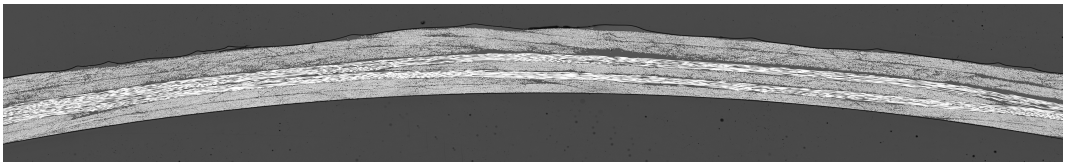

Figure 5.12: Cross-section of a circular tube with the AP-PLY fibre architecture

As the velocity of the impactor is measured before and after impact, the dissipated energy can be calculated analogous to the procedure described in Chapter 3. Looking at Table 5.8, it is immediately clear that especially for the higher impact energy levels the AP-PLY tubes dissipate less energy than the unidirectional tubes. As damage creation is a large dissipator of energy, this implies that less damage is created in the AP-PLY specimens and that the improvement is larger for higher impact energy levels.

Table 5.8: Tube dissipated energy results, averages for 5 J and 10 J.

| | **Average Dissipated Energy** [*J*] | **St. Deviation** [%] |
|---|---|---|
| Unidirectional, 5 J, 3 specimens | 2.09 | 3.12 |
| Unidirectional, 10 J, 2 specimens | 7.11 | 3.59 |
| AP-PLY, 5 J, 3 specimens | 2.10 | 22.49 |
| AP-PLY, 10 J, 2 specimens | 6.27 | 1.49 |

In Table 5.9 and Figure 5.13 the results of the C-scans are shown. Very large improvements in the projected delamination size, ranging from 50-60%, were found for the AP-PLY tubes. Also the standard deviation is much larger for the delamination size in the AP-PLY specimens. More specimens should be tested to determine more reliable material behaviour for these thin-walled tubes, but these preliminary results are promising.

Table 5.9: Tube delamination size results, averages for 5 J and 10 J.

| | **Delamination size** [$mm^2$] | **St. Deviation** [%] |
|---|---|---|
| Unidirectional, 5 J, 3 specimens | 1231 | 5.44 |
| Unidirectional, 10 J, 2 specimens | 2304 | 1.07 |
| AP-PLY, 5 J, 3 specimens | 470 | 32.96 |
| AP-PLY, 10 J, 2 specimens | 1141 | 28.63 |

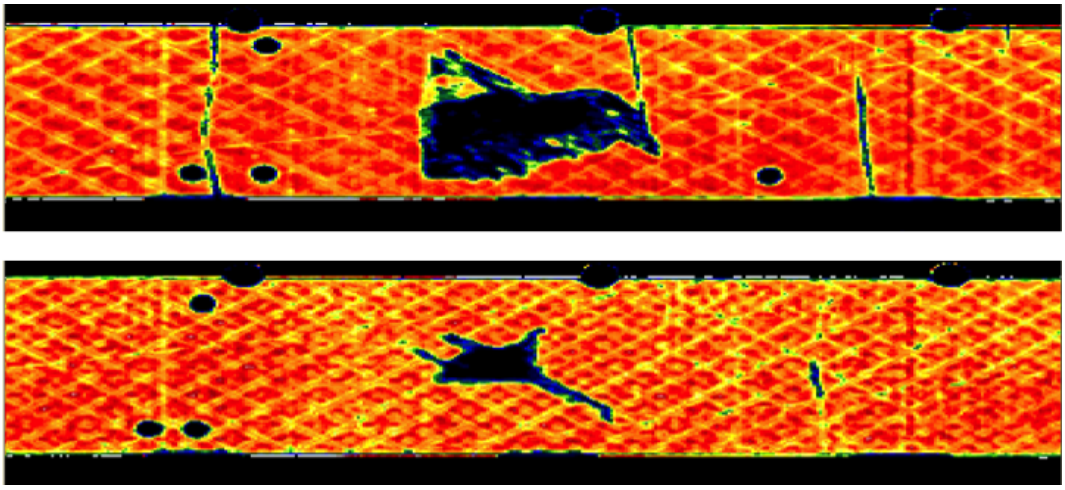

Figure 5.13: C-scans of impacted cylindrical specimens with unidirectional (top) and AP-PLY (bottom) laminates.

### 5.6.3 Summary

The performance of AP-PLY composite laminates for some important mechanical properties other than compression after impact has been tested such as open hole compression and bearing. In general, the scatter is lower and the mean values are similar or higher than those of their unidirectional counterparts. This could lead to higher allowables for design. Also in cylindrical form and in sandwich facesheets, AP-PLY can significantly improve the damage behaviour of composite laminates. In the next chapter, an attempt is made to model the delamination profile of composite laminates to further improve the AP-PLY fibre architecture.

# Chapter 6

# Delamination Prediction

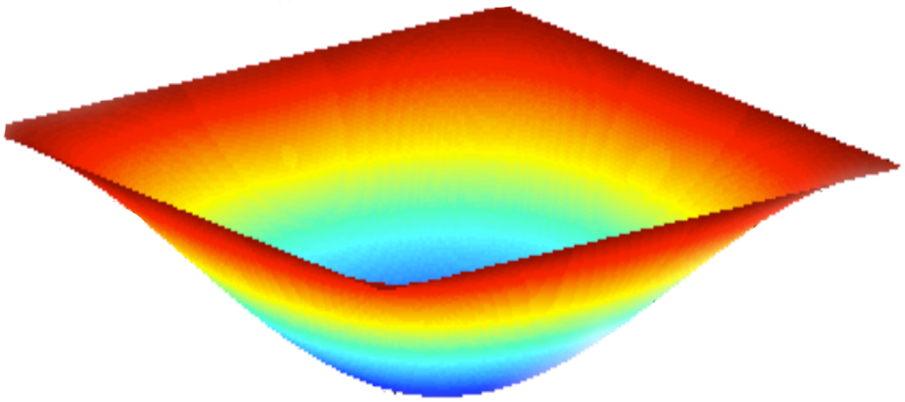

## 6.1 Introduction

In chapter 4 of this thesis, the best in-plane AP-PLY pattern of all tested conifgurations was identified using an experimental design of experiments approach. Improvements in residual strength after impact were fairly limited, whereas delamination size measurements and fracture toughness tests implied that a larger improvement can be achieved. This improvement is sought in determining the plies to interweave; when all plies are interwoven, not enough energy is dissipated or it is dissipated by damage mechanisms like fibre breakage which limit the compression after impact strength. When no plies are interwoven, almost every interface will have a large delamination. The optimal laminate is believed to lie somewhere in between, with some sacrificial plies to dissipate energy and some interwoven plies that form stable sublaminates improving the residual compressive strength after impact.

To be able to decide which plies to interweave, the tendency to delaminate for each ply interface has to be predicted. One approach is to use a stiffness and strength based model, that uses the stiffness difference between adjacent sublaminates as a measure for the tendency to delaminate. From this same model, the stresses and strains can be retrieved for applying a failure criterion, which can be used to determine which plies fail first.

## 6.2 Plate Deflection

One of the parameters that influence delamination creation is the stiffness mismatch between adjacent plies. Once delaminated, the created sublaminates have a lower buckling load than the pristine laminate and as a result, the laminate fails prematurely. In both cases, stiffness is an important characteristic of the laminate, the sublaminate and each ply. Current analytical models however are only suitable for symmetric and balanced laminates. As a starting point, the well-known out-of-plane equilibrium equation for laminated plates given by Jones (1975) can be used:

$$\begin{aligned} D_{11}w_{,xxxx} + 4D_{16}w_{,xxxy} + 2\left(D_{12} + 2D_{66}\right)w_{,xxyy} + 4D_{26}w_{,xyyy} + D_{22}w_{,yyyy} - \\ B_{11}u_{,xxx} - 3B_{16}u_{,xxy} - \left(B_{12} + 2B_{66}\right)u_{,xyy} - B_{26}u_{,yyy} - \\ B_{16}v_{,xxx} - \left(B_{12} + 2B_{66}\right)v_{,xxy} - 3B_{26}v_{,yyy} - B_{22}v_{,yyy} = p. \end{aligned} \tag{6.1}$$

For symmetric laminates $B_{ij} = 0$, so Equation 6.1 simplifies to:

$$D_{11}w_{,xxxx} + 4D_{16}w_{,xxxy} + 2\left(D_{12} + 2D_{66}\right)w_{,xxyy} + 4D_{26}w_{,xyyy} + D_{22}w_{,yyyy} = p. \tag{6.2}$$

### 6.2.1 Fourier Solution

In Equation 6.2 the well known analytical solution for the deflection of a simply supported symmetrical plate can be obtained using Fourier series:

$$w = \sum_{m=1}^{M}\sum_{n=1}^{N} \sin\frac{m\pi x}{a}\sin\frac{n\pi y}{b}. \tag{6.3}$$

For different loading conditions, this results in different expressions for composite plates.

**Concentrated Load**

For a concentrated load on a simply supported plate, the Fourier solution is given by Kassapoglou (2010):

$$w = \sum_{m=1}^{M}\sum_{n=1}^{N} \frac{\frac{4p}{ab}\sin\frac{m\pi x_0}{a}\sin\frac{n\pi y_0}{b}\sin\frac{m\pi x}{a}\sin\frac{n\pi y}{b}}{D_{11}(\frac{m\pi}{a})^4 + 2(D_{12}+2D_{66})\frac{m^2n^2\pi^4}{a^2b^2} + D_{22}(\frac{n\pi}{b})^4}. \tag{6.4}$$

**Distributed Load**

The Fourier solution for a simply supported plate under a distributed load, the solution is taken from Kollár and Springer (2009).

$$w = \sum_{m=1}^{M}\sum_{n=1}^{N} \frac{16psin\frac{m\pi x}{a}\sin\frac{n\pi y}{b}}{mn\pi^6(D_{11}(\frac{m}{a})^4 + 2(D_{12}+2D_{66})\frac{m^2n^2}{a^2b^2} + D_{22}(\frac{n}{b})^4)}. \tag{6.5}$$

Advantages of Fourier series are that the simply supported boundary conditions are automatically satisfied, and that the number of terms in the series can be increased as necessary, while they are computationally efficient. The disadvantage of these Fourier series is that the $D_{16}$ and $D_{26}$ terms are disregarded, as well as the full B-matrix making them unsuitable for unbalanced and unsymmetric laminates.

### 6.2.2 Unbalanced and Unsymmetric Laminates

For unsymmetric laminates the in-plane terms from Equation 6.1 also need to be included, which require third derivatives of the in-plane deformations $u$ and $v$. Usual sine and cosine assumptions are not suitable, as their third derivatives are not equal to the original function. For this reason so-called Legendre polynomials are used.

### 6.2.3 Legendre Polynomials

Legendre functions are solutions to Legendre's differential equation. When using power series to solve this equation, these solutions form a polynomial sequence of orthogonal polynomials called Legendre polynomials. As opposed to the more elegant Fourier series, they require a new polynomial for every higher order term.

The first five Legendre polynomials, plotted in Figure 6.1 for $x$, are:

$$\begin{aligned}
P_0(x) &= 1\\
P_1(x) &= x\\
P_2(x) &= \tfrac{1}{2}\left(3x^2-1\right)\\
P_3(x) &= \tfrac{1}{2}\left(5x^3-3x\right)\\
P_4(x) &= \tfrac{1}{8}\left(35x^4-30x^2+3\right)\\
P_5(x) &= \tfrac{1}{8}\left(63x^5-70x^3+15x\right)
\end{aligned}$$

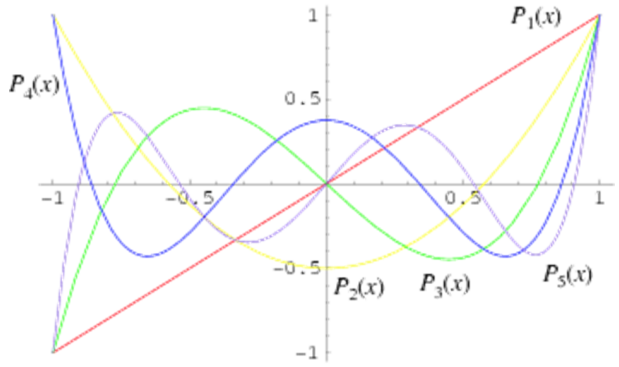


Figure 6.1: First 5 Legendre Polynomials (Source: Wolfram Mathworld)

### 6.2.4 Legendre Plate Deflection Model

A composite plate is modelled with simply supported edges to resemble the CAI test setup, which is shown in Figure 6.2. A distributed load is applied to the plate to induce the deflection that causes the stresses and strains considered in this model. At the edges, $\frac{x}{a}$ and $\frac{y}{b}$ are 1 or -1, already satisfying the boundary conditions that the bending moments are zero at the edges as $P_m''(1) = 0$.

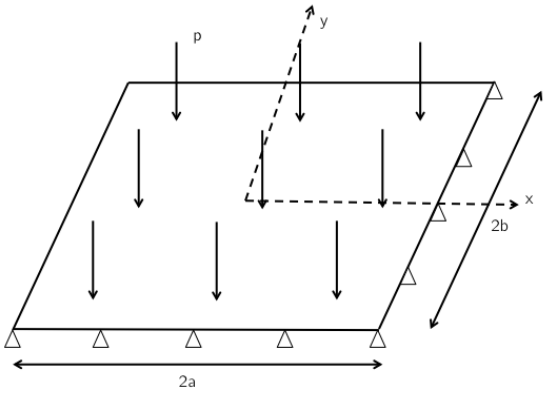


Figure 6.2: Specimen dimensions and coordinate system

The deflection of the plate is assumed to have the following shape:

$$w = \sum_{m=0}^{M} \sum_{n=0}^{N} A_{mn} P_m(\tfrac{x}{a}) P_n(\tfrac{y}{b}). \tag{6.6}$$

The distributed load $p$ is also described with Legendre polynomials:

$$p = \sum_{m=0}^{M} \sum_{n=0}^{N} B_{mn} P_m(\tfrac{x}{a}) P_n(\tfrac{y}{b}). \tag{6.7}$$

Simply supported boundary conditions are added such that all deflections and bending moments are zero at the edges.

The deflection is zero at the edges:

$$w = 0 \quad \text{at} \quad \begin{matrix} \frac{x}{a} = 1, -1 \\ \frac{y}{b} = 1, -1 \end{matrix} \tag{6.8}$$

The bending moments are zero at the edges:

$$\begin{matrix} w_{,xx} = 0 & \text{at} & \frac{x}{a} = 1, -1 \\ w_{,yy} = 0 & \text{at} & \frac{y}{b} = 1, -1 \end{matrix} \tag{6.9}$$

A system of equations is constructed in such a way that its columns are terms multiplying $A_{mn}$ and the rows are powers of $(\frac{x}{a})^i(\frac{y}{b})^j$. The rows representing the highest combined powers of $(\frac{x}{a})^i(\frac{y}{b})^j$ are replaced by boundary conditions. After a convergence study, it was decided to use $M, N = 14$, leading to a $225 \times 225$ system of equations where $8 \times 15 = 120$ rows are replaced by boundary conditions, so 105 rows are left for the original equation. This means that each of the 105 rows corresponds to a different power of $(\frac{x}{a})^i(\frac{y}{b})^j$.
The expression that has to be solved finally takes the form:

$$Ax = b \tag{6.10}$$

Where $A$ is a $225 \times 225$ coefficient matrix multiplying the vector $x$ of unknowns $A_{mn}$ and the vector $b$ in the right hand side represents the loading and values of the displacements or their derivatives according to the various boundary conditions.

Matlab's linear solver is used to calculate the values of $A_{mn}$. These can be back substituted into Equation 6.6 leading to the final expression for the deflection of the plate using Legendre Polynomials. The advantage of the present solution using Legendre polynomials is that it works when the B matrix and the $D_{16}$ and $D_{26}$ terms are non-zero, situations in which the Fourier solution fails. In the next section this model will be verified.

### Finite Element Model for Verification

A standard explicit finite element model of a $100 \times 150mm$ is constructed in Abaqus to verify the results from the Legendre model. In Figure 6.3 the linear shell plate model is shown with quad elements and a mesh size of $10 \times 10$ mm, which was sufficient for convergence.
The layup and material properties are chosen at will in the following sections for the specific verification and comparison purposes. A comparison between the finite element and Legendre series solutions can be seen in Figure 6.4.

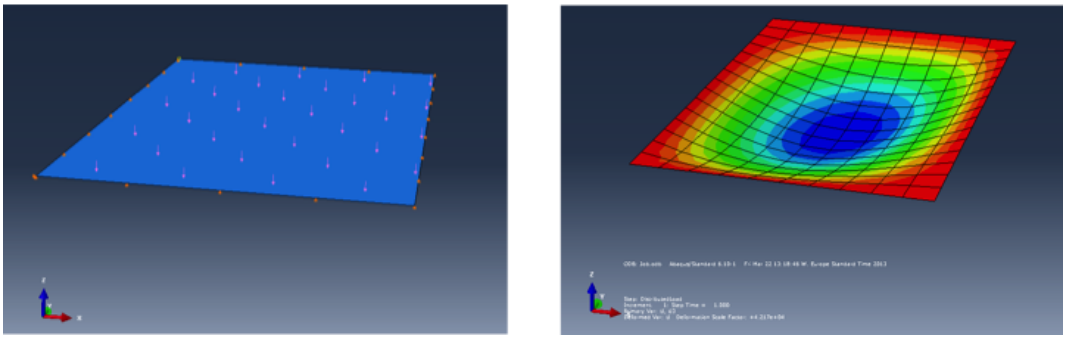

Figure 6.3: Loading of the FE model (left) and deflection example (right)

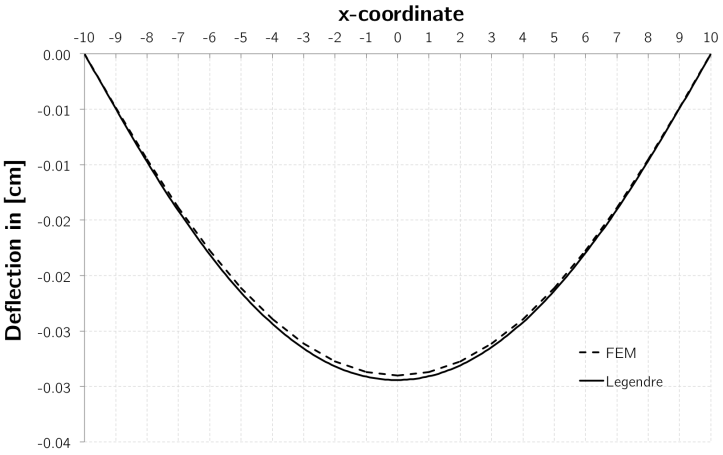


Figure 6.4: Comparison between a finite element solution and the proposed Legendre solution for a quasi-isotropic 8 ply simply supported plate under distributed loading

### Coupling Terms

Now, the Legendre deflection model is limited to symmetric and balanced laminates and verified with known solutions. To be able to include the B-matrix, also the normally ignored terms involving the B-matrix in Equation 6.1 and the in-plane equilibrium equations from Jones (1975) have to be taken into account:

$$\begin{aligned} &A_{11}u_{,xx} + 2A_{16}u_{,xy} + A_{66}u_{,yy} + A_{16}v_{,xx} + (A_{12} + A_{66})\,v_{,xy} + A_{26}v_{,yy} \\ &\quad -B_{11}w_{,xxx} - 3B_{16}w_{,xxy} - (B_{12} + 2B_{66})\,w_{,xyy} - B_{26}w_{,yyy} = 0 \end{aligned} \tag{6.11}$$

$$\begin{aligned} &A_{16}u_{,xx} + (A_{12} + A_{66})\,u_{,xy} + A_{26}u_{,yy} + A_{66}v_{,xx} + 2A_{26}v_{,xy} + A_{22}v_{,yy} \\ &\quad -B_{16}w_{,xxx} - (B_{12} + 2B_{66})\,w_{,xxy} - 3B_{26}w_{,xyy} - B_{22}w_{,yyy} = 0 \end{aligned} \tag{6.12}$$

First, for $u$ and $v$ the following expressions are selected:

$$u = \left(x^2 - a^2\right)\left(C_{10}\frac{x}{a} + C_{01}\frac{y}{b} + C_{11}\frac{x}{a}\frac{y}{b} + C_{02}\left(\frac{y}{b}\right)^2\right) \tag{6.13}$$

$$v = \left(y^2 - b^2\right)\left(F_{10}\frac{x}{a} + F_{01}\frac{y}{b} + F_{11}\frac{x}{a}\frac{y}{b} + F_{20}\left(\frac{x}{a}\right)^2\right) \tag{6.14}$$

With $C_{ij}$ and $F_{ij}$ unknown constants. Ideally, the expressions for $u$ and $v$ would be of the third order, but no converging solution could be found. Because the expressions substituted for $u$ and $v$ are of the second order, the second and third derivatives listed in Table 6.1 needed in the equilibrium equation are zero, and the corresponding stiffness terms are partly ignored. Although not perfect, the proposed model is more accurate for unsymmetric and/or unbalanced laminates than the currently used analytical expressions, which will be shown through a validation in the next section.

Table 6.1: Zero $u$ and $v$ derivatives

| Derivative | Affected Stiffness term |
|---|---|
| $u_{,yy}$ | $A_{66}$,$A_{26}$ |
| $v_{,xx}$ | $A_{16}$,$A_{66}$ |
| $u_{,xyy}$ | $B_{12} + 2B_{66}$ |
| $u_{,yyy}$ | $B_{26}$ |
| $v_{,xxx}$ | $B_{16}$ |
| $v_{,xxy}$ | $B_{12} + 2B_{66}$ |

The derivatives of these expressions are substituted in Equation 6.11 and solved for the derivatives of $w$ in terms of the constants $C_{10}$, $C_{01}$, $C_{11}$, $F_{10}$, $F_{01}$, $F_{11}$, $C_{02}$, $F_{20}$. Now, the B-related terms in the out-of-plane equilibrium equation can be taken into account while solving for $A_{mn}$.

#### Solution Process

The entire solution process of the Legendre unsymmetric and unbalanced plate deflection model is depicted in the flowchart in Figure 6.5.

### 6.2.5 Validation

Before the unsymmetric and unbalanced Legendre model is used, it is validated by comparing it to the approach by Kan and Ito (1972) and a straightforward finite element model. In Table 6.2 the material properties from Kan and Ito (1972) are shown, which were also used for validation in the Legendre and finite element model. To be able to compare the results the deflections are normalized by:

$$\frac{E_2 h^3}{F a^4} \times 10^2 \tag{6.15}$$

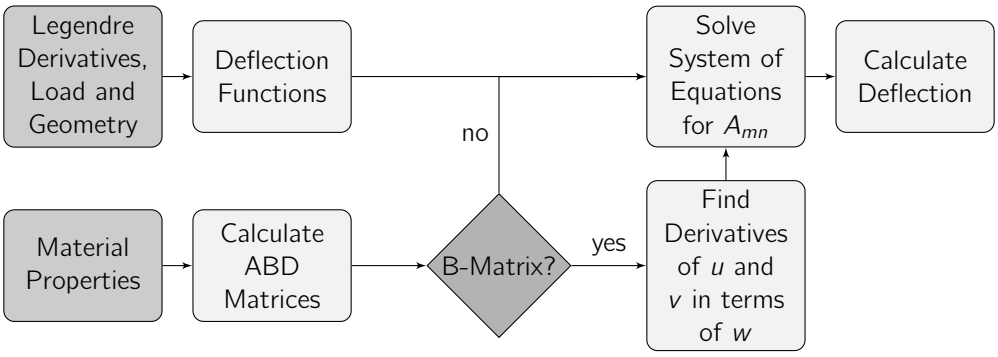


Figure 6.5: Flowchart of the solution process for the Legendre model

Table 6.2: Material and specimen properties for validation

| | | |
|---|---|---|
| $a$ | 0.1 | m |
| $F$ | -1 | N |
| $t$ | 0.1 | mm |
| $E_1$ | 400 | GPa |
| $E_2$ | 10 | GPa |
| $G_{12}$ | 10 | GPa |
| $\nu_{12}$ | 0.25 | - |

For different angle-ply layups the results are compared in Table 6.3, where $n$ is the number of plies. The table entry with 5° and $n = 6$ represents a layup of [5/-5/5/-5/5/-5].

Table 6.3: Normalized Deflections Compared to Reference [Kan and Ito, 1972]

| | $n = 2$ | | | $n = 4$ | | | $n = 6$ | | |
|---|---|---|---|---|---|---|---|---|---|
| | Ref | Leg | [%] | Ref | Leg | [%] | Ref | Leg | [%] |
| 5° | 0.4439 | 0.4030 | -9.2 | 0.4045 | 0.3931 | -2.8 | 0.3980 | 0.3921 | -1.5 |
| 30° | 0.7576 | 0.8244 | +8.8 | 0.3146 | 0.3152 | +0.2 | 0.2838 | 0.2828 | -0.4 |
| 45° | 0.7337 | 0.7547 | +2.9 | 0.2832 | 0.2829 | -0.1 | 0.2543 | 0.2563 | +0.8 |

As can be seen in Table 6.3, the results of the Legendre model correspond very well with the reference. As the laminates get thicker, for higher $n$, the deflections are smaller and the results are closer to the reference.

The layups used for verification are unsymmetric, but still balanced. To check the validity of the model for laminates which are both unbalanced and unsymmetric, a finite element model is used. In Table 6.4 the values for the deflections calculated by the Legendre, Fourier and finite element model are compared.

In all cases except for the single ply case, the Legendre model is closer to the finite element

Table 6.4: Comparison between Legendre, Fourier and FEM solutions. Deflections in *mm*.

| Layup | Legendre | Fourier | FEM |
|---|---|---|---|
| [+45] | 0.0163 | 0.0147 | 0.03139 |
| [-45] | 0.0173 | 0.0147 | 0.03139 |
| [+45/-45] | 0.0058 | 0.0018 | 0.005749 |
| [+45/-45/90/0]S | 3.0865E-5 | 3.0462E-5 | 3.165E-5 |
| [+45/-45/90/0] | 3.1002E-4 | 4.349E-4 | 2.9711E-4 |
| [0/90] | 0.0081 | 0.0034 | 0.00885 |

solution than the Fourier model. The deviation for the single ply case is most likely in the finite element model, as a single ply does not have any B-terms that can cause a deviation, but no satisfactory explanation was found. The model is deemed sufficient for the purpose of this research. For the sublaminates considered in this research, the thicker they get the more symmetric and balanced they become, and the closer the solutions are to the models that ignore the B-matrix. For further work, it would be worthwile to improve the model such that it takes all terms of the B-matrix into account.

### 6.2.6 Delamination Tendency of Multiple Quasi-Isotropic Stacking Sequences

Delaminations are created and grow during the increased load of the impactor. For different quasi-isotropic layups with 8 plies the tendency to delaminate is investigated by putting a delamination at all locations through the thickness and calculating the ratio between deflection of the top laminate and the bottom laminate for, in this case, a distributed unit load. When these ratios are added for all locations in the layup, a quantity meant to represent the total tendency to delaminate is obtained and can be compared for different alternatives. The following equation 6.16 is used to calculate the tendency to delaminate of ply interface $i$, where $N$ is the total number of plies and $\delta$ with subscript $1-i$ denotes the deflection of the part of the laminate above the delamination and $\delta$ with subscript $i-N$ denotes the deflection of the part of the laminate below the delamination:

$$tendency_i = \sum_{1}^{N} \frac{\delta_{1-i}}{\delta_{i-N}}. \tag{6.16}$$

The AS4/8552 material properties are used for the calculations in Table 6.5. The numbers in the top row indicate the ply interface number, where 1 is the lowest ply interface and 4 is the middle ply interface, where clearly the ratio is 1.
What this tendency shows is mainly the difference between different outermost ply orientations, and could be an indicator for backface splits. Because single plies are significantly softer than a package of seven or even more plies, the difference in ply orientation is more than offset by this massive stiffness difference caused by the number of plies in the other part of the laminate. As no clear distinction was found between different layups, and the results were blurred by this

Table 6.5: Tendency to delaminate based on stiffness

| Layup | 1 | 2 | 3 | 4 | Total |
|---|---|---|---|---|---|
| $[45/\text{-}45/90/0]_S$] | 291.7 | 62.5 | 0.46 | 1 | 355.66 |
| $[45/90/\text{-}45/0]_S$] | 296.2 | 36.3 | 0.15 | 1 | 333.65 |

large stiffness difference, this procedure was not deemed suitable for predicting the tendency to delaminate.

### 6.2.7 Ply Interface Failure

From the deflection shape and its curvatures, the stresses and strains for every location in every ply interface can be calculated. Details on this procedure can be found in Appendix B. Combined with a failure criterion, this gives a complete picture of in-plane failure locations for each ply interface.

#### Failure Criterion

Many criteria exist for determining composite ply failure. In this case, the combined Tsai-Hill failure criterion is chosen:

$$\frac{\sigma_1^2}{X^2} - \frac{\sigma_1\sigma_2}{X^2} + \frac{\sigma_2^2}{Y^2} + \frac{\tau_{12}^2}{S^2} = 1, \tag{6.17}$$

Where $\sigma_1$ is the stress in the principal orientation of the laminate, $\sigma_2$ is the stress in the secondary orthogonal orientation of the laminate and $\tau_{12}$ is the shear stress between the two orthogonal in-plane orientations of the laminate. In the case of compression $X$ is the failure stress of the material under compression $X_C$ and in tension $X_T$. In an analogous fashion, either $Y_C$ or $Y_T$ will be substituted for $Y$.

#### Material Properties

For all the subsequent modelling, the material properties for the thermoset AS4/8552 material processed by NLR's fibre placement machine are used. Tests are performed inhouse, and the properties are shown in Table 6.6. Also, the CAI specimen dimensions are used and the load will be varied and mentioned separately for each calculation.

#### Layup Comparison

For every location on the specimen and for every ply interface the failure index can be calculated. The size of the damage due to in-plane stresses is calculated by taking all failure indices for every location and ply interface larger than one in the 0° direction of the laminate. Every ply interface has a value corresponding to the top and bottom ply orientation, and in this case the largest value is chosen.

Table 6.6: Material and specimen properties for AS4/8552

| | | | | | |
|---|---|---|---|---|---|
| $a$ | 75 | mm | $X_C$ | 1495 | MPa |
| $b$ | 50 | mm | $X_T$ | 2042 | MPa |
| $t$ | 0.18 | mm | $Y_C$ | 257 | MPa |
| $E_1$ | 148 | GPa | $Y_T$ | 66 | MPa |
| $E_2$ | 9.65 | GPa | $S$ | 105 | MPa |
| $G_{12}$ | 4.55 | GPa | $\nu_{12}$ | 0.3 | - |

As the Legendre model is for a distributed load, and the actual impact is a point load, the value needs to be calculated from Equations 6.4 and 6.5 by calculating the value of the distributed load that induces a similar deflection to that of the point load. In Figure 6.6 the two functions are plotted. As input, a representative load from the tests is chosen to be $8000N$.

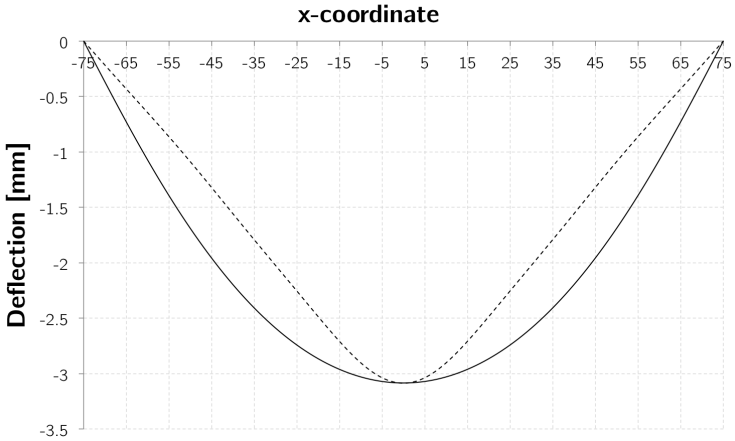


Figure 6.6: Comparison between deflections for a distributed (solid) and concentrated (dashed) load

The failure indices for the entire specimen are calculated, but only the highest values are taken for this comparison. No surprises arise from the comparison results shown in Figure 6.7 where red is a high maximum failure index and green is low: the lower plies fail first under tension, and a 90° ply high in the laminate fails early under compression. It is postulated that in-plane failure predicted with this method correlates with delaminations created at ply interfaces of adjacent failed plies. The reason is that if a ply has failed, its share of in-plane load must be transferred to adjacent (non-failed) plies by interlaminar shear which would cause delamination at the ply interface in question.

Colors are used in the pictures below, ranging from green for a small tendency to red for a high tendency to delaminate. A ply interface does not have an orientation, but for the calculation of stresses and strains this orientation is needed as input. Therefore two ply orientations are used for the interply stresses and strains, explaining the twice as high number of ply interfaces in the pictures below.

Now the failure indices are calculated for the specimens tested, with the proper layups and

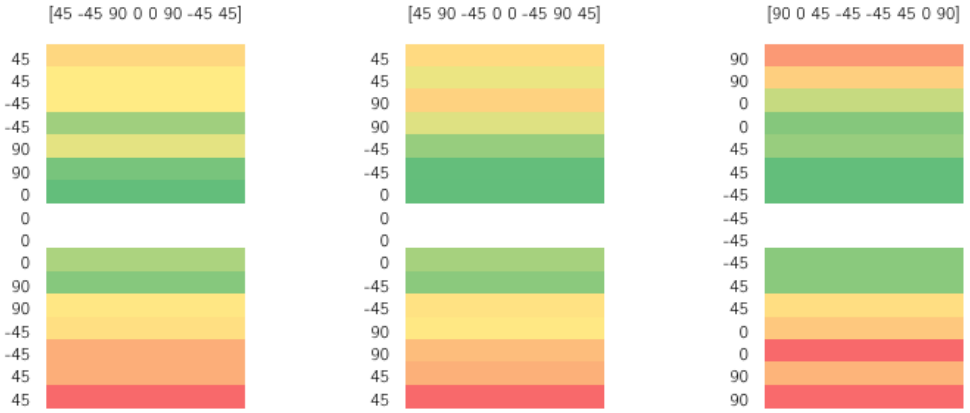


Figure 6.7: Ply interface failure

materials for the two baseline laminates. The relative comparisons in Figures 6.8 and 6.9 show the failure indices for an equivalent distributed load for a point load of 8000 $N$. Although the red areas clearly indicate which plies fail first, the failure index is nowhere higher than one and the figure is mereley illustrative and highly dependent on the applied load. For the $[45/\text{-}45/90/0]_{3S}$] layup the maximum is 0.64 and for the $[45/90/\text{-}45/0]_{3S}$] layup the maximum is 0.61.

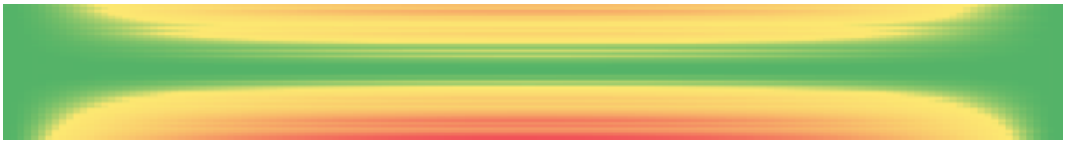

Figure 6.8: Ply interface failure for layup $[45/90/\text{-}45/0]_{3S}$] in the 0° direction of the specimen

Figure 6.9: Ply interface failure for layup $[45/\text{-}45/90/0]_{3S}$] in the 0° direction of the specimen

Apparently, the bending of the undamaged laminate is not enough to induce in-plane failure to any ply interface for an applied out-of-plane load of 8000 $N$. It is suspected that this bending induced damage results from an increased compliance of the laminate resulting from damage induced by contact force and resulting crack growth. A fracture mechanics based approach is needed to be able to predict this damage, which will then be combined with the current strength based approach.

## 6.3 Fracture Mechanics Approach

The fracture toughness, mainly in Mode II, and general ply failure due to matrix cracks and fibre breaks, play an important role in the generation of delaminations. In a fracture mechanics approach, the previously experimentally determined values for the fracture toughness are used to determine the size and location of delaminations in a composite laminate.

### 6.3.1 Fracture Toughness

The energy release rate in Mode II due to bending is calculated using a method described by [Sun and Manoharan, 1989] and [Jih and Sun, 1993], which gives a closed form expression based on classical lamination theory and Timoshenko beam theory. The model for a 3 point bending specimen defines 2 regions (Figure 6.10), where the region below the crack is neglected.

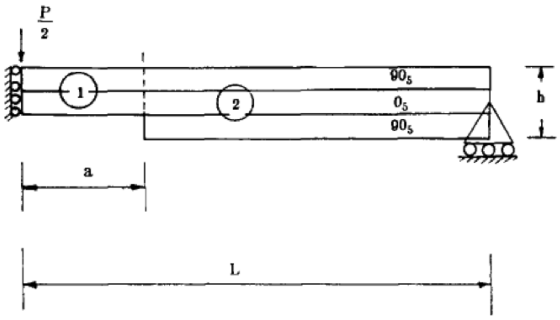


Figure 6.10: Beam Model [Sun and Manoharan, 1989]

After derivation, the equation for the energy release rate in Mode II is defined as:

$$G = \frac{P^2(L-a)^2}{8w^2}\left[\left(\frac{A_{11}}{D}\right)_1 - \left(\frac{A_{11}}{D}\right)_2\right], \tag{6.18}$$

Where $P$ is the applied force, $L$ is the length of the specimen, $a$ is the crack length, $w$ is the specimen width and $A_{11}$ the stiffness term for the two parts of the beam. $D$ is defined as:

$$D = A_{11}D_{11} - B_{11}^2 \tag{6.19}$$

#### Adaptation for CAI specimens

This model has been adapted to be able to model delaminations in a two-dimensional specimen, see Figure 6.11. The crack length $a$ is taken as the radius of the delamination, $r$, and the width of the specimen is taken as $2r$. Now expression 6.18 can be rewritten and solved for $r$ with values for the critical fracture toughness $G_{IIC}$ and specimen length $L = 75$.
As an illustration, the value for the fracture toughness $G$ in each ply interface is plotted against delamination diameter $r$ in Figure 6.12 for a UD 90° CAI specimen. The dotted red line shows

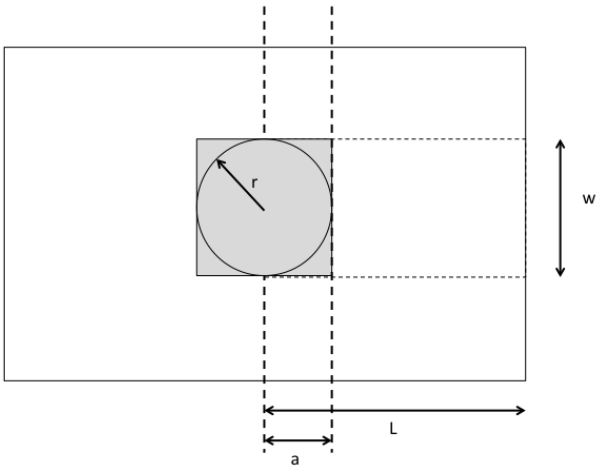


Figure 6.11: Configuration of the adapted delamination model

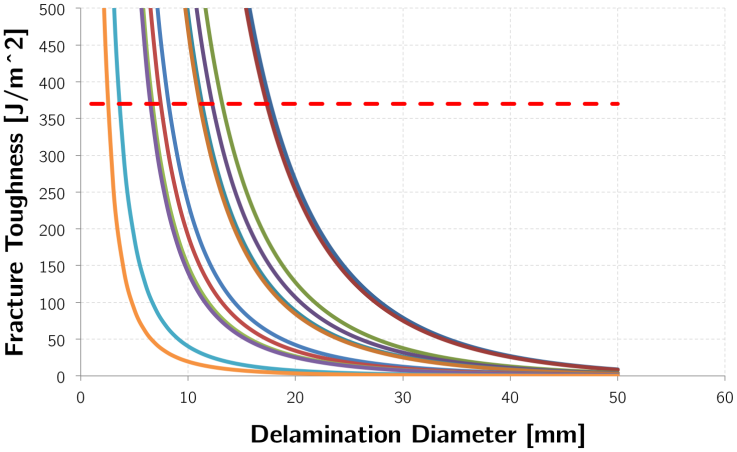


Figure 6.12: Plot of the fracture toughness vs delamination diameter in each ply interface below the mid-plane, with the rightmost curve for the mid-plane and the leftmost curve for the lowest ply interface

the critical fracture toughness $G_{IIC}$. For the same UD 90° specimen, also the delamination radius is plotted against the load in Figure 6.13.

This approach will always yield a value for $r$, as the width of the specimen is adapted together with the crack length. With delaminations above the mid-plane, this model does not give reliable results. Therefore only delamination profiles below the mid-plane are calculated using this model. Looking at cross-sections after impact (Chapter 3), this corresponds with the largest amount of damage. As laminates have to be symmetrical for practical usage, it is deemed a proper approach to look at the lower half of the laminate. In Table 6.7, the delamination profile from the mid-plane down is shown for a UD 90° layup and a UD 45° layup, with the $G_{IIC}$ value for the unidirectional ply interfaces as determined in previous tests.
The delamination sizes as calculated are the same order of magnitude (35 $mm$)of the projected

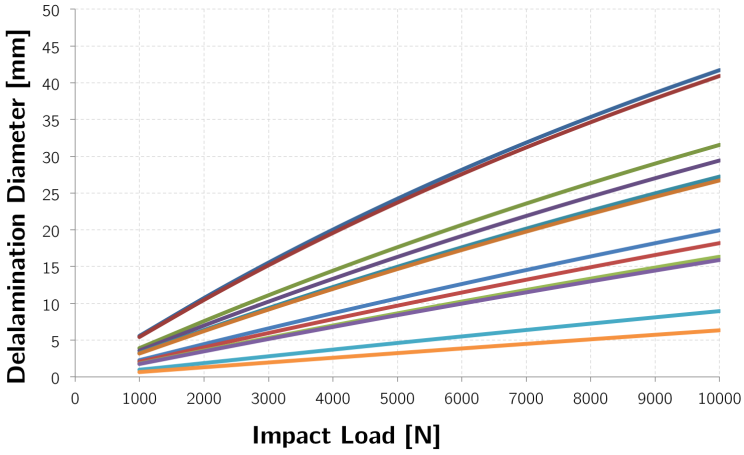


Figure 6.13: Plot of the delamination diameter vs the applied load in each ply interface below the mid-plane, with the top curve for the mid-plane and the bottom curve for the lowest ply interface

delamination sizes from the C-scans discussed in Chapter 4. As C-scans show only the projected delamination size, no detailed information is available on the size of each delamination. The two layups show no significant difference; again, as this is a stiffness approach comparing the top and bottom halves of a delaminated laminate, the more plies are added the more the two stiffnesses resemble each other.

### 6.3.2 Tendency to Delaminate; the combined approach

A model is proposed where both the fracture toughness and ply failures are taken into account to decide which plies in a laminate to interweave, which is depicted in the flowchart in Figure 6.14. After calculating the delamination profile from the fracture toughness model the largest delamination width is used the decrease the stiffness of the laminate by splitting it in two regions. The reduced bending stiffness is calculated to use in the Legendre model for calculating the ply interface stresses and strains. WIth the failure criterion, the location and the extent of the ply interface failures are calculated and the two models are superimposed. The largest delaminations from both determine the delamination profile of the laminate.

#### Stiffness Adaptation

The reduced bending stiffness is calculated by Kollár and Springer (2009):

$$D^* = D - BA^{-1}B, \tag{6.20}$$

Where the stiffness of the delaminated part is calculated in series:

$$D^*_{2,3} = D^*_2 + D^*_3, \tag{6.21}$$

Table 6.7: Delamination diameters in *mm* using the fracture toughness approach with $G_{IIC} = 370 J/m^2$

| Ply interface | UD 90° | UD 45° |
|---|---|---|
| 12 | 35 | 36 |
| 13 | 35 | 35 |
| 14 | 26 | 31 |
| 15 | 25 | 23 |
| 16 | 23 | 22 |
| 17 | 22 | 21 |
| 18 | 16 | 19 |
| 19 | 15 | 14 |
| 20 | 13 | 13 |
| 21 | 13 | 12 |
| 22 | 7 | 11 |
| 23 | 5 | 5 |

And the stiffness of the total width of the specimen $W$ is calculated in parallel, using the following relation:

$$\frac{w}{D^*_{tot}} = \frac{l_1}{D_1} + \frac{a}{D^*_{2,3}} + \frac{l_1}{D_3} + \frac{l_4}{D_4}. \tag{6.22}$$

This new stiffness $D^*_{tot}$ is fed into the Legendre model to calculate the size of the damage using the strength approach described previously.

### 6.3.3 Combined delamination profile

Parameters that influence the delamination damage profile in this approach are the material properties, the layup and the material's critical fracture toughness in Mode II, $G_{IIC}$. The two quasi-isotropic layups that were tested before in this research will be taken as baselines to be improved, namely $[45/\text{-}45/90/0]_{3S}$ and $[45/90/\text{-}45/0]_{3S}$. The impact force is again taken as 8000 $N$, material is AS4/8552 and the specimen has the standard CAI dimensions. In Tables 6.8 and 6.9 the full delamination profiles are shown for the UD 90° and the UD 45° layup respectively.

Comparing these values to the experiments is difficult as the C-scans show very irregularly shaped delaminations while the model assumes circular delaminations, and only the projected size can be measured with reasonable accuracy. More experimental study is needed, possibly with specifically designed specimens, to validate the model. In this study, the model serves as a qualitative guide to determine the best through-the-thickness distribution of the interwoven AP-PLY layers.

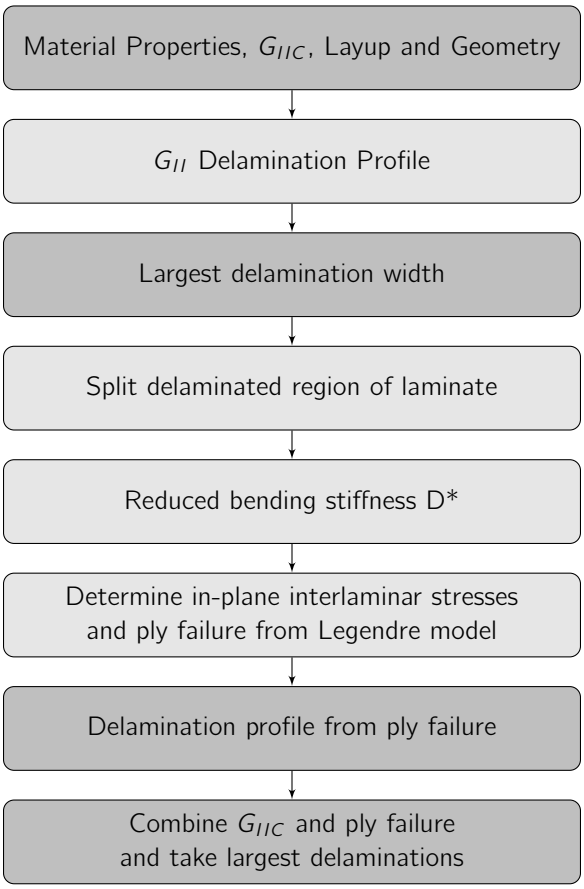


Figure 6.14: Delamination tendency model structure

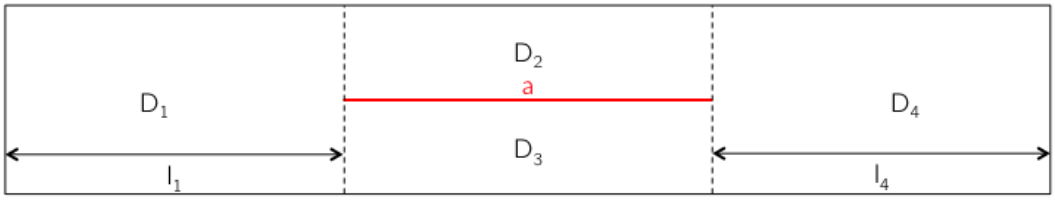


Figure 6.15: Sideview of the specimen with the largest delamination in red, and resulting regions with different stiffness

### 6.3.4 Summary and Improved Layups

A general, analytical model using Legendre polynomials is presented to calculate the deflection of unsymmetric and unbalanced composite laminates, from which also the ply stresses and strains can be calculated. Together with a fracture mechanics based model the delamination profile of a composite laminate with a certain layup can be predicted. Next, a few assumptions are made to derive the improved layups from the previously calculated delamination profiles:

Table 6.8: Delamination Profile for $[45/\text{-}45/90/0]_{3S}$

| Ply Interface | Orientation | $G_{IIC}$ | $G_{II}$ Del. Size | Failure Del. Size | Total Del. Size |
|---|---|---|---|---|---|
| Ply Interface | [°] | $[\frac{J}{m^2}]$ | $[mm]$ | $[mm]$ | $[mm]$ |
| 12 | 0 | 370 | 35 | 0 | 35 |
| 13 | 90 | 370 | 35 | 0 | 35 |
| 14 | -45 | 370 | 26 | 0 | 26 |
| 15 | 45 | 370 | 25 | 0 | 25 |
| 16 | 0 | 370 | 23 | 40 | 40 |
| 17 | 90 | 370 | 22 | 0 | 22 |
| 18 | -45 | 370 | 16 | 82 | 82 |
| 19 | 45 | 370 | 15 | 95 | 95 |
| 20 | 0 | 370 | 13 | 106 | 106 |
| 21 | 90 | 370 | 13 | 108 | 108 |
| 22 | -45 | 370 | 7 | 115 | 115 |
| 23 | 45 | 370 | 5 | 118 | 118 |

- Energy has to be dissipated by plies that contribute less to the residual strength; i.e. 45° and 90° plies
- As AP-PLY introduces a fairly limited improvement in $G_{IIC}$, interweaving layers with the AP-PLY pattern will only reduce the predicted delamination size by a fairly small amount. Therefore, mainly ply interfaces with fairly small predicted delaminations will be interwoven
- Clusters of plies that did not delaminate have to carry the load under compression, so 0° plies should be interwoven in these sublaminates
- Clusters of at least 3-4 plies have to be formed
- The laminate has to stay symmetric and balanced, including the interwoven layers

Together with the calculated delamination profiles, these assumptions lead to a new through-the-thickness distribution of the AP-PLY pattern. The final AP-PLY pattern designed on the basis of these assumptions is discussed in detail in Chapter 7. Not included are the considerations regarding damage growth due to cyclic loading. Only compression after impact is taken into account. All other loading types, such as fatigue, would be excellent topics for future research.

Table 6.9: Delamination Profile for $[45/90/-45/0]_{3S}$

| Ply Interface | Orientation | $G_{IIC}$ | $G_{II}$ Del. Size | Failure Del. Size | Total Del. Size |
|---|---|---|---|---|---|
| Ply Interface | [°] | $[\frac{J}{m^2}]$ | $[mm]$ | $[mm]$ | $[mm]$ |
| 13 | 0 | 370 | 36 | 0 | 36 |
| 14 | -45 | 370 | 35 | 0 | 35 |
| 15 | 90 | 370 | 31 | 0 | 31 |
| 16 | 45 | 370 | 23 | 0 | 23 |
| 17 | 0 | 370 | 22 | 34 | 34 |
| 18 | -45 | 370 | 21 | 49 | 49 |
| 19 | 90 | 370 | 19 | 56 | 56 |
| 20 | 45 | 370 | 14 | 92 | 92 |
| 21 | 0 | 370 | 13 | 106 | 106 |
| 22 | -45 | 370 | 12 | 108 | 108 |
| 23 | 90 | 370 | 11 | 110 | 110 |
| 24 | 45 | 370 | 5 | 117 | 117 |

Chapter 7

# Improved Layup Test Results

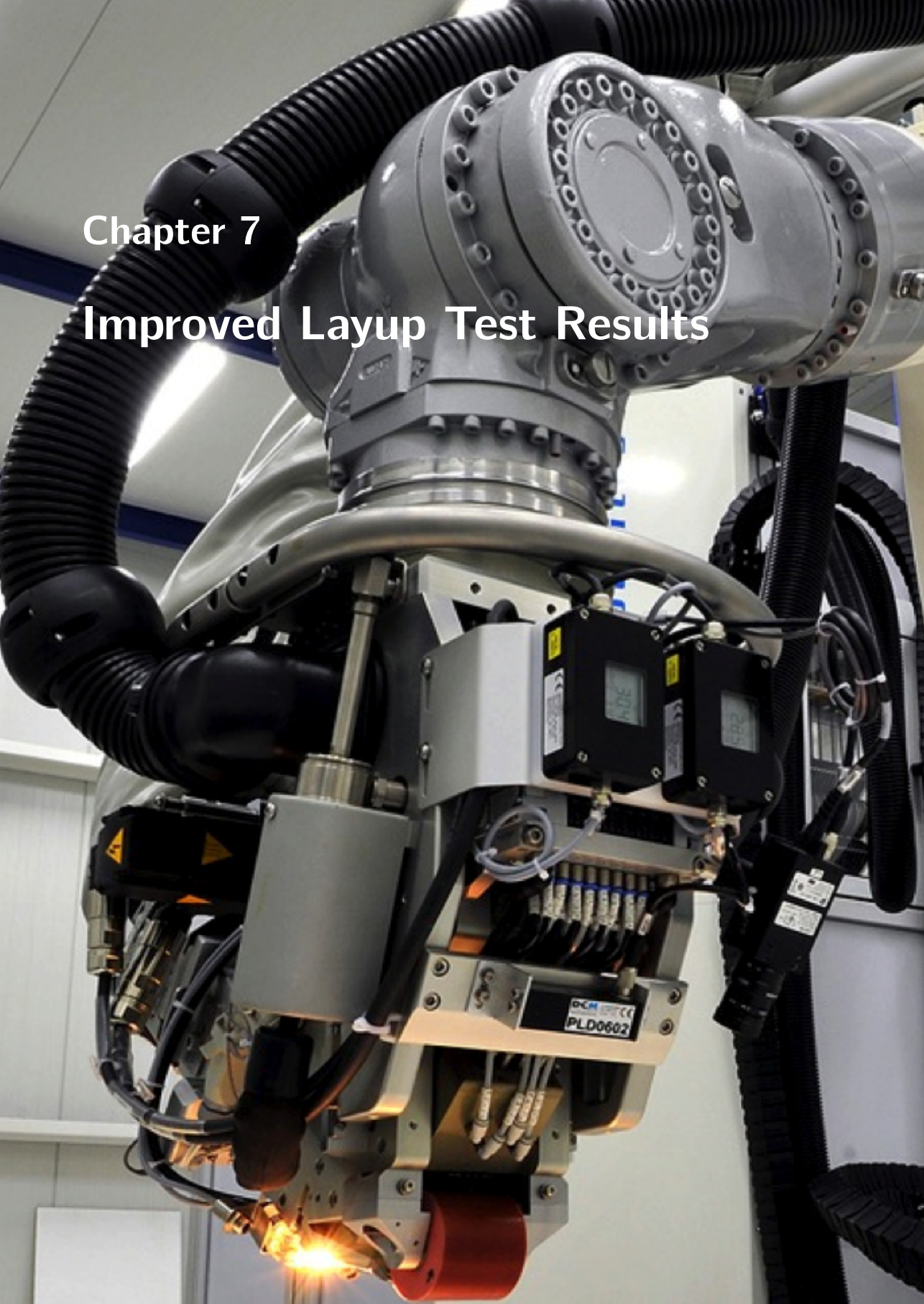

## 7.1 Introduction

As a final exercise, an improved layup is proposed based on the findings of the first series of AP-PLY tests and the modelling of the tendency to delaminate. One of the lessons from the design of experiments and literature is that not only the size of the delaminations matters, but also the location of delaminations through the thickness, which determines the thickness and layup of sublaminates. Another lesson is that when delaminations do not get a chance to initiate and/or grow, other forms of damage are needed to dissipate the energy of the impact. Depending on the loading, those can also have an adverse effect on after impact performance. Since the damage behaviour could be tuned, more improvement in the residual strength was expected based on the delamination size improvement than was seen in the first series of tests. This chapter motivates an improved layup based on findings from the previous chapter, literature, communication with experts and engineering common sense.

## 7.2 Improved Layups

The quasi-isotropice layup $[45/\text{-}45/90/0]_{3S}$ is chosen as the baseline for the last optimisation step. From Chapter 4, the best results were achieved with skipping one tow width between fibre tows in a series pattern, with a tow-width of $1/4$".

Outside +45°/-45° layers are commonly avoided in industry, because of the large difference (90°) between the two subsequent ply angles. Their advantage however is a 'softer' outer shell which is relieving stresses in open hole and bearing, and protection of the more important load carrying plies. With AP-PLY, the two 45° plies on the outside can be interwoven, what could decrease the disadvantages of this configuration because the two layers would be less susceptible to delaminations. Another possible advantage of two interwoven 45° plies could be in attachment of subcomponents, for instance stringers. Often it is seen that, in the case of adhesive bonding, the stringer pulls off the top layer of the laminate. Instead of gluing them on a single unidirectional ply, they can be attached to two directions each of which is held down by the other, decreasing or avoiding stringer pull-off.

AP-PLY has a negative impact on manufacturing time, when no adaptations are made to the fibre placement machine. Therefore, a layup with AP-PLY and UD plies combined also has two advantages combined: shorter manufacturing times and more energy dissipation due to delaminations in the UD interfaces than full AP-PLY laminates.

A first improvement to the configuration is a minimum configuration with AP-PLY only on the outside 45° layers, which will be referred to as configuration 1. The layup thus becomes:

$$[(45/\text{-}45)_{1\times 1/4}/90/0/45/\text{-}45/90/0/45/\text{-}45/90/0]_S$$

A second improvement to the configuration is a configuration with 5 plies interwoven with AP-PLY protected by three sacrificial outside plies, which will be referred to as configuration 2. The layup thus becomes:

$$[45/\text{-}45/90/(0/45/\text{-}45/90/0)_{1\times 1/4}/45/\text{-}45/90/0]_S$$

### Manufacturing time

For comparison purposes, manufacturing times normalised for a single ply are estimated and shown in Table 7.1 for the two new configurations proposed in the previous section, and compared to the normalised baseline with 24 unidirectional plies. AP-Plies are taken to require twice the placement time of a unidirectional ply, when no adaptations are made to the fibre placement machine.

Table 7.1: Placement time of AP-PLY configurations compared to the normalised reference UD

| Configuration | UD Plies | AP-Plies | Normalised Time | Difference |
|---|---|---|---|---|
| UD | 24 | 0 | 24 | - |
| Configuration 1 | 20 | 4 | 28 | +17% |
| Configuration 2 | 14 | 10 | 34 | +42% |
| Full AP-PLY | 0 | 24 | 48 | +100% |

## 7.3 Test Results

The two improved layups are tested for compression after impacted, using the same three design comparators as in Chapter 4 for the discussion in this section.

### 7.3.1 Indentation

From the indentation behaviour shown in Figure 7.1 a difference can only be seen for the higher impact energies, although on the 40 *J* energy level only one specimen was impacted. The almost identical behaviour to the baseline implies that a similar amount of energy is dissipated, and no significant difference in damage modes is expected. Previously, higher indentation values were linked to more fibre breakage and matrix cracks instead of delaminations.

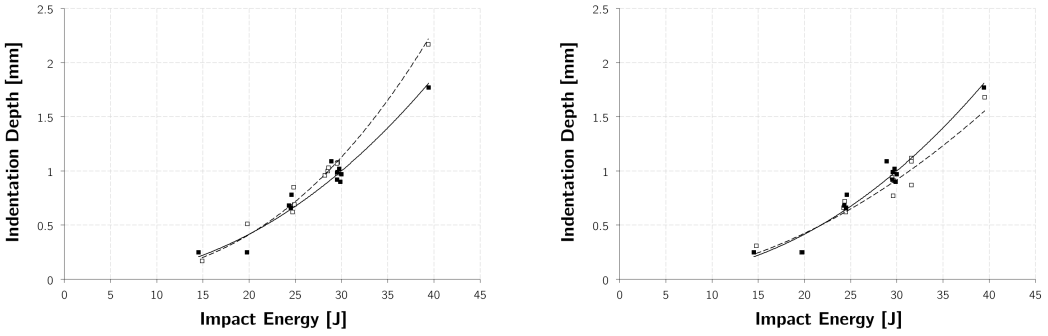


Figure 7.1: Indentation depth versus impact energy for configurations 1 (left) and 2 (right), in AP-PLY (black) and baseline (white)

### Impact force measurements

Analogous to Chapter 3, also for these tests the force during impact was recorded as well as the velocity right before and right after impact. The results for the dissipated energy are calculated from those velocities and plotted in Figure 7.2. As seen before, no clear difference can be found between the two different AP-PLY configurations and the baseline.

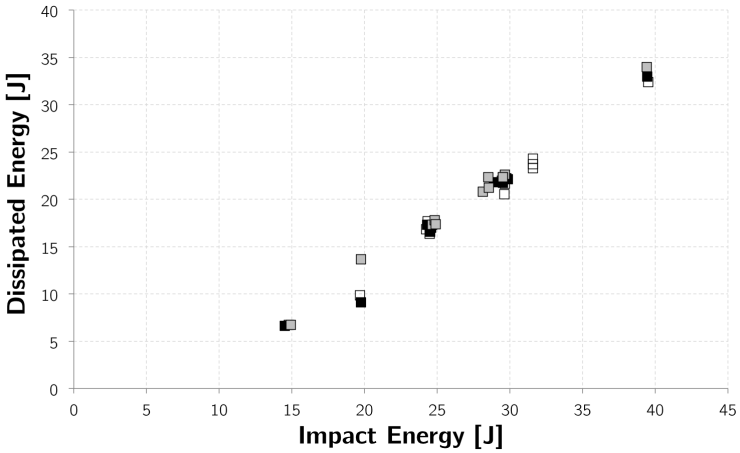


Figure 7.2: Dissipated energy versus impact energy for configuration 1 (grey), configuration 2 (black) and baseline (white)

Again an eigenfrequency was found in the Force-time signal. For this series of tests, the eigenfrequency was found to be around $11.500Hz$. All frequencies higher than $10.000Hz$ were filtered out and the average maximum force and impact time for 3 impacts at $30J$ are shown in Table 7.2.

Table 7.2: Average maximum force during impact and impact time at $30J$

| | **Maximum Force** $[N]$ | **Impact Duration** $[ms]$ |
|---|---|---|
| Baseline | 8840 | 3.84 |
| Configuration 1 | 7485 | 4.19 |
| Configuration 2 | 7721 | 3.74 |

Two main observations from Table 7.2 are that the maximum force during impact is very high for the baseline as compared to the AP-PLY configurations, and that the impact time is longest for configuration 1 with only AP-PLY in the outside two layers. The lower maximum force for AP-PLY is consistent with the measurements from the full AP-PLY specimens. An explanation for the longer impact duration in configuration 1 could be the different contact behaviour between AP-PLY and UD outside layers. A stronger outside layer could make it harder for the impactor to penetrate the specimen. Comparing these values with the results from Chapter 3 is difficult as these specimens were manufactured with a different fibre placement machine and a different batch of material.

### 7.3.2 Delamination

As predicted in the model, large delaminations arise in the outermost ply interfaces. As the configuration with those plies interwoven will decrease the size of those delaminations determining the projected delamination size, it is no surprise that its projected delamination sizes are smaller as can be seen in Figure 7.3. In configuration two, the behaviour is almost similar to the baseline, which is due to the outside unidirectional plies that result in large delaminations determining the projected delamination size.

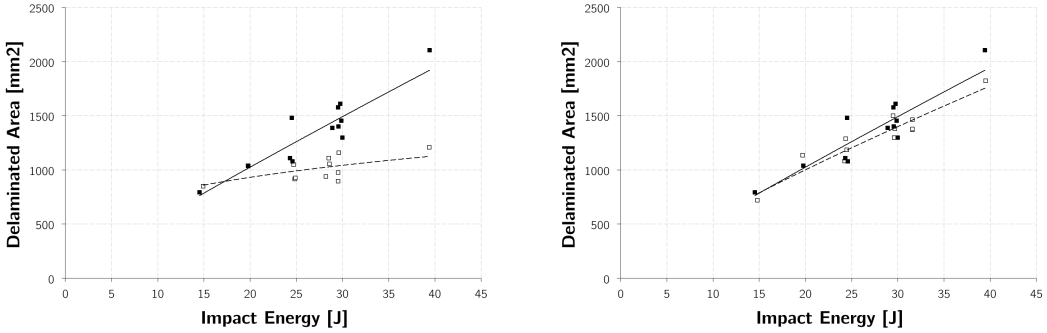


Figure 7.3: Projected delamination size versus impact energy for configurations 1 (left) and 2 (right), in AP-PLY (black) and baseline (white)

### 7.3.3 Damage Profiles

In this section, section cuts are shown in both the 0° lengthwise and 90° width direction of the specimen, to have a more complete picture of the damage profile. In the C-scans, white is the indentation at the top, between yellow and green is the mid-plane and blue is the bottom. On the top and right side of the C-scan, the B-scans of the delaminations are shown. In the vacuum bagging of the new configurations, no cover plate is used which was the case for the previous configurations. Very small thickness differences due to the pattern were observed, in the order of 0.05 *mm*, which also show up in the C-scans. Although not significant, this part of the manufacturing process of AP-PLY is something that needs further research.

#### Baseline

In the section cuts in Figure 7.4 it can be clearly seen that the delaminations are largest along the orientation of the lower ply of an interface; the whiter plies are along the direction of the section cut and all delaminations are in the resin interface above that ply. The C-scans in Figure 7.5 are merely a reference to compare the two improved AP-PLY configurations to. In the blue part, clearly the backside split is visible typical for laminates with unidirectional plies.

#### Configuration 1

In configuration 1, only the outside two plies are interwoven. In the section cut in Figure 7.6, clearly no delaminations can be seen between the outside two plies, which were visible in the

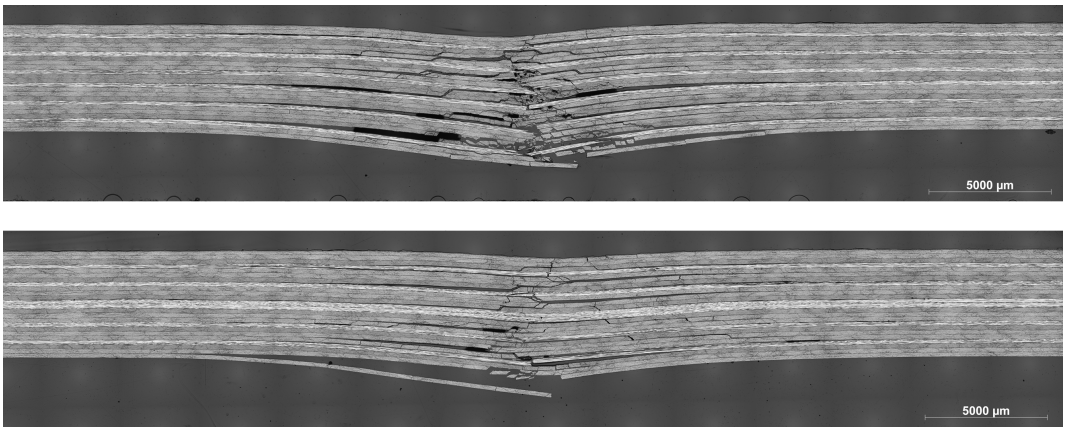


Figure 7.4: Section cut of a baseline specimen impacted with 25 $J$, cut in the 90° (top) and 0° fibre orientation (bottom)

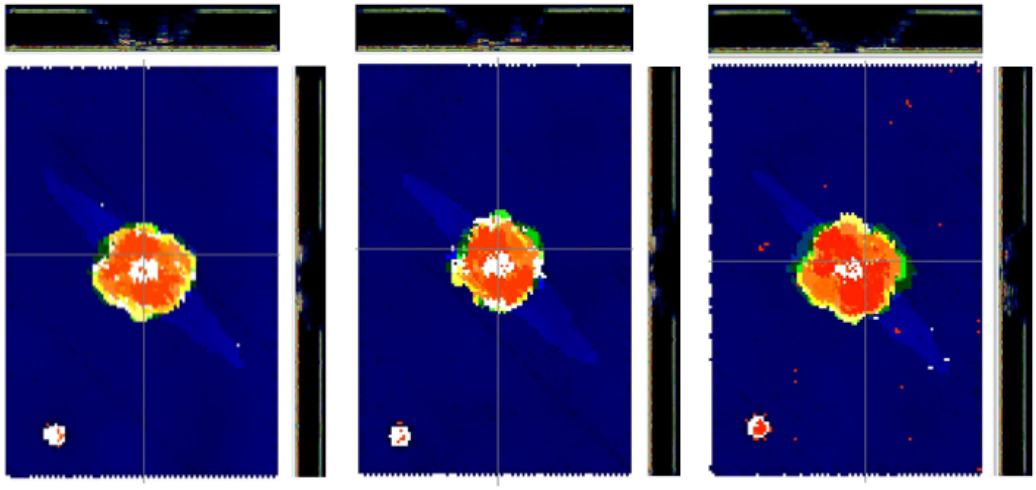

Figure 7.5: Delamination C-scans of 3 baseline specimens impacted at 30 $J$

baseline specimens. The rest of the damage, which is mainly shear matrix cracks, compares very well to the baseline.

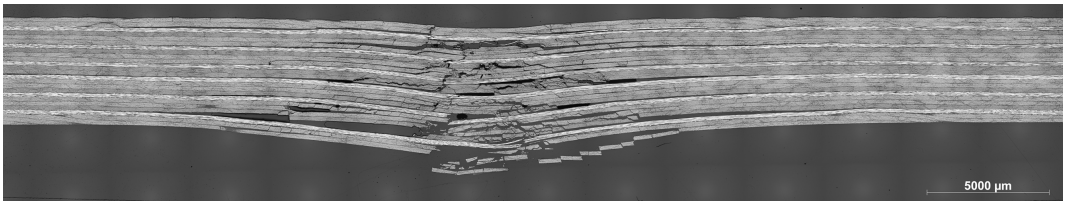


Figure 7.6: Section cut of a specimen of configuration 1 impacted with 25 $J$, cut in the 90° fibre orientation

Looking at the C-scans in Figure 7.7, clearly smaller and differently shaped delaminations are visible. The large green delamination in the leftmost picture and the smaller yellow one in the rightmost picture indicate that when delaminations are blocked by the AP-PLY pattern, the plies that do delaminate will do so in a more aggressive fashion. Also the backside splits are smaller and of different shape, as was seen before in Chapter 4.

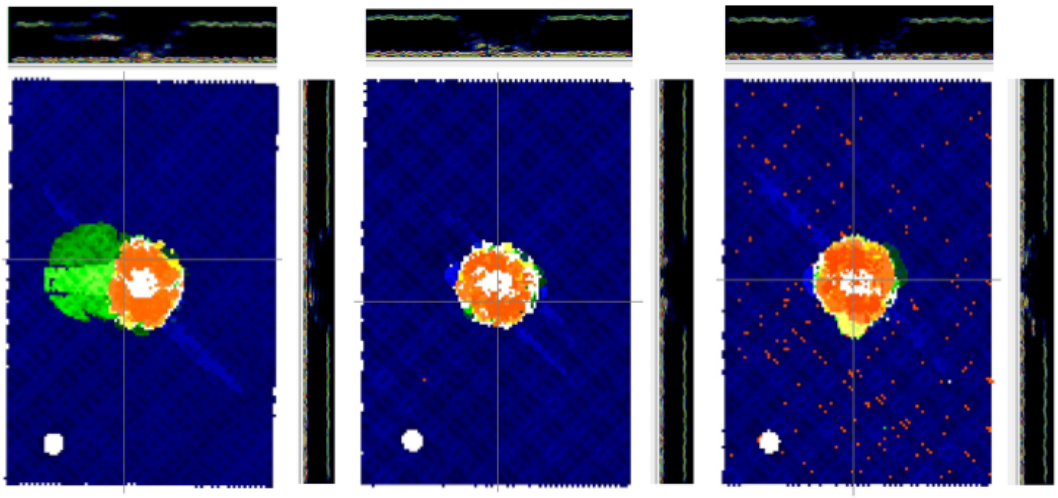

Figure 7.7: Delamination C-scans of 3 configuration 1 specimens impacted at 30 $J$

**Configuration 2**

In the section cuts of configuration 2 specimens shown in Figure 7.8, clearly more undulations due to the two packages of 5 interwoven AP-PLY plies are present. Especially the 0° direction shows less matrix cracks in the top part than the 90° direction. Large delaminations are seen in the bottom and top ply interfaces and the mid-plane, which are undirectional and allowed to delaminate. Because of the unidirectional outside plies, again large backside splits are visible in the C-scans of configuration 2 shown in Figure 7.9. Fewer 'red' delaminations are seen, indicating that the delaminations are located further to the bottom of the laminate, which is supported by the bottom section cut in Figure 7.8 and the B-scans.

### 7.3.4 Residual Strength

As the final and most important part of the CAI tests, the residual strength is plotted against the impact energy for both new configurations compared to the baseline in Figure 7.10. Configuration 1 shows an improvement, especially at 30 $J$, although small. Configuration 2 is the clear winner, with all specimens performing better than their baseline counterparts. As previous results for full AP-PLY laminates could sometimes be explained as within experimental scatter, this new configuration raises no doubt about the better performance of composite laminates with judicious use of the AP-PLY fibre placement architecture. The plies that are interwoven play an important role in energy dissipation and creating sublaminates that survive the impact.

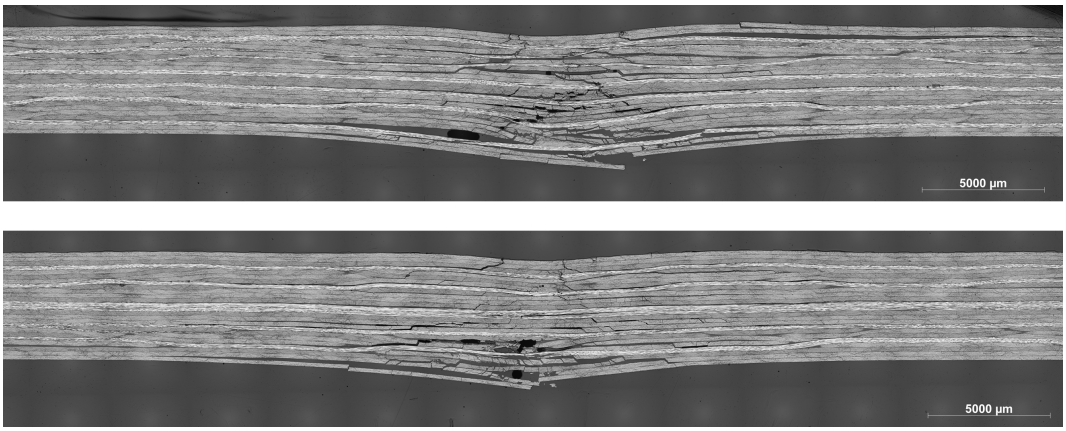


Figure 7.8: Section cut of a specimen of configuration 2 impacted with 25 *J*, cut in the 90° (top) and 0° fibre orientation (bottom)

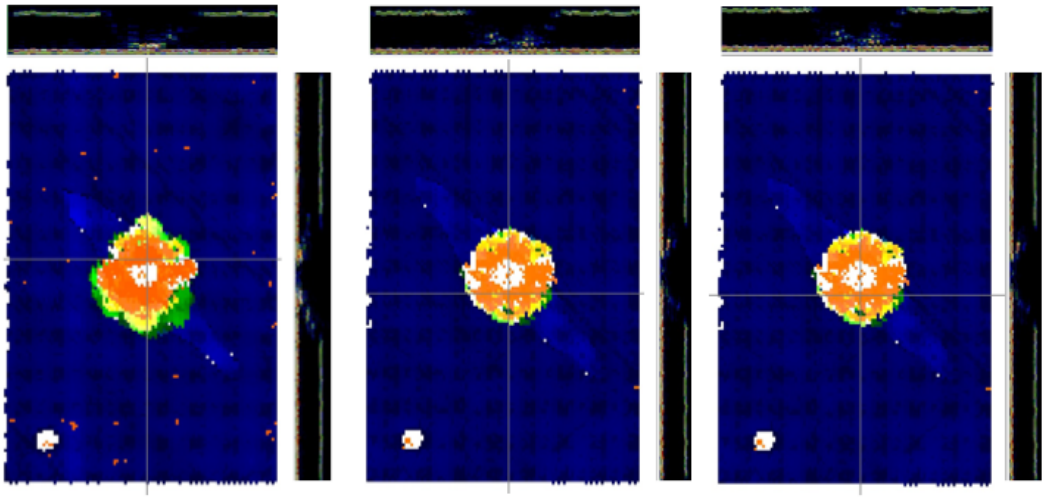

Figure 7.9: Delamination C-scans of 3 configuration 2 specimens impacted at 30 *J*

With an improved model of the damage behaviour with an AP-PLY pattern, it is expected that even better combinations of AP-PLY and UD plies in composite laminates can be designed.

### 7.3.5 Summary

In Table 7.3 the results for all impacts of both configurations are shown compared to the baseline. Both configurations perform better than the baseline laminate with unidirectional plies, in terms of the most important parameter residual strength. The same percentage improvement as with full AP-PLY laminates is achieved with interweaving only 4 plies, although the full impact energy spectrum should be taken into account. The indentation depth of the baseline and configuration 1 are similar, while configuration 2 had smaller indentation depths.

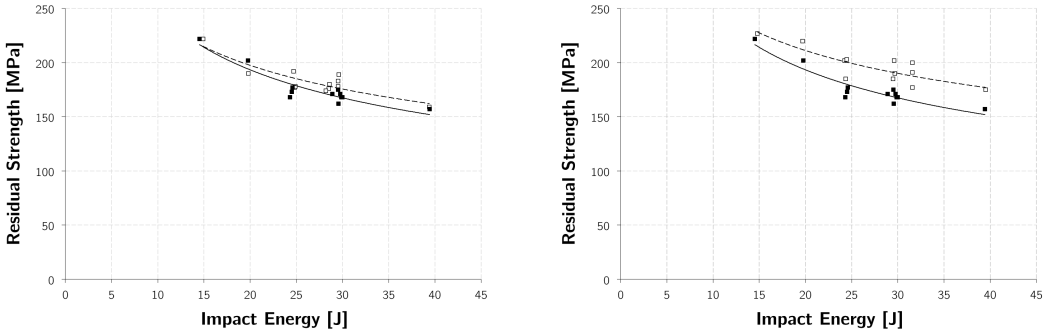


Figure 7.10: Residual strength versus impact energy for configurations 1 (left) and 2 (right), in AP-PLY (black) and baseline (white)

Projected delamination size is smaller for configuration one and similar for configuration 2.

Table 7.3: Relative differences in [%] between the two tested configuration and the baseline, where ID is indentation depth, DS is delamination size and RS is residual strength

| | **Configuration 1** | | | **Configuration 2** | | |
|---|---|---|---|---|---|---|
| | **ID** | **DS** | **RS** | **ID** | **DS** | **RS** |
| 15 | - 32 | + 6.9 | 0 | + 24.0 | - 9.3 | + 2.3 |
| 20 | + 22.6 | - 0.4 | - 5.9 | - 5.1 | + 9.2 | + 8.9 |
| 25 | + 1.9 | - 21.1 | + 5.6 | - 5.7 | - 3.1 | + 13.9 |
| BVID | + 5.3 | - 33.2 | + 3.11 | + 8.5 | - 9.2 | + 10.5 |
| 30 | + 2.6 | - 25.8 | + 9.8 | - 14.1 | + 2.2 | + 15.2 |
| 40 | + 22.6 | - 42.6 | + 1.27 | - 5.1 | - 13.4 | + 11.5 |

The improvement is larger for configuration 2, and it can be said with more confidence taking into account the experimental scatter. In Figure 7.11 the relative improvement of the two configurations with respect to the baseline unidirectional laminate are plotted against the energy levels. Although some of the values, especially the highest and the lowest ones, are based on only one test specimen, ascending trends can be distinguished, meaning that a larger improvement can be expected when energy levels, or damage states, are higher. More tests at high energy levels are needed to support this conclusion.

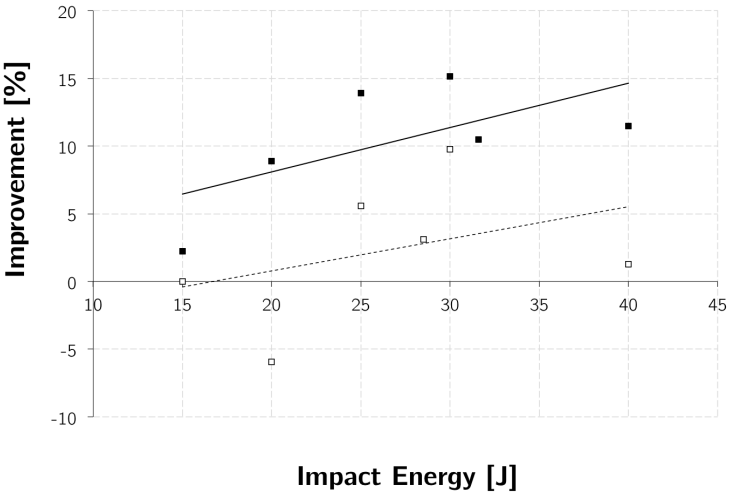


Figure 7.11: Relative improvement at different energy levels for configuration 1 (white) and configuration 2 (black)

# Chapter 8

# Conclusions and Recommendations

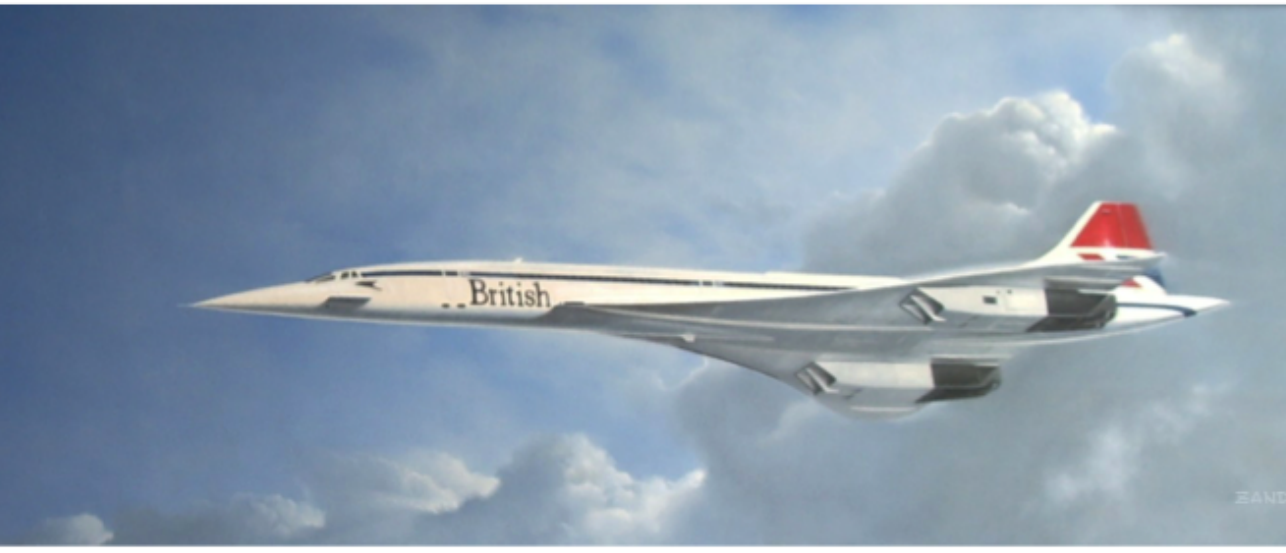

## 8.1 Conclusions

A new concept for designing and manufacturing fibre placed composite laminates was presented in this thesis. This fibre placement architecture improves the damage tolerance over laminates with unidirectional layers by interweaving layers in a pattern, creating through-the-thickness reinforcements. An attempt was made to discover and describe the most basic behaviour of these laminates in an empirical and experimental fashion.

Looking at the literature on impact damage behaviour of composite laminates the following conclusions are important for this research:

- Besides delaminations, also fibre breakage and matrix cracks play a role in after damage compressive strength.
- Not only the size but also the location of the delaminations through the thickness determines the after impact compression strength and thus the damage tolerance of composite laminates.
- Fibre architectures with fibres running in the thickness direction other than fabrics and braids can improve the after damage compressive strength, while maintaining in-plane properties as compared to unidirectional laminates.

An example of such a fibre architecture is presented and named AP-PLY. In compression after impact tests and destructive and non-destructive inspections, the behaviour of these new laminate configurations are studied in both a qualitative and a quantitative manner.

- As AP-PLY is a geometric principle, it is applicable to any resin and fibre combination, preferably one that is already been used and thus available for fibre placement. Thermoset prepregs, thermoplastic tapes and dry fibres have been used successfully.
- No adaptation of the current fibre placement machines is needed for them to be able to manufacture AP-PLY laminates. For the preferred configuration from this research, manufacturing time will increase by 42%.
- Only very small undulation angles are present in AP-PLY and no stiffness decrease is measured by applying the AP-PLY fibre architecture.
- In AP-PLY laminates, the maximum force during impact is lower than in unidirectional laminates with the same layup. This indicates that less delaminations are created during impact which is favourable for the laminate's stiffness.
- The indentation for the same energy level is higher in thermoset AP-PLY laminates as compared to their counterparts with unidirectional layers, leading to an earlier barely visible impact damage. In thermoplastic materials, this behaviour is opposite.
- The projected delamination size is considerably smaller for AP-PLY, where the specific values depend on the pattern, layup and material system.
- Depending on the pattern, interweaving all layers in a layup leads to an increase in after impact compression strength between 5-10%.

- The larger the damage, so with thinner laminates or higher impact energies, the larger the improvement in damage tolerance achieved by using AP-PLY.

As many parameters in the pattern can be changed, a design of experiments approach was used to determine the influence of the individual pattern parameters on the impact damage behaviour and subsequent compressive strength. When designing laminates with the AP-PLY fibre placement architecture, the following has to be taken into account:

- In the AP-PLY fibre placement architecture, skipping two tow widths does not yield such a significant improvement over skipping three tow-widths to justify the longer manufacturing time.
- The smaller from the two bandwidths tested has the highest residual strength after impact and smaller scatter, indicating that smaller bandwidths are favourable.
- Interweaving more than two layers using AP-PLY increases the after impact performance. Simply applying the original pattern to four layers increases the undulations and irregularity. A new pattern is proposed that interweaves every package of two interwoven layers with the package of layers above and the package of layers below.

Not only monolithic, flat, quasi-isotropic laminate configurations have been tested for compression after impact behaviour, but also cylindrical tubes, sandwich panels and other mechanical properties in order to have a full understanding of the mechanical behaviour of this new family of composite laminates.

- Sandwich panels with AP-PLY facesheets show a 10% improvement in after impact compression strength.
- In a relatively thin cylindrical configuration the decrease in projected delamination size by using AP-PLY was as high as 60%.
- Bearing and open hole compression tests show similar values for AP-PLY and laminates with unidirectional layers, but considerably smaller scatter. This could lead to higher A- and B-basis allowables.
- A specimen was designed to test the fracture toughness of the AP-PLY pattern. Both Mode I and Mode II fracture toughness are increased by the AP-PLY Pattern. Mode I fracture toughness is increased with 89% and Mode II fracture toughness is increased by 20%.

The higher fracture toughness values and the significantly smaller delaminations imply that more improvement can be reached than what is currently seen in the compression after impact tests. To design an improved AP-PLY configuration, an attempt was made to model the behaviour of composite laminates under an impact loading analytically.

- A new method to calculate the deflection of unsymmetric and unbalanced composite laminates under an out-of-plane load using Legendre polynomials was developed.
- Using this method combined with a fracture mechanics approach, the size and location of delaminations could be predicted with reasonable comparison to test results.

Continuing from the conclusions of the analytical model, a final AP-PLY configuration has shown to be very promising in damage tolerance with less negative influence on the manufacturing time than previous configurations.

- Considering impact, making every ply interface in a laminate stronger does not make the entire laminate stronger as not enough impact energy will be dissipated. This could also apply to fibre architectures other than AP-PLY and fibre placement, such as weaving, braiding and filament winding.
- An improved AP-PLY configuration is presented where 10 out of 24 plies are interwoven, increasing the after impact compression strength by 15%.

## 8.2 Recommendations

The research presented in this thesis is merely a starting point. As the AP-PLY concept is still very young, it needs more work to mature before it can be applied in aerospace structures. The following topics could be addressed:

- The influence of the interweaving angle on the AP-PLY performance should be investigated; depending on the angle, more or less overlap exists between the layers.
- To be able to design properly with AP-PLY, a model is needed to simulate its behaviour. The model should take into account the physical properties of AP-PLY to optimize both the in-plane pattern and the stacking through the thickness. A start could be a finite element model to incorporate the fracture toughness behaviour in cohesive elements between stacked shell layers.
- An adaptation of the fibre placement head should be investigated to eliminate the disadvantage of the longer fabrication time of AP-PLY as compared to unidirectional layers.
- Larger series of similar AP-PLY specimens should be tested to investigate the scatter in mechanical properties, in both static and impact loading.
- Elements and subcomponents should be designed, built and tested to prove the AP-PLY principle higher in the building-block pyramid.
- The fatigue behaviour of AP-PLY laminates should be looked at. As the Mode I results show a large improvement, it is expected that in delamination growth AP-PLY can have even more benefits than in the Mode II dominated delamination creation what was tested in this research.
- The optimal machine motions, especially through the air between courses, should be found to minimise the increase in fabrication time.
- Even more unorthodox fibre placement architectures can be thought of to make better use of the advantage of composites and their automated manufacturing processes.

# Bibliography


Abdalla, Mostafa M., Shahriar Setoodeh, and Zafer Gürdal (2007). "Design of variable stiffness composite panels for maximum fundamental frequency using lamination parameters". In: *Composite Structures* 81.2, pp. 283 –291.

Abrate, S. (1991). "Impact on Laminated Composite Materials". In: *Applied Mechanics Review* 44.4, pp. 155 –190.

AITM (2009). *1.0010*. Airbus Industry Test Method.

Akhavan, Hamed and Pedro Ribeiro (2011). "Natural modes of vibration of variable stiffness composite laminates with curvilinear fibers". In: *Composite Structures* 93.11, pp. 3040 – 3047.

Arzoni, V., M.H. Nagelsmit, and P.J. van Langen (2012). "Improving the damage tolerance of composite sandwich panels by use of AP-PLY". In: *Proceedings SAMPE SEICO 2012*, pp. 1–6.

ASTM (2007). *D5528*. American Society for the Testing of Materials.

— (2009a). *D5961-Standard Test Method for Bearing Response of Polymer Matrix Composite Laminates*. American Society for the Testing of Materials.

— (2009b). *D7136*. American Society for the Testing of Materials.

— (2009c). *D7137*. American Society for the Testing of Materials.

Baker, A.A., R. Jones, and R.J. Callinan (1985). "Damage Tolerance of Graphite/Epoxy Composites". In: *Composite Structures* 8, pp. 15–44.

Bannister, Michael (2001). "Challenges for composites into the next millennium - a reinforcement perspective". In: *Composites Part A: Applied Science and Manufacturing* 32.7, pp. 901 –910.

Beukers, A. and E. van Hinte (2005). *Lightness: The Inevitable Renaissance of Minimum Energy Structures*. 010 Publishers.

Bibo, G.A. and P.J. Hogg (1996). "Review: The role of reinforcement architecture on impact damage mechanisms and post-impact compression behaviour". In: *Journal of Materials Science* 31, pp. 1115 –1137.

Blom, Adriana W., Patrick B. Stickler, and Zafer Gürdal (2010). "Optimization of a composite cylinder under bending by tailoring stiffness properties in circumferential direction". In: *Composites Part B: Engineering* 41.2, pp. 157 –165.

Blom, Adriana W. et al. (2008). "Design of variable-stiffness conical shells for maximum fundamental eigenfrequency". In: *Computers & Structures* 86.9, pp. 870 –878.

Box, G.E.P., W.G. Hunter, and J.S. Hunter (1978). *Statistics for Experimenters*. John Wiley and Sons.

Camanho, P.P. and M. Lambert (2006). "A design methodology for mechanically fastened joints in laminated composite materials". In: *Composites Science and Technology* 66.15, pp. 3004 –3020.

Campbell, F.C. (2010). *Structural Composite Materials*. ASM International.

Campen, Julien M.J.F. van, Christos Kassapoglou, and Zafer Gürdal (2012). "Generating realistic laminate fiber angle distributions for optimal variable stiffness laminates". In: *Composites Part B: Engineering* 43.2, pp. 354 –360.

Cantwell, W.J. and J. Morton (1991). "The impact resistance of composite materials - a review". In: *Composites* 22.5, pp. 347 –362.

Dost, E.F. et al. (1991). "Effects of stacking sequence on impact damage resistance and residual strength for quasi-isotropic laminates". In: *Composite Materials Fatigue and Fracture* 3, pp. 476–500.

Dransfield, Kimberley, Caroline Baillie, and Yiu-Wing Mai (1994). "Improving the delamination resistance of CFRP by stitching - a review". In: *Composites Science and Technology* 50.3, pp. 305 –317.

Feraboli, Paolo (2006). "Some Recommendations for Characterization of Composite Panels by Means of Drop Tower Impact Testing". In: *Journal of Aircraft* 43.6, pp. 1710–1718.

Feraboli, Paolo and Keith T. Kedward (2006). "A new composite structure impact performance assessment program". In: *Composites Science and Technology* 66.10, pp. 1336 –1347.

Garcia, Enrique J., Brian L. Wardle, and A. John Hart (2008). "Joining prepreg composite interfaces with aligned carbon nanotubes". In: *Composites: Part A* 39, pp. 1065–1070.

Gürdal, Z. and R. Olmedo (1993). "In-plane response of laminates with spatially varying fiber orientations : variable stiffness concept". In: *AIAA Journal* 31, pp. 751–758.

Hart-Smith, L.J. (1993). "The Ten-Percent Rule for preliminary sizing of fibrous composite structures". In: *Aerospace Materials* 5.2, pp. 10–16.

IJsselmuiden, S.T. (2011). "Optimal Design of Variable Stiffness Composite Structures using Lamination Parameters". PhD thesis. Delft University of Technology.

ISO (2002). *ISO 15114 - Fibre-reinforced plastic composites - Determination of apparent mode II interlaminar fracture toughness for unidirectionally reinforced materials*. European Committee for Standardization.

Jih, C.J. and C.T. Sun (1993). "Prediction of Delamination in Composite Laminates Subjected to Low Velocity Impact". In: *Journal of Composite Materials* 27.7, pp. 684–701.

Jones, R.M. (1975). *Mechanics of Composite Materials*. Scripta Book Co.

Kan, Y.R. and Y.M. Ito (1972). "Analysis of Unbalanced Angle-Ply Rectangular Plates". In: *Int. J. Solids Structures* 8, pp. 1283–1297.

Kassapoglou, C. (2010). *Design and Analysis of Composite Structures*. John Wiley and Sons.

Khani, A. et al. (2011). "Design of variable stiffness panels for maximum strength using lamination parameters". In: *Composites Part B: Engineering* 42.3, pp. 546 –552.

Khokar, N. (1996). "3D Fabric-forming Processes: Distinguishing Between 2D-weaving, 3D-weaving and an Unspecified Non-interlacing Process". In: *Journal of The Textile Institute* 87.1, pp. 97–106.

Kim, J.-K. (1998). "Methods for improving impact damage resistance of CFRPs". In: *Key engineering materials* 141-143, pp. 149–168.

Kollár, L.P. and G.S. Springer (2009). *Mechanics of Composite Structures*. Cambridge University Press.

Kostopoulos, V. et al. (2010). "Impact and after-impact properties of carbon fibre reinforced composites enhanced with multi-wall carbon nanotubes". In: *Composites Science and Technology* 70.4, pp. 553 –563.

Leong, K.H. et al. (2000). "The potential of knitting for engineering composites "a review". In: *Composites Part A: Applied Science and Manufacturing* 31.3, pp. 197 –220.

Lopes, C.S. et al. (2009). "Low-velocity impact damage on dispersed stacking sequence laminates. Part I: Experiments". In: *Composites Science and Technology* 69, pp. 926–936.

Martin, R.H. and B.D. Davidson (1999). "Mode II fracture toughness evaluation using four point bend, end notched flexure test". In: *Plastics, Rubber and Composites* 28.8, pp. 401–406.

MIL-HDBK-17-3F (2002). *Composite Materials Handbook Volume 3*. Department of Defense.

MIL-HDBK-5J (2003). *Metallic Materials and Elements for Aerospace Vehicle Structures*. Department of Defense.

Mouritz, A.P. (2007). "Review of z-pinned composite laminates". In: *Composites Part A: Applied Science and Manufacturing* 38.12, pp. 2383 –2397.

Mouritz, A.P. et al. (1999). "Review of applications for advanced three-dimensional fibre textile composites". In: *Composites Part A: Applied Science and Manufacturing* 30.12, pp. 1445 –1461.

Nagelsmit, M., C. Kassapoglou, and Z. Gürdal (2011a). "Fiber Placement Process for AP-PLY Composite Components". In: *Proceedings SAMPE SETEC 2011*, pp. 195–202.

Nagelsmit, M.H., C. Kassapoglou, and Z. Gürdal (2011b). *Influence of Multidirectional Weave (AP-PLY) Pattern Parameters on Composite Impact Damage Behaviour*. NLR-TP-2011-566.

Nagelsmit, M.H. et al. (Jan. 2010). *Method for making a composite material and structure, composite material and end product*.

Naumann, Niko et al. (2012). "Recent advances in robotic automated deposition of different materials". In: *Proceedings SAMPE SEMAT*, pp. 158–164.

Niu, Micheal (1992). *Composite Aircraft Structures*. Hong Kong Conmilit Press Ltd.

Reinhart, Gunther, Andreas Glück, and Claudia Ehinger (2012). "Automated process chain for the manufacturing of fiber reinforces plastics (FRP)". In: *Proceedings SAMPE SEMAT*, pp. 144–149.

Roeseler, William G., Branko Sarh, and Max U. Kismarton (2007). "Composite structures: the first 100 years". In: *16th International Conference on Composite Materials, Kyoto, Japan*, pp. 1–10.

Rousseau, J., D. Perreux, and N. Verdière (1999). "The influence of winding patterns on the damage behaviour of filament-wound pipes". In: *Composites Science and Technology* 59.9, pp. 1439 –1449.

Sebaey, T.A. (2012). "Characterization and Optimization of Dispersed Composite Laminates for Damage Resistant Aeronautical Structures". PhD thesis. Universitat de Girona.

Sebaey, T.A. et al. (2013). "Damage resistance and damage tolerance of dispersed CFRP laminates: Effect of the mismatch angle between plies". In: *Composite Structures* In press.

Setoodeh, Shahriar, Mostafa M. Abdalla, and Zafer Gürdal (2006). "Design of variable stiffness laminates using lamination parameters". In: *Composites Part B: Engineering* 37.4-5, pp. 301 –309.

Setoodeh, Shahriar et al. (2009). "Design of variable-stiffness composite panels for maximum buckling load". In: *Composite Structures* 87.1, pp. 109 –117.

Shen, Frank C. (1995). "A filament-wound structure technology overview". In: *Materials Chemistry and Physics* 42.2, pp. 96 –100.

Sierakowski, R.L. and G.M. Newaz (1995). *Damage Tolerance in Advanced Composites*. Technomic Publishing Company.

Sun, C.T. and M.G. Manoharan (1989). "Growth of delamination cracks due to bending in a $[90_5/0_5/90_5]$ laminate". In: *Composites Science and Technology* 34, pp. 365–377.

Thuis, H.G.S.J. et al. (1998). "The influence of stitching fibre and stitching density on the failure strains of CFRP fabrics". In: *Proceedings European Conference on Composite Materials 8*, pp. 133–142.

Tong, L., A.P. Mouritz, and M. Bannister (2002). *3D Fibre Reinforced Polymer Composites*. Elsevier Science Ltd.

Zhang, X., L. Hounslow, and M. Grassi (2006). "Improvement of low-velocity impact and compression-after-impact performance by z-fibre pinning". In: *Composites Science and Technology* 66.15, pp. 2785 –2794.

# Appendix A

# Derivations

As the plate is simply supported at the edges, the boundary conditions yield new conditions to solve the system of equations:

$$w = 0 \quad \text{at} \quad \begin{matrix} \frac{x}{a} = 1, -1 \\ \frac{y}{b} = 1, -1 \end{matrix} \tag{A.1}$$

From Equation A.1:

$$\sum_{m=0}^{14} \sum_{n=0}^{14} A_{mn} P_m(\tfrac{x}{a}) P_n(1) = 0$$

$$\sum_{m=0}^{14} \sum_{n=0}^{14} A_{mn} P_m(\tfrac{x}{a}) P_n(-1) = 0$$

$$\sum_{m=0}^{14} \sum_{n=0}^{14} A_{mn} P_m(-1) P_n(\tfrac{y}{b}) = 0$$

$$\sum_{m=0}^{14} \sum_{n=0}^{14} A_{mn} P_m(1) P_n(\tfrac{y}{b}) = 0$$

$$M = w_{xx} = w_{yy} = 0 \quad \text{at} \quad \begin{matrix} \frac{x}{a} = 1, -1 \\ \frac{y}{b} = 1, -1 \end{matrix} \tag{A.2}$$

$$\sum_{m=0}^{14} \sum_{n=0}^{14} A_{mn} P_m(\tfrac{x}{a}) P_n''(1) = 0$$

$$\sum_{m=0}^{14} \sum_{n=0}^{14} A_{mn} P_m(\tfrac{x}{a}) P_n''(-1) = 0$$

$$\sum_{m=0}^{14}\sum_{n=0}^{14} A_{mn} P_m''(-1) P_n(\tfrac{y}{b}) = 0$$

$$\sum_{m=0}^{14}\sum_{n=0}^{14} A_{mn} P_m''(1) P_n(\tfrac{y}{b}) = 0$$

For the distributed load also the external force $p$ is described with Legendre polynomials:

$$p = \sum_{m=0}^{14}\sum_{n=0}^{14} B_{mn} P_m(\tfrac{x}{a}) P_n(\tfrac{y}{b}) \tag{A.3}$$

Multiply both sides with $P_q(\frac{x}{a}) P_r(\frac{y}{b})$ and integrate:

$$\int_{-a}^{a}\int_{-b}^{b} p P_q(\tfrac{x}{a}) P_r(\tfrac{y}{b})\,\mathrm{d}x\,\mathrm{d}y = \int_{-a}^{a}\int_{-b}^{b} B_{mn} P_m(\tfrac{x}{a}) P_n(\tfrac{y}{b}) P_q(\tfrac{x}{a}) P_r(\tfrac{y}{b})\,\mathrm{d}x\,\mathrm{d}y \tag{A.4}$$

Because Legendre polynomials are orthogonal over (-1,1) and taking $(\frac{x}{a}) = z$ and $(\frac{y}{b}) = s$:

$$\int_{-1}^{1} P_m(z) P_q(z) a\,\mathrm{d}z = \begin{cases} a\frac{2}{2m+1} & \text{if } m = q \\ 0 & \text{if } m \neq q \end{cases} \tag{A.5}$$

$$\int_{-1}^{1} P_n(s) P_r(s) b\,\mathrm{d}s = \begin{cases} b\frac{2}{2n+1} & \text{if } n = r \\ 0 & \text{if } n \neq r \end{cases} \tag{A.6}$$

The equation becomes:

$$p I_m I_n = B_{mn} \frac{4ab}{(2m+1)(2n+1)} \tag{A.7}$$

Where, again with $(\frac{x}{a}) = z$ and $(\frac{y}{b}) = s$:

$$I_m = \int_{-a}^{a} P_m(\tfrac{x}{a})\,\mathrm{d}x = \int_{-1}^{1} P_m(z) a\,\mathrm{d}z = \frac{P_{m-1}(0) - P_{m+1}(0)}{2m+1} = \begin{cases} 2a & \text{if } m = 0 \\ 0 & \text{if } m \neq 0 \end{cases} \tag{A.8}$$

$$I_n = \int_{-b}^{b} P_n(\tfrac{y}{b})\,\mathrm{d}y = \int_{-1}^{1} P_n(s) b\,\mathrm{d}s = \frac{P_{n-1}(0) - P_{n+1}(0)}{2n+1} = \begin{cases} 2b & \text{if } n = 0 \\ 0 & \text{if } n \neq 0 \end{cases} \tag{A.9}$$

So looking at Equation A.4, $a$ and $b$ cancel on both sides and $m, n = 0$, resulting in:

$$B_{mn} = B_{00} = p \tag{A.10}$$

Resulting is a system of equations where only the $A_{mn}$ are unknown:

$$GE \times A_{mn} = B_{mn} \times P_m(\tfrac{x}{a}) P_n(\tfrac{y}{b}) = p \tag{A.11}$$

# Appendix B

# Derivation of Ply Stresses and Strains

Most failure criteria make use of ply strains and stresses, hence these have to be retrieved from the model in the following way.

From the Legendre model, the curvatures of the total panel can be calculated:

$$\kappa_x = -\frac{\mathrm{d}^2 w}{\mathrm{d}x^2}$$
$$\kappa_y = -\frac{\mathrm{d}^2 w}{\mathrm{d}y^2}$$
$$\kappa_{xy} = -2\frac{\mathrm{d}^2 w}{\mathrm{d}x\,\mathrm{d}y}$$

From these curvatures, the laminates global strains can be calculated:

$$\epsilon_x = \epsilon_{x0} + z\kappa_x$$
$$\epsilon_y = \epsilon_{y0} + z\kappa_y$$
$$\gamma_{xy} = \gamma_{xy0} + z\kappa_{xy}$$

Mid-plane strains $\epsilon_{x0}$,$\epsilon_{y0}$ and $\gamma_{xy0}$ are zero for balanced and symmetric laminates, according to the Kirchhoff assumption. For this case of unbalanced and/or unsymmetric laminates after the first ply failure, the mid-plane strains follow from the expressions for the in-plane displacements $u$ and $v$:

$$\epsilon_{x0} = \frac{\mathrm{d}u}{\mathrm{d}x} = \frac{3C_{10}x^2b + 2xC_{01}ya + 3C_{11}x^2y - a^2C_{10}b - a^2C_{11}y}{(ab}$$

$$\epsilon_{y0} = \frac{\mathrm{d}v}{\mathrm{d}y} = \frac{2yF_{10}xb - 3F_{01}y^2a - 3F_{11}xy^2 + b^2F_{01}a + b^2F_{11}x)}{ab}$$

$$\gamma_{xy0} = \frac{\mathrm{d}u}{\mathrm{d}y} + \frac{\mathrm{d}v}{\mathrm{d}x} = -(-x^2 + a^2)\frac{(C_{01}a + C_{11}x)}{ab} - (-y^2 + b^2)\frac{(F_{10}b + F_{11}y)}{ab}$$

Now that the strains in each ply are know in the laminate's coordinate system, they need to be translated to the ply's coordinate system. This means they need to be rotated by the ply orientation angle using the following transformation matrix that also takes into account the fact that the engineering shear strain is twice the $\gamma_{xy}$:

$$\begin{Bmatrix} \epsilon_1 \\ \epsilon_2 \\ \gamma_{12} \end{Bmatrix} = \begin{bmatrix} \cos^2\theta & \sin^2\theta & \sin\theta\cos\theta \\ \sin^2\theta & \cos^2\theta & -\sin\theta\cos\theta \\ -2\sin\theta\cos\theta & 2\sin\theta\cos\theta & (\cos^2\theta - \sin^2\theta) \end{bmatrix} \begin{Bmatrix} \epsilon_x \\ \epsilon_y \\ \gamma_{xy} \end{Bmatrix}$$

Going from strains to stresses, the strains have to be multiplied by the ply stiffness, which are just the orthotropic values as defined before in calculating the ABD-matrices.

$$\begin{Bmatrix} \sigma_1 \\ \sigma_2 \\ \sigma_{12} \end{Bmatrix} = \begin{bmatrix} Q_{11} & Q_{12} & Q_{16} \\ Q_{12} & Q_{22} & Q_{26} \\ Q_{16} & Q_{26} & Q_{66} \end{bmatrix} \begin{Bmatrix} \epsilon_1 \\ \epsilon_2 \\ \gamma_{12} \end{Bmatrix}$$

As the ply itself is orthotropic, $Q_{16}$ and $Q_{26}$ are zero.
Both stresses and strains are known for each ply in the laminate.

# Appendix C

# Compression After Impact Test Results

Table C.1: TS UD 90°

| **Specimen ID** | **IE [$J$]** | **ID [$mm$]** | **DA [$mm^2$]** | **RS [$MPa$]** |
|---|---|---|---|---|
| 3142-1 | 40 | 2.51 | 1183 | 157 |
| 3142-2 | 15 | 0.2 | 816 | 231 |
| 3142-3 | 20 | 0.61 | 972 | 206 |
| 3142-4 | 25 | 0.81 | 1036 | 191 |
| 3142-5 | 30 | 1.54 | 1167 | 173 |
| 3142-6 | 30 | 1.38 | 1130 | 161 |
| 3142-7 | 30 | 1.4 | 1132 | 173 |
| 3142-8 | 26.48 | 1.13 | 1041 | 180 |
| 3142-9 | 26.48 | 1.03 | 1095 | 186 |
| 3142-10 | 26.48 | 1.03 | 1061 | 183 |
| 3142-11 | 20 | 0.59 | 973 | 203 |
| 3142-12 | 20 | 0.48 | 1183 | 203 |

Table C.2: TS AP-PLY 2 90° 1/2

| **Specimen ID** | **IE [$J$]** | **ID [$mm$]** | **DA [$mm^2$]** | **RS [$MPa$]** |
|---|---|---|---|---|
| 3143-1 | 40 | 2.95 | 1040 | 178 |
| 3143-2 | 15 | 0.18 | 675 | 238 |
| 3143-3 | 20 | 0.55 | 770 | 218 |
| 3143-4 | 25 | 0.87 | 882 | 201 |
| 3143-5 | 30 | 1.70 | 931 | 176 |
| 3143-6 | 30 | 1.68 | 796 | 186 |
| 3143-7 | 30 | 1.55 | 979 | 179 |
| 3143-8 | 25.88 | 0.99 | 1043 | 186 |
| 3143-9 | 25.88 | 1.01 | 835 | 193 |
| 3143-10 | 25.88 | 1.06 | 938 | 198 |
| 3143-11 | 20 | 0.53 | 906 | 202 |
| 3143-12 | 20 | 0.40 | 753 | 213 |

Table C.3: TS AP-PLY 1 90° 1/2

| **Specimen ID** | **IE [$J$]** | **ID [$mm$]** | **DA [$mm^2$]** | **RS [$MPa$]** |
|---|---|---|---|---|
| 3144-1 | 40 | 4.16 | 1004 | 174 |
| 3144-2 | 15 | 0.21 | 785 | 228 |
| 3144-3 | 20 | 0.58 | 716 | 231 |
| 3144-4 | 25 | 0.93 | 819 | 194 |
| 3144-5 | 30 | 1.69 | 799 | 187 |
| 3144-6 | 30 | 1.77 | 937 | 182 |
| 3144-7 | 30 | 1.57 | 905 | 187 |
| 3144-8 | 25.06 | 1.04 | 808 | 192 |
| 3144-9 | 25.06 | 0.74 | 663 | 209 |
| 3144-10 | 25.06 | 0.74 | 680 | 217 |
| 3144-11 | 20 | 0.56 | 633 | 220 |
| 3144-12 | 20 | 0.55 | 769 | 208 |

Table C.4: TS UD 45°

| **Specimen ID** | **IE [$J$]** | **ID [$mm$]** | **DA [$mm^2$]** | **RS [$MPa$]** |
|---|---|---|---|---|
| 3145-1 | 40 | 2.64 | 1304 | 170 |
| 3145-2 | 15 | 0.18 | 1067 | 229 |
| 3145-3 | 20 | 0.43 | 937 | 210 |
| 3145-4 | 25 | 0.76 | 1108 | 203 |
| 3145-5 | 30 | 1.20 | 1264 | 181 |
| 3145-6 | 30 | 1.43 | 1212 | 186 |
| 3145-7 | 30 | 1.20 | 1110 | 188 |
| 3145-8 | 27.63 | 1.09 | 1220 | 195 |
| 3145-9 | 27.63 | 0.96 | 1281 | 205 |
| 3145-10 | 27.63 | 0.96 | 1221 | 202 |
| 3145-11 | 20 | 0.34 | 988 | 240 |
| 3145-12 | 20 | 0.41 | 969 | 227 |

Table C.5: TS AP-PLY 2 45° 1/2

| **Specimen ID** | **IE [$J$]** | **ID [$mm$]** | **DA [$mm^2$]** | **RS [$MPa$]** |
|---|---|---|---|---|
| 3152-1 | 40 | 3.07 | 1929 | 174 |
| 3152-2 | 15 | 0.21 | 934 | 229 |
| 3152-3 | 20 | 0.48 | 1010 | 227 |
| 3152-4 | 25 | 0.88 | 1195 | 218 |
| 3152-5 | 30 | 1.25 | 1196 | 195 |
| 3152-6 | 30 | 1.56 | 1197 | 191 |
| 3152-7 | 30 | 1.60 | 1764 | 170 |
| 3152-8 | 26.25 | 0.86 | 1352 | 200 |
| 3152-9 | 26.25 | 1.27 | 1133 | 205 |
| 3152-10 | 26.25 | 1.03 | 1060 | 208 |
| 3152-11 | 20 | 0.43 | 1175 | 243 |
| 3152-12 | 20 | 0.43 | 1052 | 231 |

Table C.6: TS AP-PLY 1 45° 1/2

| **Specimen ID** | **IE [$J$]** | **ID [$mm$]** | **DA [$mm^2$]** | **RS [$MPa$]** |
|---|---|---|---|---|
| 3153-1 | 40 | 4.03 | 1242 | 173 |
| 3153-2 | 15 | 0.27 | 1025 | 236 |
| 3153-3 | 20 | 0.44 | 1149 | 234 |
| 3153-4 | 25 | 0.96 | 1019 | 213 |
| 3153-5 | 30 | 1.66 | 1192 | 190 |
| 3153-6 | 30 | 1.46 | 1077 | 195 |
| 3153-7 | 30 | 1.44 | 1281 | 197 |
| 3153-8 | 25.4 | 1.02 | 955 | 212 |
| 3153-9 | 25.4 | 1.16 | 1035 | 204 |
| 3153-10 | 25.4 | 1.21 | 842 | 213 |
| 3153-11 | 20 | 0.57 | 982 | 238 |
| 3153-12 | 20 | 0.48 | 930 | 241 |

Table C.7: Alternating TS AP-PLY 2 90° 1/2

| **Specimen ID** | **IE [$J$]** | **ID [$mm$]** | **DA [$mm^2$]** | **RS [$MPa$]** |
|---|---|---|---|---|
| 3157-1 | 40 | 2.95 | 1200 | 180 |
| 3157-2 | 15 | 0.22 | 755 | 229 |
| 3157-3 | 20 | 0.46 | 949 | 219 |
| 3157-4 | 25 | 0.94 | 847 | 217 |
| 3157-5 | 30 | 1.47 | 990 | 181 |
| 3157-6 | 30 | 1.37 | 1611 | 198 |
| 3157-7 | 30 | 1.75 | 872 | 176 |
| 3157-8 | 26.05 | 1.38 | 767 | 186 |
| 3157-9 | 26.05 | 1.16 | 879 | 202 |
| 3157-10 | 26.05 | 1.10 | 940 | 202 |
| 3157-11 | 20 | 0.59 | 746 | 212 |
| 3157-12 | 20 | 0.43 | 930 | 225 |

Table C.8: TP AP-PLY 1 45° 1/2

| **Specimen ID** | **IE [$J$]** | **ID [$mm$]** | **DA [$mm^2$]** | **RS [$MPa$]** |
|---|---|---|---|---|
| 3188-1 | 40.1 | 1.23 | 737 | 275 |
| 3188-2 | 35.4 | 0.95 | 510 | 281 |
| 3188-3 | 35.2 | 0.79 | 544 | 278 |
| 3188-4 | 35.1 | 0.74 | 531 | 312 |
| 3188-5 | 30.3 | 0.60 | 492 | 333 |
| 3188-6 | 40.2 | 1.15 | 503 | 283 |
| 3188-7 | 40.2 | 1.14 | 455 | 302 |
| 3188-8 | 30.1 | 0.54 | 536 | 343 |
| 3188-9 | 30.2 | 0.54 | 635 | 306 |
| 3188-10 | 49.9 | 1.74 | 736 | 237 |
| 3188-11 | 25.1 | 0.38 | 506 | 332 |
| 3188-12 | 19.9 | 0.32 | 451 | 369 |

Table C.9: TP UD 45°

| **Specimen ID** | **IE [$J$]** | **ID [$mm$]** | **DA [$mm^2$]** | **RS [$MPa$]** |
|---|---|---|---|---|
| 3189-1 | 39.7 | 1.16 | 601 | 277 |
| 3189-2 | 35.4 | 1.09 | 871 | 274 |
| 3189-3 | 35.1 | 1.05 | 654 | 250 |
| 3189-4 | 35.4 | 0.95 | 481 | 304 |
| 3189-5 | 30.3 | 0.75 | 577 | 305 |
| 3189-6 | 40.2 | 1.42 | 622 | 258 |
| 3189-7 | 40.2 | 1.21 | 635 | 263 |
| 3189-8 | 30.4 | 0.68 | 765 | 276 |
| 3189-9 | 30.1 | 0.57 | 602 | 312 |
| 3189-10 | 50.5 | 3.01 | 749 | 229 |
| 3189-11 | 25.2 | 0.42 | 550 | 314 |
| 3189-12 | 19.9 | 0.32 | 656 | 337 |

Table C.10: TS AP-PLY 1 45° 1/2 Four

| **Specimen ID** | **IE [$J$]** | **ID [$mm$]** | **DA [$mm^2$]** | **RS [$MPa$]** |
|---|---|---|---|---|
| 3330-1 | 40.7 | 2.64 | 983 | 174 |
| 3330-2 | 15.1 | 0.17 | 657 | 237 |
| 3330-3 | 20.2 | 0.32 | 798 | 222 |
| 3330-4 | 25.1 | 0.61 | 1098 | 212 |
| 3330-5 | 30.4 | 1.08 | 1446 | 203 |
| 3330-6 | 30.5 | 1.13 | 1141 | 193 |
| 3330-7 | 30.4 | 1.44 | 1104 | 192 |
| 3330-8 | 28.3 | 1.07 | 860 | 198 |
| 3330-9 | 28.4 | 1.03 | 852 | 197 |
| 3330-10 | 28.6 | 0.74 | 1231 | 200 |
| 3330-11 | 25.3 | 0.62 | 1146 | 202 |
| 3330-12 | 25.2 | 0.90 | 692 | 202 |

Table C.11: TS AP-PLY 1 45° 1/4

| **Specimen ID** | **IE [$J$]** | **ID [$mm$]** | **DA [$mm^2$]** | **RS [$MPa$]** |
|---|---|---|---|---|
| 3329-1 | 40.7 | 3.30 | 1195 | 175 |
| 3329-2 | 15.2 | 0.19 | 910 | 239 |
| 3329-3 | 20.3 | 0.41 | 1042 | 237 |
| 3329-4 | 25.2 | 0.88 | 997 | 214 |
| 3329-5 | 29.9 | 1.25 | 1318 | 204 |
| 3329-6 | 30.3 | 1.18 | 963 | 205 |
| 3329-7 | 30.5 | 1.25 | 957 | 199 |
| 3329-8 | 27.3 | 0.95 | 971 | 219 |
| 3329-9 | 27.1 | 1.01 | 1181 | 196 |
| 3329-10 | 27.2 | 0.91 | 955 | 208 |
| 3329-11 | 25.3 | 0.85 | 940 | 211 |
| 3329-12 | 25.3 | 0.84 | 1247 | 212 |

Table C.12: Total TS AP-PLY 1 45° 1/2

| **Specimen ID** | **IE [$J$]** | **ID [$mm$]** | **DA [$mm^2$]** | **RS [$MPa$]** |
|---|---|---|---|---|
| 3358-1 | 40.7 | 2.07 | 999 | 175 |
| 3358-2 | 15.2 | 0.17 | 1013 | 252 |
| 3358-3 | 20.3 | 0.46 | 888 | 224 |
| 3358-4 | 25.0 | 0.74 | 877 | 210 |
| 3358-5 | 30.2 | 1.02 | 1126 | 200 |
| 3358-6 | 30.4 | 1.32 | 981 | 200 |
| 3358-7 | 30.4 | 1.15 | 993 | 198 |
| 3358-8 | 28.7 | 0.94 | 864 | 194 |
| 3358-9 | 29.0 | 1.00 | 1294 | 192 |
| 3358-10 | 28.9 | 1.07 | 1022 | 203 |
| 3358-11 | 25.2 | 0.80 | 1365 | 199 |
| 3358-12 | 25.3 | 0.70 | 1035 | 190 |

Table C.13: TS AP-PLY 1 90° 1/4 Configuration 1

| **Specimen ID** | **IE [$J$]** | **ID [$mm$]** | **DA [$mm^2$]** | **RS [$MPa$]** |
|---|---|---|---|---|
| 4098-1 | 14.9 | 0.17 | 849 | 222 |
| 4098-2 | 39.4 | 2.17 | 1208 | 159 |
| 4098-3 | 19.8 | 0.51 | 1036 | 190 |
| 4098-4 | 24.7 | 0.62 | 1048 | 192 |
| 4098-5 | 29.6 | 1.08 | 1160 | 189 |
| 4098-6 | 29.5 | 1.07 | 895 | 178 |
| 4098-7 | 29.5 | 0.98 | 977 | 183 |
| 4098-8 | 28.5 | 1.00 | 1110 | 176 |
| 4098-9 | 28.2 | 0.96 | 939 | 174 |
| 4098-10 | 28.6 | 1.03 | 1055 | 180 |
| 4098-11 | 24.8 | 0.85 | 916 | 177 |
| 4098-12 | 24.9 | 0.69 | 926 | 178 |

Table C.14: TS AP-PLY 1 90° 1/4 Configuration 2

| Specimen ID | IE [$J$] | ID [$mm$] | DA [$mm^2$] | RS [$MPa$] |
|---|---|---|---|---|
| 4243-1 | 39.5 | 1.68 | 1824 | 175 |
| 4243-2 | 14.8 | 0.31 | 720 | 227 |
| 4243-3 | 19.7 | 0.25 | 1136 | 220 |
| 4243-4 | 24.2 | 0.66 | 1081 | 202 |
| 4243-5 | 29.6 | 0.77 | 1297 | 202 |
| 4243-6 | 29.7 | 0.91 | 1381 | 190 |
| 4243-7 | 29.5 | 0.94 | 1500 | 185 |
| 4243-8 | 31.6 | 0.87 | 1466 | 200 |
| 4243-9 | 31.6 | 1.12 | 1370 | 177 |
| 4243-10 | 31.6 | 1.09 | 1379 | 191 |
| 4243-11 | 24.3 | 0.72 | 1287 | 185 |
| 4243-12 | 24.5 | 0.62 | 1184 | 203 |

Table C.15: TS UD 90° 2

| Specimen ID | IE [$J$] | ID [$mm$] | DA [$mm^2$] | RS [$MPa$] |
|---|---|---|---|---|
| 4244-1 | 39.4 | 1.77 | 2106 | 157 |
| 4244-2 | 14.5 | 0.25 | 794 | 222 |
| 4244-3 | 19.8 | 0.25 | 1040 | 202 |
| 4244-4 | 24.6 | 0.78 | 1078 | 177 |
| 4244-5 | 29.6 | 0.99 | 1403 | 162 |
| 4244-6 | 28.9 | 1.09 | 1388 | 171 |
| 4244-7 | 30.0 | 0.97 | 1298 | 168 |
| 4244-8 | 29.5 | 0.92 | 1577 | 175 |
| 4244-9 | 29.9 | 0.90 | 1456 | 168 |
| 4244-10 | 29.8 | 1.02 | 1611 | 171 |
| 4244-11 | 24.3 | 0.68 | 1108 | 168 |
| 4244-12 | 24.5 | 0.66 | 1481 | 173 |

Table C.16: Sandwich AP-PLY

| Specimen ID | IE [$J$] | ID [$mm$] | ML [$kN$] |
|---|---|---|---|
| 1-1 | 5.0 | 2.30 | 27.5 |
| 1-2 | 2.5 | 0.82 | 28.8 |
| 1-3 | 2.5 | 0.90 | 30.4 |
| 1-4 | 2.5 | 1.10 | 29.0 |
| 1-5 | 3.5 | 1.38 | 27.1 |
| 1-6 | 3.5 | 1.28 | 29.9 |
| 1-7 | 1.5 | 0.47 | 30.1 |
| 1-8 | 1.5 | 0.45 | 29.0 |

Table C.17: Sandwich UD

| **Specimen ID** | **IE [$J$]** | **ID [$mm$]** | **ML [$kN$]** |
|---|---|---|---|
| 2-1 | 5.0 | 2.01 | 22.4 |
| 2-2 | 2.5 | 0.86 | 25.4 |
| 2-3 | 2.5 | 0.92 | 27.6 |
| 2-4 | 2.5 | 0.93 | 26.2 |
| 2-5 | 3.5 | 1.37 | 25.7 |
| 2-6 | 3.5 | 1.25 | 29.1 |
| 2-7 | 1.5 | 0.31 | 27.3 |
| 2-8 | 1.5 | 0.39 | 26.3 |

# Appendix D

# SBC, OHC and Bearing Test Results

Table D.1: Baseline Plain Compression

| **Specimen ID** | **Compression Modulus [$GPa$]** | **Maximum Stress [$MPa$]** | **Strain [$\mu$]** |
|---|---|---|---|
| 3442-19 | 43.5 | 617.3 | 14200 |
| 3442-20 | 43.9 | 632.7 | 14400 |
| 3442-21 | 44.2 | 625.1 | 14160 |
| | | | |
| Mean | 43.85 | 625.0 | 14250 |
| Standard Deviation | 0.29 | 6.29 | |

Table D.2: AP-PLY Plain Compression

| **Specimen ID** | **Compression Modulus [$GPa$]** | **Maximum Stress [$MPa$]** | **Strain [$\mu$]** |
|---|---|---|---|
| 3443-19 | 45.2 | 580.3 | 12840 |
| 3443-20 | 45.2 | 613.5 | 13580 |
| 3443-21 | 45.0 | 603.2 | 13400 |
| | | | |
| Mean | 45.1 | 599.0 | 13270 |
| Standard Deviation | 0.074 | 13.875 | |

Table D.3: Baseline Open Hole Compression

| **Specimen ID** | **Maximum Stress [$MPa$]** | **Strain [$\mu$]** |
|---|---|---|
| 3442-13 | 352.2 | 8030 |
| 3442-14 | 328.7 | 7500 |
| 3442-15 | 319.0 | 7270 |
| 3442-16 | 315.2 | 7190 |
| 3442-17 | 318.2 | 7260 |
| 3442-18 | 329.9 | 7520 |
| | | |
| Mean | 327.20 | |
| Standard Deviation | 13.6 | |
| Coefficient of Variation | 4.2% | |

Table D.4: AP-PLY Open Hole Compression

| **Specimen ID** | **Maximum Stress [$MPa$]** | **Strain [$\mu$]** |
|---|---|---|
| 3443-13 | 338.3 | 7500 |
| 3443-14 | 328.8 | 7290 |
| 3443-15 | 340.0 | 7530 |
| 3443-16 | 330.4 | 7320 |
| 3443-17 | 331.6 | 7350 |
| 3443-18 | 306.8 | 6800 |
| | | |
| Mean | 329.30 | 7300 |
| Standard Deviation | 11.909 | |
| Coefficient of Variation | 3.62% | |

Table D.5: Baseline Bolt Bearing

| **Specimen ID** | **Bearing Yield Strength [$MPa$]** | **Ultimate Bearing Strength[$MPa$]** |
|---|---|---|
| 3442-1 | 1035 | 1066 |
| 3442-2 | 980 | 1034 |
| 3442-3 | 1009 | 1057 |
| 3442-4 | 1014 | 1100 |
| 3442-5 | 1030 | 1127 |
| 3442-6 | 1039 | 1071 |
| | | |
| Mean | 1018 | 1076 |
| Standard Deviation | 21.9 | 33.0 |
| Coefficient of Variation | 2.2% | 3.1% |

Table D.6: AP-PLY Bolt Bearing

| **Specimen ID** | **Bearing Yield Strength [$MPa$]** | **Ultimate Bearing Strength[$MPa$]** |
|---|---|---|
| 3443-1 | 1041 | 1076 |
| 3443-2 | 1007 | 1067 |
| 3443-3 | 997 | 1023 |
| 3443-4 | 1014 | 1065 |
| 3443-5 | 1042 | 1080 |
| 3443-6 | 999 | 1084 |
| | | |
| Mean | 1017 | 1066 |
| Standard Deviation | 20.0 | 21.9 |
| Coefficient of Variation | 2.0% | 2.1% |

Table D.7: Baseline Pin Bearing

| **Specimen ID** | **Bearing Yield Strength [$MPa$]** | **Ultimate Bearing Strength[$MPa$]** |
|---|---|---|
| 3442-7 | 622 | 641 |
| 3442-8 | 596 | 701 |
| 3442-9 | 591 | 665 |
| 3442-10 | 607 | 684 |
| 3442-11 | 589 | 687 |
| 3442-12 | 625 | 674 |
| | | |
| Mean | 605 | 677 |
| Standard Deviation | 15.5% | 20.7 |
| Coefficient of Variation | 2.6% | 3.1% |

Table D.8: AP-PLY Pin Bearing

| **Specimen ID** | **Bearing Yield Strength [$MPa$]** | **Ultimate Bearing Strength[$MPa$]** |
|---|---|---|
| 3443-7 | 578 | 705 |
| 3443-8 | 621 | 674 |
| 3443-9 | 559 | 686 |
| 3443-10 | 612 | 689 |
| 3443-11 | 601 | 684 |
| 3443-12 | 621 | 674 |
| | | |
| Mean | 598 | 685 |
| Standard Deviation | 25.0 | 11.2 |
| Coefficient of Variation | 4.2% | 1.6% |

# Appendix E

# Fracture Toughness Test Results

Table E.1: Baseline Mode I Fracture Toughness

| **Specimen ID** | **Fracture Toughness [$J/m^2$]** |
|---|---|
| 4044-8 | 221.0 |
| 4044-9 | 203.1 |
| 4044-10 | 220.9 |
| 4044-11 | 192.7 |
| 4044-12 | 202.1 |
| 4044-13 | 187.6 |
| | |
| Mean | 204.6 |
| Coefficient of Variation | 6.8% |

Table E.2: AP-PLY Mode I Fracture Toughness

| **Specimen ID** | **Fracture Toughness [$J/m^2$]** |
|---|---|
| 4106-1 | 367.4 |
| 4106-2 | 397.3 |
| 4106-3 | 410.3 |
| 4106-4 | 365.9 |
| 4106-5 | 354.8 |
| 4106-6 | 427.0 |
| | |
| Mean | 387.1 |
| Coefficient of Variation | 7.4% |

Table E.3: Baseline Mode II Fracture Toughness

| **Specimen ID** | **Fracture Toughness [$J/m^2$]** |
|---|---|
| 4044-2 | 339.5 |
| 4044-3 | 361.4 |
| 4044-4 | 385.0 |
| 4044-5 | 363.9 |
| 4044-6 | 384.6 |
| | |
| Mean | 366.9 |
| Coefficient of Variation | 5.2% |

Table E.4: AP-PLY Mode II Fracture Toughness

| **Specimen ID** | **Fracture Toughness [$J/m^2$]** |
|---|---|
| 4105-1 | 450.7 |
| 4105-2 | 456.8 |
| 4105-3 | 429.0 |
| 4105-4 | 441.6 |
| 4105-5 | 434.1 |
| 4105-6 | 430.3 |
| | |
| Mean | 440.4 |
| Coefficient of Variation | 2.6% |

# List of Publications

Nagelsmit, M.H., Kassapoglou, C. & Gürdal, Z. (2010, June 4). A new fibre placement architecture for improved damage tolerance. Pitea, Sweden, 21st SICOMP Conference.

Nagelsmit, M.H., Kassapoglou, C. & Gürdal, Z. (2011). AP-PLY: A New Fibre Placement Architecture for Improved Damage Tolerance. In AJM Ferreira (Ed.), ICCS16 (pp. 597-597). Porto: FEUP.

Nagelsmit, M.H., Kassapoglou, C. & Gürdal, Z. (2011). AP-PLY: A New Fibre Placement Architecture for Fabric Replacement. SAMPE Journal, 47(no 2), 36-45.

Nagelsmit, M.H., Kassapoglou, C. & Gürdal, Z. (2010, October 5). AP-PLY: A new fibre placement architecture for fabric replacement. Marknesse, Nederland, ISCM 5/1/2010.

Nagelsmit, M.H., Kassapoglou, C. & Gürdal, Z. (2010, September 30). AP-PLY: A new fibre placement architecture for improved impact resistance. Barcelo, Valencia, Spain, GOCarbon Fibre 2010.

Mistry, M., Gandhi, F., Nagelsmit, M.H. & Gürdal, Z. (2011). Actuation Requirements of a Warp Induced Variable Twist Rotor Blade. Journal of Intelligent Material Systems and Structures, 22(9), 919-933.

Mistry, M., Gandhi, F., Nagelsmit, M.H. & Gürdal, Z. (2010). Actuation requirements of a wrap induced variable twist rotor blade. In s.n. (Ed.), Proceedings of the ASME 2010 Conference on Smart Materials, Adaptive Structures & Intelligent Systems (pp. 1-21). Philadelphia, USA: ASME.

Nagelsmit, M.H., Kassapoglou, C. & Gürdal, Z .(2011). Fiber Placement Process for AP-PLY Composite Components. In s.n. (Ed.), Proceedings SAMPE SETEC 2011 (pp. 195-202). Leiden: Sampe Europe.

Arzoni, V., Nagelsmit, M.H. & Langen, P.J. de (2012). Improving the damage tolerance of composite sandwich panels by use of AP-PLY. In M Erath (Ed.), SAMPE SEICO 12 (pp. 1-6). Paris, France: SAMPE Europe.

Nagelsmit, M.H., Kassapoglou, C., Thuis, H.G.S.J., Gürdal, Z. & Wildvank, W.A.R. (08-

04-2011). Method for Making a Composite Material, Composite Material and End Product. no WO2011/092271 A1.

Nagelsmit, M.H. & Gerrits, W. (2013). Influence of Steering Radius on Mechanical Properties of Non-Conventional Fibre Placed Laminates. In AJM Ferreira (Ed.), ICCS17 . Porto: FEUP.

# Acknowledgements

First of all, thank you for reading this thesis! That is already a compliment and reassuring that it was actually worth writing it and I hope you enjoy reading it.

While the words usually flow from my keyboard, it is hard to express my gratitude sufficiently to those who deserve it. The conciseness I started to appreciate by now means you will be acknowledged in bullits, implying an arbitrary order and completeness. With these last words pulled out of my heart and keyboard I will start making it up to you, there's so much more to come!

- I am writing this preface while staying with my lovely parents, who have always supported me. Always a warm welcome when I stayed over and only worked on my thesis all evening, and never a dull moment with 'Broertjes' Eelco and Jorrit.
- Floor, another chapter is closed and we can continue with the next, and the next, and the next...
- Grandma, you were here first so you got the first copy of this thesis!
- Paul, Inge, Klaas and Daan, thanks for Floor and the great sailing trips.
- Zafer Gürdal, every conversation with you is walking on your toes, being hard and fun at the same time. You were the one that kept me in engineering while the tempations were great. I'm eternally greatful for that. Good luck on the other side of the pond!
- Christos, you are my example in terms of knowledge, politeness, engineering, science and work ethic. You always said $\nu\alpha\iota$ to my requests and knew everything I didn't.
- Everybody else from the Aerospace Structures and Computational Mechanics group: Jan, Gillian, Laura, Miranda, Sonell, Yujie, Ali, Farid, Julien, Mohammed, Ke, Roeland, Glenn, Sam, Christian, Attila, Zhenpei, Dan, Sergio, Pooria, Sourena, Louis, Sathis, Eddy, Weiling, Mostafa, Agnes, Claudio and ofcourse professors Arbocz and Rothwell.
- NLR! Bert, for initiating and supporting this research and all my crazy ideas. Peter, for the discussions while all other offices were dark, Michiel, for making all these ridiculous laminates, Frank, for destroying them, Gerrit, Karel, Roel, Gerard, Ludmila, Marcelo, Robert, Wilco, Frank, Chris, Ralf, Marc, Jan, Wim, Henri, Ronald, Bart, Nico, Richard, Michiel N, Axel, Joachim, Senne, Ellen and Bianca. All the other people from the S-building; Ton, Niels, Hotze, Paul, Gert, Lourens, Jacco, Tim, Arnoud, Dion, etc. Even

the A-building with Marco, Wouter, Gerben and everybody else. The Amsterdam office for their hospitality and being closer to home.

- Without the help of AP-PLY interns Roy, Ruben, and Vincent we wouldn't be so far with AP-PLY as we are now.
- I had great Michelin star dinners with my roommates in Blokzijl; Jan, Stephan, Marino and Arno.
- Club Marsch, another excuse for a party, on a Tuesday... Good luck with the present!
- Club van Delft, Nathan and Bob, thanks for the support, the creative inspiration and the entrepreneurship.
- The Delftsche Ballen and the P-Haven for the breadneeded distraction.
- Sebastiaan and Matthieu for being my paranymphs as a crown on all the support.
- Everybody else I have neglected in the past four years!

I started drawing airplanes in kindergarten and it will probably never stop, while the level of detail keeps increasing with the years. Now that I have reached the material behaviour, I'm looking forward to zoom out again.

# Curriculum Vitae

Martin was born on 3 September 1983 in Leiderdorp, The Netherlands, and after growing up, dreaming of becoming a pilot and attending the Esdal College in the more rural eastern part of the country he went back to Holland to become a 'Delftenaar'. The cute little city of Delft offered him a student rowing club, Laga, where he was president, a big band where he blew his trumpet, the best friends he could dream of and he even ended up with one of the rare girls. In summary: the time of his life. At Delft University of Technology he earned his BSc degree at the Aerospace Engineering faculty followed by an MSc degree with the Aerospace Structures chair, where he analysed, built and flew (!) morphing wings, partially at the Pennsylvania State University in the USA. To complete this standard resumé of a Dutch kid studying Aerospace Engineering in Delft he started working at the Dutch National Aerospace Laboratory (NLR) as a PhD student, and currently as an R&D Engineer at the Structures Technology department of the Aerospace Vehicles division.